COHERENT RADIO OVER FIBER LINKS FOR BROADBAND WIRELESS ACCESS NETWORKS

Xiang Chen

A thesis submitted in partial fulfillment of the requirements for the Doctorate in Philosophy degree in Electrical and Computer Engineering

Ottawa-Carleton Institute of Electrical and Computer Engineering
School of Electrical Engineering and Computer Science
Faculty of Engineering
University of Ottawa

uOttawa

May 2017

ABSTRACT

The ever-increasing demand for high date rate is beyond what is provided by the present wireless and wired access networks. Radio-over-fiber (RoF) technology which can provide broadband wireless access has been considered the most practical and efficient solution. In recent years, RoF with coherent detection has been shown to have better performance than that with direct detection in terms of receiver sensitivity and spectral efficiency. However, RoF with coherent detection suffers from phase noise introduced from both the transmitter and local oscillator (LO) laser sources, which degrades the performance significantly. This study is focused on coherent RoF links for broadband wireless access networks. The thesis consists of four parts.

In the first part, a new approach to cancel the phase noise and the unstable frequency difference introduced from the transmitter and LO laser sources based on digital signal processing (DSP) in an RoF link with coherent detection is presented. The proposed schemes rival the RoF link with direct detection in complexity while maintaining a high receiver sensitivity. In addition, a high spectral efficiency coherent RoF link with phase noise cancellation, which can detect both intensity- and phase- modulated signals carried by the same optical carrier, is studied and demonstrated.

In the second part, to achieve full-duplex transmission and increase the capacity of an RoF link, radio over wavelength division multiplexing passive optical network (WDM-PON) is studied. To eliminate the requirements of light sources and wavelength management at the optical network units (ONUs), which reduces the cost and eases the installation for a radio over WDM-

PON system, a new approach to reuse the downstream wavelength at the ONU with coherent detection and DSP at the optical line terminal (OLT) is investigated. The performance in terms of error vector magnitude (EVM) and bit rate error (BER) is evaluated for both downlink and uplink. In the scheme, the coherent detection improves the receiver sensitivity for the uplink and compensate for the degraded data transmission performance due to the utilization of a wavelength-reused downstream optical signal. Furthermore, since the future internet traffic will become highly symmetric, a symmetrical radio over a colorless WDM passive optical network (PON) with wavelength reuse based on polarization multiplexing and coherent detection is proposed and studied.

In the third part, a coherent RoF link based on optical single sideband with no optical carrier (OSSB) modulation with low-cost free-running laser sources for ultra-dense wavelength division multiplexing passive optical networks (UDWDM-PONs) is studied. In a UDWDM-RoF-PON, the channel spacing is very small, thus a WDM filter may not be able to de-multiplex the ultra-dense channels. However, through coherent detection, the channel separation can be realized by using electrical filters at the output of the coherent receiver. In addition, to utilize the spectrum in each channel more efficiently, OSSB modulation is employed. In the proposed scheme, an RoF signal based OSSB modulation with coherent detection is experimentally demonstrated. The channel spacing can be as narrow as 3 GHz.

Finally, for 5th generation wireless systems (5G), multi-input and multi-output (MIMO) is a key technology which can multiple the capacity. To seamlessly integrate MIMO into RoF links, it is required that an RoF link can transmit multiple wireless signals over a single wavelength. To enable 4 × 4 MIMO, in the fourth part, an RoF link to transmit four wireless signals with an identical microwave center frequency without using frequency-division multiplexing (FDM) over a single optical wavelength based on optical independent sideband (OISB) modulation and optical orthogonal modulation incorporating optical coherent detection and digital signal processing (DSP) is studied. To increase the spectral efficiency further, a novel high spectral efficiency (20.62 bit/s/Hz) RoF link based on coherent detection and DSP with the spectral efficiency improved by employing both intensity and phase modulation and polarization multiplexing to transmit four microwave signals over a single optical carrier is investigated.

ACKNOWLEDGMENTS

My thesis covers almost all the research achievements I have made throughout my four years' Ph.D. study and it condenses not only my own painstaking efforts but also many others', to whom I would like, therefore, give my sincere thanks.

My heartfelt gratitude goes first of all to my supervisor, Professor Jianping Yao for his consistent encouragement and inspiration, his invaluable, methodical and patient guidance during all those unforgettable four years' study and my thesis writing. His enthusiasm for, dedication and serious attitude towards scientific research has had an inestimable impact on me and contributed greatly to the successful completion of my thesis writing.

My sincere thanks then go to my former lab mates, Wangzhe Li and Hiva Shahoei, who provided enormous support and help for me academically and to get used to the new surrounding shortly after I arrived in Ottawa. Their support and help ensured me to have a good start for my Ph.D. study.

I would like also give my sincere thanks to Weilin Liu, Weifeng Zhang and Jiejun Zhang, who are currently working together with me in the same lab. From joining in their academic discussions either formally or informally that took place in the lab, I was greatly benefitted. The discussions would either enlighten me about answers to some questions I was considering or help me create some new ideas in research.

My thanks then go to my parents for their unconditional love and their support both spiritually and economically for all my study life. They can understand me better and can share my troubles and joys in my study as they were both university professors before they got retired. Finally, I would like to thank my girlfriend, who is very considerate and caring. She has never

refused to help me out whenever I met with difficulties in my life so that I could focus my attention on my study and research work and successfully finish the thesis work.

PUBLICATION LIST

Refereed journal papers

1 H. Deng, J. Zhang, **X. Chen**, and J. P. Yao, "Photonic generation of a phase-coded chirp microwave waveform with increased TBWP," *IEEE Photon. Technol. Lett.*, moderate revisions.

2 **X. Chen** and J. P. Yao, "Data rate quadrupled coherent microwave photonic link," *IEEE Photon. Technol. Lett.*, to be published.

3 **X. Chen** and J. P. Yao, "Wavelength reuse in an RoF link based on CS-DSB modulation, coherent detection and DSP," *IEEE Photon. Technol. Lett.*, vol. 29, no. 12, pp. 975-978, Jun. 15, 2017.

4 **X. Chen** and J. P. Yao, "A 4 × 4 multiple-input multiple-output coherent microwave photonic link with optical independent sideband and optical orthogonal modulation," *OSA Chin. Opt. Lett.*, vol. 15, no. 1, pp. 010008 (2017), Jan. 2017. (**Invited paper**)

5 X. Han, **X. Chen** and J. P. Yao, "Simultaneous even- and third-order distortion suppression in a microwave photonic link based on orthogonal polarization modulation, balanced detection and optical sideband filtering," *Opt. Exp.*, vol. 24, no. 13, pp. 14812-14827, Jun. 2016.

6 **X. Chen** and J. P. Yao, "High spectral efficiency coherent RoF system based on OSSB modulation with low-cost free-running laser sources for UDWDM-PONs," *J. Lightw. Technol.*, vol. 34, no. 11, pp. 2789-2795, Jun. 2016.

7 **X. Chen** and J. P. Yao, "Wavelength reuse in a symmetrical radio over WDM-PON based on polarization multiplexing and coherent detection," *J. Lightw. Technol.*, vol. 34, no. 4, pp. 1150-1157, Feb. 15, 2016.

8 R. Li, X. Han, **X. Chen**, X. Chen, and J. P. Yao, "A phase-modulated microwave photonic link with an extended transmission distance," *IEEE Photon. Technol. Lett.*, vol. 27, no. 24, pp. 2563-2566, Sept. 2015.

9 **X. Chen** and J. P. Yao, "A high spectral efficiency coherent microwave photonic link employing both amplitude and phase modulation with digital phase noise cancellation," *J. Lightw. Technol*., vol. 33, no. 14, pp. 3091-3097, Jul. 15, 2015.

10 **X. Chen**, W. Li, and J. P. Yao, "Dynamic range enhancement for a microwave photonic link based on a polarization modulator," *IEEE Trans. Microw. Theory Tech.*, vol. 63, no. 7, pp. 2384-2389, Jul. 2015.

11 **X. Chen**, T. Shao, and J. P. Yao, "Digital phase noise cancellation for a coherent-detection microwave photonic link," *IEEE Photon. Technol. Lett.*, vol. 26, no. 8, pp. 805-808, Apr. 2014. (**Hot paper, selected by the Editorial Board of IEEE Photonics Technology Letters**)

12 **X. Chen**, W. Li, and J. P. Yao, "Microwave photonic link with improved dynamic range using a polarization modulator," *IEEE Photon. Technol. Lett*., vol. 25, no. 14, pp. 1373-1376, Jul. 2013.

Conference Papers

1 J. Li, **X. Chen** and J. P. Yao, "A microwave photonic filter with an improved spurious-free dynamic range," Photonics North 2017, Ottawa, Ontario, Canada, 6-8 June 2017, accepted.

2 **X. Chen** and J. P. Yao, "Microwave photonic link based on coherent detection using low-cost free-running laser sources Incorporating optical independent sideband and optical orthogonal modulation for 4 × 4 MIMO," 2017 Optical Fiber Communication Conference and Exposition **(OFC 2017)**, W3F.3, Los Angeles Convention Center, Los Angeles, California, USA, 19-23 March 2017.

3 **X. Chen** and J. P. Yao, "Coherent microwave photonic link based on optical orthogonal modulation with phase noise cancellation for 2 × 2 MIMO," IEEE International Topical Meeting on Microwave Photonics, 31 Oct.-1 Nov. 2016, Long beach, California, USA.

4 **X. Chen** and J. P. Yao, "High spectral efficiency coherent radio-over-fiber link with low-cost free-running laser sources for UDWDM-PONs, " 2016 Optical Fiber Communication Conference and Exposition **(OFC 2016)**, Tu3B.2, Anaheim Convention Center, Anaheim, California, USA, 20-24 March 2016.

5 **X. Chen** and J. P. Yao, “Wavelength reuse in a symmetrical radio over WDM-PON based on polarization multiplexing and coherent detection with digital phase noise cancellation,” 2015 IEEE International Topical Meeting on Microwave Photonics, 26-29 Oct. 2015, Paphos, Cyprus.

6 **X. Chen** and J. P. Yao, “Radio over colorless WDM-PON with wavelength reuse based on polarization multiplexing and coherent detection incorporating digital phase noise cancellation,” 2015 Optical Fiber Communication Conference and Exposition **(OFC 2015)**, W1F.2, Los Angeles Convention Center, Los Angeles, California, USA, 22-26 March 2015.

7 **X. Chen** and J. P. Yao, “A coherent microwave photonic link with digital phase noise cancellation,” 2014 IEEE International Topical Meeting on Microwave Photonics, 20-23 Oct. 2014, Sapporo, Japan. (oral presentation)

TABLE OF CONTENTS

LIST OF FIGURES

LIST OF TABLES

LIST OF ACRONYMS

ADC	Analog to digital
AFC	Automatic frequency control
AMP	Amplifier
AWG	Arrayed waveguide grating
AxC	Antenna-carrier
BBU	Baseband unit
BPD	Balanced photodetector
BER	Bit error rate
BS	Base station
BTB	Back to back
CS	Central station
CW	Continuous wave
CWs	Control words
DEMUX	Wavelength division de-multiplexer
DFB	Distributed-feedback
DP-MZM	Dual-parallel Mach-Zehnder modulator
DPSK	Differential phase shift keying
DS	Downstream signal
DSB	Double sideband
DSO	Digital storage oscillocope
DSP	Digital signal processing
EDFA	Erbium-doped fiber amplifier
ELOs	Electrical local oscillators
EPON	Ethernet passive optical network
ER	Extinction ratio
ESA	Electrical spectrum analyzer
5G	5^{th} generation wireless systems

FDM	Frequency-division multiplexing
FP-LD	Fabry-Pérot laser diode
GPON	Gigabit passive optical network
IF	Intermediate frequency
IM/CD	Intensity modulation and coherent detection
IM/DD	Intensity modulation and direct detection
IPSec	Internet protocol security
I&Q	In-phase and quadrature
LD	Laser diode
LED	Light-emitting diode
LO	Local oscillator
LTE	Long term evolution
MAC	Medium access control
MIMO	Multi-input multi-output
MUX	Wavelength division multiplexer
MZM	Mach-Zehnder modulator
OC	Optical coupler
ODN	Optical distribution network
ODSB+C	Optical double-sideband with carrier
OISB	Optical independent sideband
OLT	Optical line terminal
ONU	Optical network unit
OOK	ON-OFF-keying
OSSB	Optical single-sideband with no carrier
OSSB+C	Optical single-sideband with carrier
PBS	Polarization beam splitter
PBC	Polarization beam combiner
PC	Polarization controller
PD	Photodetector
PLL	Phase-locked loop
PM	Phase modulator

PNC	Phase noise cancellation
PON	Passive optical network
PolM	Polarization modulator
PR	Polarization rotator
PSK	Phase shift keying
PM/CD	Phase modulation and coherent detection
QAM	Quadrature amplitude modulation
QPSK	Quadrature phase shift keying
RAN	Remote access node
RF	Radio frequency
ROF	Radio over fiber
RRH	Remote radio head
RSOA	Reflective semiconductor optical amplifier
SMF	Single-mode fiber
SOA	Semiconductor optical amplifier
TDM	Time-division multiplexing
TDMA	Time division multiple access
TLS	Tunable laser source
UDWDM	Ultra-dense wavelength division multiplexing
US	Upstream signal
WDM	Wavelength division multiplexing
WiFi	Wireless fidelity

CHAPTER 1 INTRODUCTION

1.1 Background

In recent years, an ongoing growth of the global IP traffic has been generated due to the advent of new services and applications, for example, video on demand, video conferencing, interactive multimedia, e-commerce, intelligent transport and traffic information, which has placed huge capacity and low latency requirements not only for the long-haul networks but also for the last mile access networks. Optical access networks (e.g. Gigabit passive optical network (GPON), Ethernet PON (EPON)), which can satisfy the demands of the rising bandwidth and phenomenal growth of global IP traffic, has emerged in response to the needs of times. However, GPON and EPON are both time-division multiplexing (TDM) based PONs. So several users have to share the same bandwidth provided by one laser source. This requires scheduling mechanisms and burst mode transmission, which inherently limit the latency and the data rate for each user [1]. Thus it may not meet the requirements of the future access networks. These problems can be mitigated by implementing wavelength division multiplexed (WDM)-PONs. WDM-PONs can provide per user dedicated wavelength and dedicated bandwidth, which enables a continued transmission mode. Thus ultra-low latency and full unshared bandwidth become possible. On the other hand, the mobile data traffic has grown 4,000-fold over the past 10 years and almost 400-million-fold over the past 15 years, since mobile and wireless access bring great convenience to people to reach each other and access the Internet if they wish whenever and wherever they go, which in turn stimulates the rapid development of mobile and wireless access networks [2]. It is estimated that between 2015 and 2020 global mobile data traffic will increase nearly eightfold. Nowadays, for home and business local area networks, wireless fidelity (WiFi) is the most popular wireless access technology. The most prominent standard is IEEE (Institute of Electrical and Electronics Engineers) 802.11 n, supporting transmission rates of 600 Mb/s per access point. However, the achievable transmission rate in practice is much lower, depending on distance and environment. For mobile access, long-term evolution (LTE) technologies are widely used in the world. LTE technologies, as the 4^{th} generation wireless technology, can provide at most 300 Mb/s if 4×4 multi-input and multi-output (MIMO) is employed [3].

In conclusion, for access networks, wireless access networks provide great mobility and flexibility while fiber optical access network provide abundant bandwidth and capacity. Apparently the convergence of optical and wireless access system is the trend for the future broadband access. However, for the WiFi based access networks (WiFi + GPON or EPON), since frequency allocation, modulation and demodulation scheme, multiplexing are all located within the WiFi hot spots, upgrading (e.g. changing the center frequency or modulation and demodulation scheme) and maintaining become very complicated. In addition, cell-edge performance is not good since coordination between adjacent cells is not easy to realize. For the mobile access network, digitized in-phase (I) and quadrature (Q) waveforms of the wireless signals, as well as control words (CWs) are transmitted from baseband units (BBUs) to remote radio heads (RRHs) in a binary sequence through an optical link [4]. Although modulation and demodulation scheme are located within the BBUs, it still has some disadvantages. Firstly, at the RRHs, electrical local oscillators (ELOs) with different frequencies for different wireless signals, which are used to realize frequency up conversion and down conversion, are required, making the RRH very costly. Secondly, in the optical domain, the spectral efficiency is very low since binary ON-OFF-keying (OOK) is employed as the modulation format. Thirdly, time division multiple access (TDMA) is employed, which inherently limits the latency of the system and the sustained data rate with the number of active users. In addition, de-multiplexing is realized in RRHs, which increases the complexity [4].

Radio over fiber (RoF) system maybe one of the potential cost-effective solutions for the problems of the current access network mentioned above. RoF makes it possible to centralize all the functions, such as frequency allocation, modulation and demodulation scheme, multiplexing, switching, routing and medium access control (MAC) in one shared location (central station (CS)), which simplifies the design of the BSs. The radio signals are delivered to simplified BSs via optical fiber directly. The primary functions of the BSs are optoelectronic conversion and amplification functions. No ELOs is needed in BSs. Besides, RoF also has some other benefits. 1) The antenna site installation is simplified. The install and repair time on site can be shortened. In addition, due to simple BS structure, the BSs maintenance becomes simple. 2) The CSs are located in a physically secured locations thus Internet Protocol Security (IPSec) for the link between CSs and core network is no longer needed. 3) The RoF link is transparent to radio interface format (modulation and demodulation scheme, radio frequency, bit rate and so on) and protocol. Thus, LTE, WiFi and mmWave may all work together. Furthermore, this centralized network architecture allows a dynamic radio resource configuration and capacity allocation. Also, centralized upgrading is possible. 4) Since CSs are connected with BSs via low loss fibers, large distances between CSs and BSs are possible [5, 6]. In RoF links, intensity-modulation and direct-detection (IM/DD) links have been widely studied and used, since it is easy to implement and is less costly [7, 8]. Besides, recently RoF based on coherent detection has attracted much attention, since it can provide high receiver sensitivity and high spectral efficiency [9]. However, such links are sensitive to the phase noise and the unstable frequency difference introduced from the transmitter laser source and LO source. So proper technology have to be used to cancel the phase noise and the unstable frequency difference. A few solutions have been proposed in recent years, such as the use of an optical phase-locked loop (OPLL) to lock the phase of the LO laser source [10, 11] and the use of a dual-mode local light source [12, 13]. For OPLL, it is difficult to achieve effective phase locking and system stability if the transmitter laser source and LO laser source have large phase noise and frequency drift. The technical difficulty in OPLL has not been solved perfectly even when we use state-of-the art distributed-feedback (DFB) semiconductor lasers [7]. The use of a dual-mode local light source may solve this problem, but at the receiver a dual-mode local light source has to be used which increases the complexity [12].

To increase the capacity of RoF links, applying wavelength division multiplexing (WDM) passive optical networks (PONs) technology is an effective way to increase the useable bandwidth of the fiber. For full-duplex radio over WDM-PONs, since the access network environment is very sensitive to variations in capital and operational costs, colorless optical network units (ONUs) are essential [1]. At the colorless ONUs, the light sources and wavelength management are not required, which ease the installation and maintenance. In addition, the manufactory and inventory cost can be saved dramatically. Numerous schemes to implement colorless ONUs are proposed, such as spectrum slicing of a broadband light source that covers a spectral range of all the transmission wavelengths [14, 15], colorless ONUs based on injection locking [16, 17], wavelength-seeded [18] or self-seeding [19]-[21], and the reuse of the downstream wavelengths. In [14, 15], an arrayed waveguide grating (AWG) was used to spectrally slice the spectrum of a broadband optical light source located in the OLT or ONU into multi-channel narrowband optical light sources for upstream transmission [14, 15]. But the high spectral-slicing losses and the poor quality of a broadband optical light source limits the communication date rate (<155 Mb/s) and the transmission distance for the upstream signals. Alternative solutions were proposed to increase the date rate for the upstream transmission based on either an injection-locked Fabry-Pérot laser diode (FP-LD) [16, 17] or a wavelength-seeded reflective semiconductor optical amplifier (RSOA) [18] of which the emission wavelength is identical to that of the seeding light originated from a spectrum-sliced broadband light source. In order to further decrease the cost of the systems [19]-[21], the centralized broadband source was removed by using self-injection-locking of an FP-LD [19] or self-seeding of an RSOA with an optical feedback element [20]. More recently, schemes based on wavelength reuse of a downstream optical signal sent from the OLT for upstream transmission were proposed, including injection locking of a FP-LD [22, 23], gain-saturation of a semiconductor optical amplifier (SOA) [24] or a RSOA [25, 26] and the reuse of the optical carrier with an optical filter [27]-[30]. However, the analog bandwidth of an SOA or RSOA is very limited (typically around 1 GHz). In addition, in [22], [25, 26], to minimize the influence of the downstream modulation on the upstream data, the extinction ratio (ER) of the downstream signal has to be very low which limits the performance for the downstream transmission. Furthermore, in [27, 28] an optical filter with a different center frequency has to be used at a different ONU, so the ONU is not colorless. To reduce the crosstalk from the downstream signal, [22], [25, 26], the phase modulation were used for downstream signals to facilitate the erase of the downstream signals [31]. Since direct detection can only detect intensity information on the optical carrier, the downstream phase-modulated signal can be erased totally. However, since the downstream signal was phase modulated, direct detection with the assistance of a delay interferometer has to be used. What's more, the data rate for the downstream was not transparent because of using a fixed-time delay interferometer. To solve this problem, two schemes were proposed [32]-[34]. In the first scheme, two orthogonally polarized light waves, both are phase-modulated by a downstream signal at a polarization modulator (PolM) for the downstream transmission, are utilized for wavelength reuse [32, 33]. In the second scheme, an intensity-modulated optical signal is polarization multiplexed with a pure optical carrier and then transmitted to the receiver [34]. The pure optical carrier is separated using a polarization demultiplexer and used for wavelength reuse in the ONU. The main limitation of the schemes in [32]-[34] is that polarization multiplexing cannot be implemented to double the data rate since two orthogonally polarized light waves which carry only one radio signal are utilized for the purpose of wavelength reuse (If polarization multiplexing is implemented, two different radio signals with the same center frequency can be transmitted in an radio over fiber (RoF) system, which improves the spectral efficiency). Therefore, the spectral efficiency and the data rate for the whole system is not increased. Three typical colorless ONU technologies are discussed in detailed in Chapter 2.3.

To further increase the capacity and data rate of the RoF links, MIMO, as one of the promising air interface for the 5G broadband wireless communications, providing reliable wireless communications with high spectral efficiency can be employed [35]. On one hand, MIMO can multiply the capacity by transmitting multiple signals over multi co-located antennas without the need for an additional bandwidth. On the other hand, it can also be used for beamforming, to achieve spatial selectivity, or for diversity to mitigate the multipath situations and improve the quality of the received signals. However, to realize seamless integration of the RoF links and MIMO, it is required to transmit multiple wireless signals over a single wavelength. Various approaches to transmit multiple wireless signals over a single wavelength are described in detailed in Chapter 2.4.

1.2 Major contributions of this research

In the thesis, schemes based on coherent detection and DSP to cancel the unstable frequency difference and phase noise introduced from the transmitter laser source and the LO laser source, to increase the spectral efficiency of an RoF link, to reuse a wavelength from a downstream signal in an ONU of a coherent radio over colorless WDM-PON, and to integrate 4 × 4 MIMO into a coherent RoF link, have been proposed and demonstrated.

First, two different approaches to realize RoF links based on coherent detection with phase noise cancellation are proposed and demonstrated. Coherent detection is sensitive to the phase noise and unstable frequency difference introduced from the transmitter laser source and the LO laser source. Thus, in order to recover effectively a signal at a receiver, in the first approach, a technique to cancel the phase noise and the unstable frequency difference introduced from two laser sources is investigated. The performance of the RoF link in terms of error vector magnitudes (EVMs) is studied. In an experimental demonstration, for an LO laser source with a linewidth of 1 MHz, the RF signal still can be recovered after phase noise cancellation (PNC) which proves the effectiveness of the PNC approach. For a signal with a bit rate of 834 Mb/s, the receiver sensitivity of the proposed RoF link can reach -24.5 dBm, which is better than that based on an RoF link with direct detection.

To increase the spectral efficiency, in the second approach, an RoF link with both amplitude and phase modulation is proposed. By using coherent detection, both the phase information and amplitude information can be recovered. In addition, the phase noise and the unstable frequency difference introduced from both the transmitter laser source and the LO laser source can also be cancelled. The performance of the RoF link is investigated in terms of EVMs and estimated bit rate error (BER). A sub-band spectral efficiency of 10 bit/s/Hz is demonstrated.

Second, two different approaches to realize wavelength reuse in a radio over colorless WDM-PON based on coherent detection with PNC are proposed and demonstrated. In the first approach, a radio over colorless WDM-PON with wavelength reuse based on polarization multiplexing and coherent detection incorporating PNC is proposed and experimentally demonstrated. Since coherent detection is used for the uplink to extract the uplink RoF signal from the reused downlink optical signal, the ONUs are colorless and simplified. In addition, it enables the compensation for the degraded data transmission performance due to the utilization of a reused optical carrier, since compared with direct detection, coherent detection can provide a higher optical receiver sensitivity. To the best of my knowledge, at that time it was the first time to realize wavelength reuse based on optical coherent detection. Furthermore, to realize symmetric operation of the network, a symmetrical radio over WDM-PON based on polarization multiplexing and coherent detection incorporating wavelength reuse is proposed. In the experiment, the transmission of two 2.5-Gb/s 16 quadrature amplitude modulation (16-QAM) downstream microwave vector signals and two 2.5-Gb/s 16-QAM upstream microwave vector signals over a 10.5-km single-mode fiber (SMF) is experimentally demonstrated. Compared with the RSOA-based or the FP-LD based colorless ONUs, proper controlling the optical power, wavelength and the ER of the downstream signals at the ONUs are not necessary.

Third, to improve the spectral efficiency and energy efficiency of a conventional optical double-sideband with carrier (ODSB+C) modulation RoF link, a coherent RoF link based on optical single-sideband modulation with no optical carrier (OSSB) is proposed. Thanks to the OSSB modulation, the optical carrier and one of the two optical sidebands carrying exactly the same information are eliminated, which improves the spectral efficiency and energy efficiency. The OSSB RoF signal can be recovered by optical coherent detection with PNC module incorporating low-cost free-running laser sources. The proposed scheme is very attractive for radio over ultra-dense WDM-PONs, since in each channel the spectrum can be utilized efficiently and channel spacing can be very narrow. The cannel spacing can be as narrow as 3 GHz and the data rate for each channel can reach 2.5 Gbit/s.

Finally, two RoF links are proposed which enable 4 × 4 MIMO without using FDM. For the first scheme, an RoF link to transmit four wireless signals with an identical microwave center frequency over a single optical wavelength based on optical independent sideband (OISB) modulation and optical orthogonal modulation incorporating optical coherent detection and digital signal processing (DSP) is proposed and experimentally demonstrated. To increase the spectral efficiency and make the RoF link transparent to the center frequency of the transmitted microwave signal, a 20.62 bit/s/Hz coherent RoF employing both intensity and phase modulation and polarization multiplexing to transmit four microwave signals over a single optical carrier is proposed.

1.3 Organization of this thesis

The thesis consists of seven chapters.

In Chapter 1, a background review of optical and wireless access networks and the necessity of RoF links with coherent detection is presented, as well as the summarized major contributions of the research.

In Chapter 2, the principle of conventional IM/DD RoF links and RoF links based on coherent detection is given. In addition, a review about the phase noise cancellation for coherent RoF link is presented. Then, techniques to realize colorless ONU are introduced. Finally, three ways to transmit multiple signals over an optical wavelength are discussed for enabling MIMO.

In Chapter 3, an RoF link based on coherent detection with phase noise cancellation is presented. To increase the spectral efficiency of the RoF link, a high spectral efficiency coherent RoF link employing both amplitude and phase modulation with phase noise cancellation is studied.

In Chapter 4, two approaches to realize radio over colorless WDM-PON with wavelength reuse based on coherent detection incorporating PNC are discussed.

In Chapter 5, a novel high spectral efficiency coherent RoF link based on OSSB modulation with low-cost free-running laser sources for UDWDM-PONs is investigated.

In Chapter 6, two coherent RoF links are proposed which enable 4×4 MIMO.

Finally, a conclusion is drawn in Chapter 7 with recommendations for future work.

CHAPTER 2 THEORETICAL OVERVIEW

In this chapter, firstly the theoretical principle of a conventional IM/DD RoF link and an RoF link based on coherent detection are given. Secondly, a review about the PNC for coherent RoF link is presented. Then, techniques to realize colorless ONU are introduced. Finally, three ways to transmit multiple signals over an optical link are discussed.

2.1. Radio over fiber link with direct detection

Radio over fiber link followed by direct detection is the universal choice in applications today [36]-[65]. Fig. 2.1 shows the schematic diagram of a conventional RoF link with direct detection. An RoF link with direct detection typically includes a laser source, an Mach-Zehnder modulator, a photodetector and a DC bias controller.

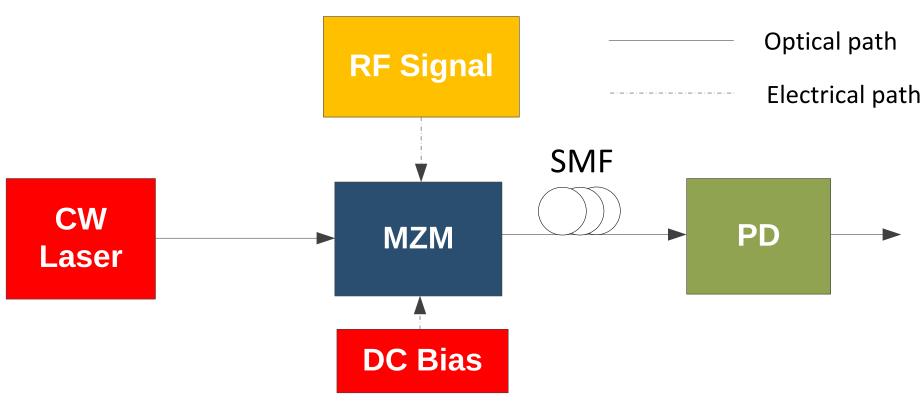

Fig. 2.1. A conventional RoF link with direct detection.

As can be seen, the light wave from a continuous-wave (CW) laser source is sent to an MZM. A radio frequency (RF) signal is applied to the MZM via the RF port. The MZM is biased at the quadrature point of the transmission curve. At the output of the MZM, an intensity-modulated RoF signal is sent to the optical receiver via a length of single-mode fiber (SMF). At the receiver, a photodetector is used to detect the RoF signal. The benefits of the RoF link with direct detection are simple structure and easy to implement. However, direct detection can only detect the intensity of the optical wave. All frequency and phase information of the optical carrier are lost, which decreases the spectral efficiency of the RoF link. In addition, the receiver sensitivity is very low [7, 8].

2.2. Radio over fiber link with coherent detection

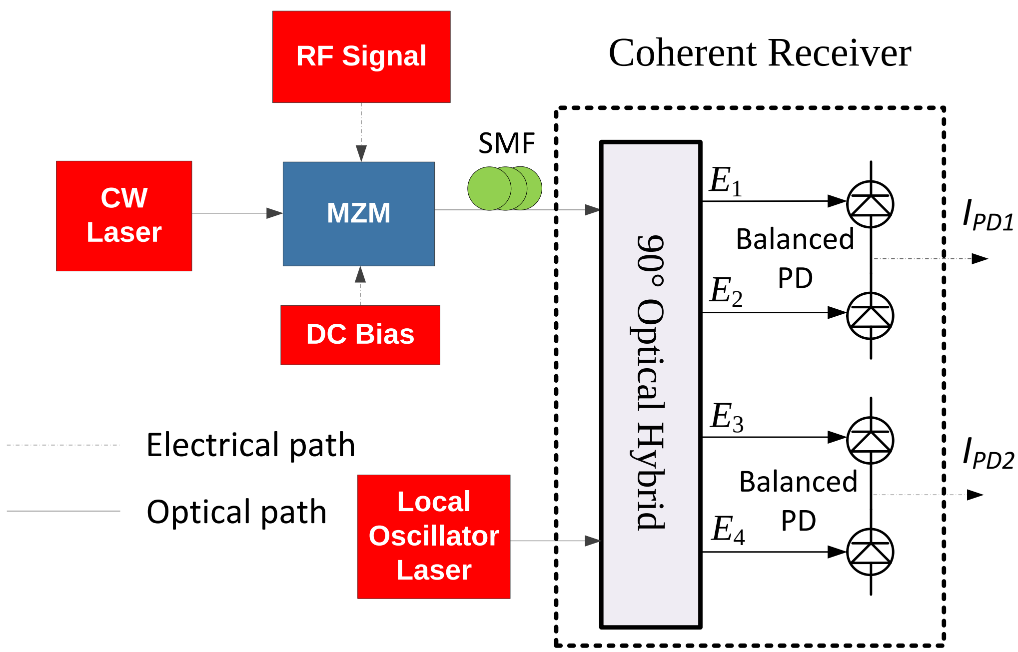

Fig. 2.2. An RoF link with coherent detection.

Another way to detect the RoF signal is coherent detection [66]-[80]. As can be seen in Fig. 2.2, at the receiver side, a coherent receiver with a LO laser source is used to detect the intensity-modulated RoF signal. In Fig. 2.2, the MZM is biased at the quadrature point, the optical field at the output of the MZM is given by

$$E_s(t) = \sqrt{2P_s L_s}\cos\left(\pi x(t)/2V_\pi + \pi/4\right)e^{j\left(\omega_c t + \phi_c(t)\right)} \tag{2-1}$$

where P_s is the optical output power of the light wave from the transmitter laser source, ω_c is the angular frequency of the light wave, $x(t)$ is the RF input signal, $\phi_c(t)$ is the phase term of the transmitter laser source, V_π is the half-wave voltage of the MZM, and L_s is the link loss between the coherent receiver and the transmitter. Similarly, the optical field at the output of the LO laser source can be written as

$$E_{LO}(t) = \sqrt{2P_{LO}}e^{j\left(\omega_{LO} t + \phi_{LO}(t)\right)} \tag{2-2}$$

where P_{LO} is the optical power of the light wave from the LO laser source, $\phi_{LO}(t)$ is the phase term, and ω_{LO} is the angular frequency.

The optical signal from the transmitter and the light wave from the LO laser source are co-polarized and are applied to a 90° optical hybrid. At the four outputs of the 90° optical hybrid, we have four optical fields given by

$$E_1 = \sqrt{L}(E_s + E_{LO}) \tag{2-3}$$

$$E_2 = \sqrt{L}(E_s - E_{LO}) \tag{2-4}$$

$$E_3 = \sqrt{L}(E_s + E_{LO}e^{j\pi/2}) \tag{2-5}$$

$$E_4 = \sqrt{L}(E_s - E_{LO}e^{j\pi/2}) \tag{2-6}$$

where L is the link loss caused by the 90° optical hybrid.

By applying E_1 and E_2, and E_3 and E_4 to two balanced photodetectors, we have two output photocurrents given by

$$I_{PD1} = 4RL\sqrt{P_s P_{LO} L_s}\left[\cos\left(\pi x(t)/2V_\pi + \pi/4\right)\cos\left(\left(\Delta\omega\right)t + \phi(t)\right)\right] \quad (2\text{-}7)$$

$$I_{PD2} = 4RL\sqrt{P_s P_{LO} L_s}\left[\cos\left(\pi x(t)/2V_\pi + \pi/4\right)\sin\left(\left(\Delta\omega\right)t + \phi(t)\right)\right] \quad (2\text{-}8)$$

where $\Delta\omega$ is the frequency difference between the transmitter laser source and the LO laser source, $\Delta\omega = \omega_c - \omega_{LO}$, $\phi(t)$ is the phase noise introduced by both the transmitter laser source and the LO laser source, $\phi(t) = \phi_c(t) - \phi_{LO}(t)$ and R is the responsivity of the photodetector. The power of the signal is proportional to the power of the LO laser source, thus coherent detection require less modulated optical power than direct detection for the same signal-to-noise ratio. However, as can be seen in (2-7) and (2-8), to recover the signal from the photodetectors after the coherent receiver, the unstable frequency $\Delta\omega$ and the phase noise $\phi(t)$ introduced from the transmitter laser source and LO laser source have to be cancelled. In next section, techniques to cancel the phase noise and unstable frequency difference are presented [81].

2.2.1. Phase noise cancellation based on dual-mode local light source

Fig. 2.3 shows the schematic diagram about phase noise cancellation for the RoF with coherent detection based on dual-mode local light source [12, 13]. A continuous wave (CW) light wave is intensity modulated by a millimeter-wave signal. After a length of SMF transmission, the RoF signal is coherently detected by a coherent receiver with a dual-mode local light. The dual-mode local light is composed of two optical carriers which has a frequency separation of f_{LO}. The frequency of the two optical carriers are f_{lo}-$f_{LO}/2$, $f_{lo}+f_{LO}/2$. f_{lo} is the center frequency of the dual-mode local light. At the output of the coherent receiver, the transmitted millimeter-wave signal is down-converted. The center frequency of the down-converted millimeter-wave signal is f_c-f_{lo}-f_{RF}+f_{LO}/2. In addition, a pilot tone with a center frequency of f_c-f_{lo}-f_{LO}/2 is obtained. Since the signal and the pilot tone carry the same phase noise, through mixing the phase noise in the signal can be cancelled.

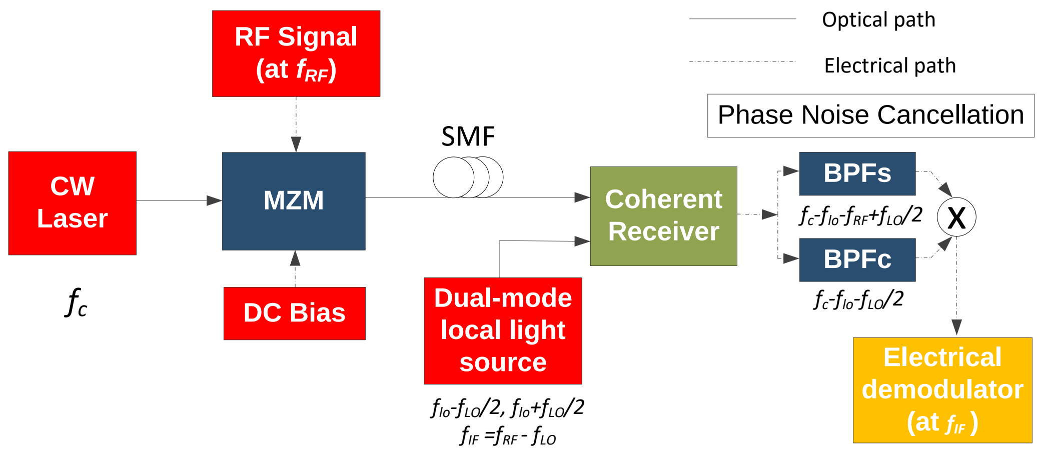

Fig. 2.3. Phase noise cancellation for the RoF link with coherent detection based on dual-mode local light source.

The disadvantages of this scheme are 1) a dual-mode local light has to be used, which increases the complexity and cost; 2) to cancel the phase noise, two electrical filters with fixed center frequency have to be used. Thus, the RoF link is not transparent to the data rate and center frequency of the transmitted signal.

2.2.2. Phase noise cancellation based on optical phase lock loop

Fig. 2.4 shows an example of the optical phase lock loop (OPLL)-type coherent receiver for binary phase-shift keying (BPSK) modulation [82]. The OPLL is used to recover the carrier phase. At the output of the coherent receiver, the in-phase component $\sin\left(\theta_s\left(t\right)+\theta_n\left(t\right)\right)$ and the quadrature component $\cos(\theta_s(t)+\theta_n(t))$ are obtained, where $\theta_s(t)$ (BPSK modulation: $\theta_s(t)$ is equal to 0 or π) and $\theta_n(t)$ are phase modulation and phase noise. To recover the carrier phase, the product between the in-phase component and the quadrature component is taken, which eliminating BPSK modulation and leading to the phase error $\theta_n(t)$ between the transmitter laser source and LO laser source. The phase error is used to control the frequency of the LO laser source so that the phase of the LO laser source tracks the carrier phase of the light from the transmitter. The disadvantage of the OPLL is that it is very complex. Besides, the pull-in range of an OPLL is usually several hundred MHz at most. Furthermore, it is difficult to maintain the system stability when the transmitter laser source and the LO laser source have large phase noise and frequency drift. Thus, narrow linewidths laser sources should be selected so that effective phase locking can be achieved. Finally, the OPLL bandwidth is usually limited below 300 MHz because of large loop delay.

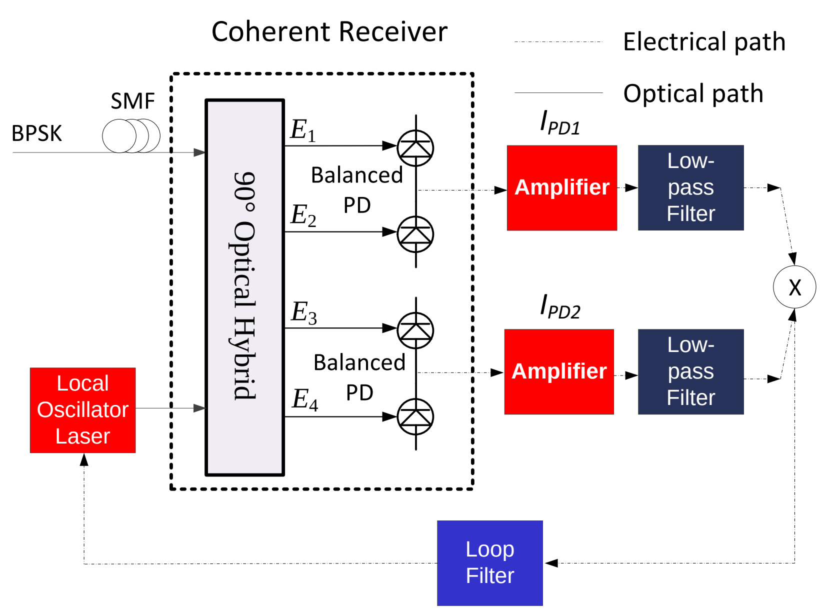

Fig. 2.4. OPLL-type coherent receiver for BPSK modulation.

2.3. Colorless optical network units in a WDM-PON

In a WDM-PON, making the ONUs colorless, which can ease the installation and cost, is very essential, since the optical access network environment is very cost-sensitive. In literature, there exists many schemes that facilitate the colorless feature in ONUs which have been mentioned in Chapter 1.1. Here, three typical schemes are described.

2.3.1. Colorless ONUs based on spectral-slicing technique

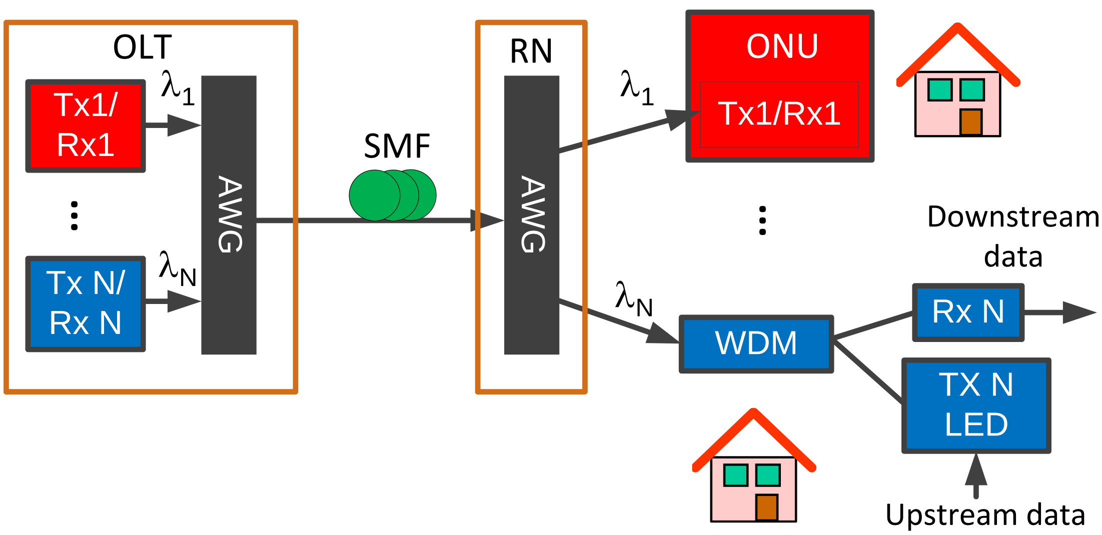

Fig. 2.5. Colorless ONUs based on spectral-slicing.

Fig. 2.5 shows the schematic diagram of the colorless ONUs based on spectral-slicing technique [14, 15]. For the uplink, at each ONU a light-emitting diode (LED) as a broadband optical source which is modulated by the upstream data is implemented. The spectral-slicing occurred at the arrayed waveguide grating (AWG). At the OLT, only a narrowband of sliced-spectrum is received. Due to the poor quality of the spectrum sliced broadband light source the modulation bandwidth is usually very narrow. In addition, such scheme suffers from high slicing losses.

2.3.2. Colorless ONUs based on injection-locked FP-LD

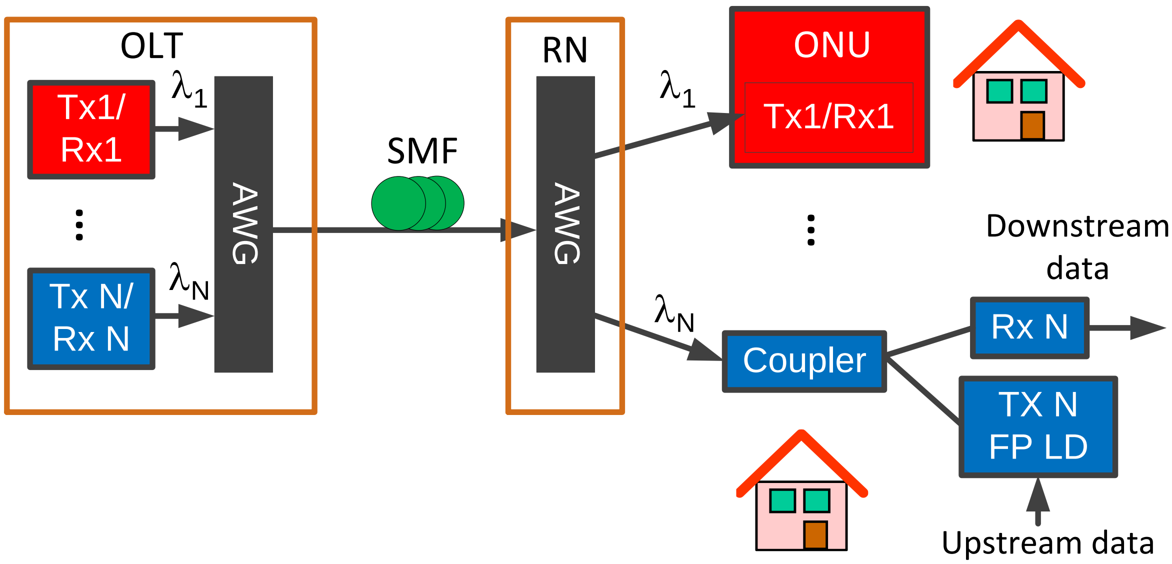

Fig. 2.6. Colorless ONUs based on injection-locked FP-LD.

To increase the modulation bandwidth, using an external optical light injected into an FP-LD can result in the excitation of only one stable mode for high-speed modulation. Fig. 2.6 shows the schematic diagram of the colorless ONU based on injection-locked FP-LD [16, 17]. The FP-LD which is injection locked by the downstream optical signal is placed at each ONU. At the output of the FP-LD, an optical carrier whose wavelength is the same as that of the injected downstream signal is generated for the uplink modulation. To achieve a stable injection locking, the injected power and the wavelength must be confined in a region. Therefore, properly controlling the injected wavelength and power is necessary. In addition, to generate a clear optical carrier, a low modulation depth of the downstream optical signal is required, which limits the transmission performance of the downlink.

2.3.3. Colorless ONUs based on RSOA

The third approach to realize colorless ONUs is to use an RSOA at the ONU. An example of deploying RSOAs as colorless transmitters in a WDM-PON is shown in Fig. 2.7 [25, 26]. At the OLT, the optical carrier from each channel is intensity modulated by the downstream signal. All the intensity-modulated signals from different channels are then wavelength multiplexed. After a length of SMF transmission, at the remote node, the downstream optical signals are wavelength de-multiplexed and sent to corresponding ONUs. At each ONU, the downstream optical signal is divided into two portions. One portion is detected by a photodiode (PD). Another portion of the downstream optical signal is applied to an RSOA for wavelength reuse.

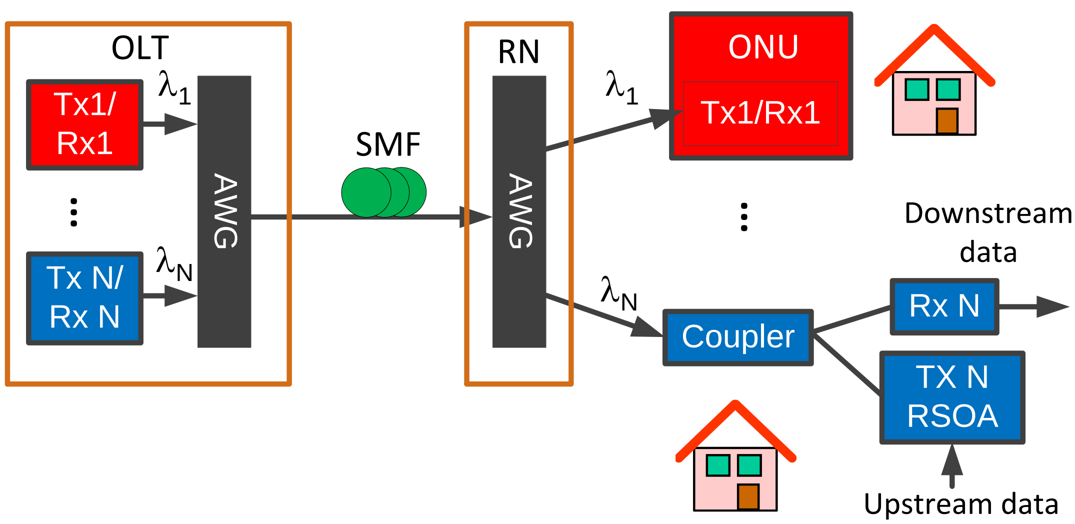

Fig. 2.7. Colorless ONUs based on RSOA.

Fig. 2.8 shows the input-output characteristic of the RSOA, which indicates that the RSOA output power saturates as the input power increases. As can be seen, if the power of downstream optical signal is in the saturation region of the RSOA, the extinction ratio (ER) of the output downstream signal is significantly reduced compared with that of the input signal, which means the intensity-information carried by the downstream optical signal can be almost erased. At the same time, if the RSOA is modulated by an upstream signal, an upstream signal is generated, which has an identical wavelength of the downstream signal. However, the ER of the input downstream signal has to be low, otherwise, the influence of the downstream modulation on the upstream signal becomes severe reducing the signal to noise ratio (SNR) of the upstream signal. Thus, the ERs of the downstream signals have to be controlled to balance the performance between the downstream and upstream signals.

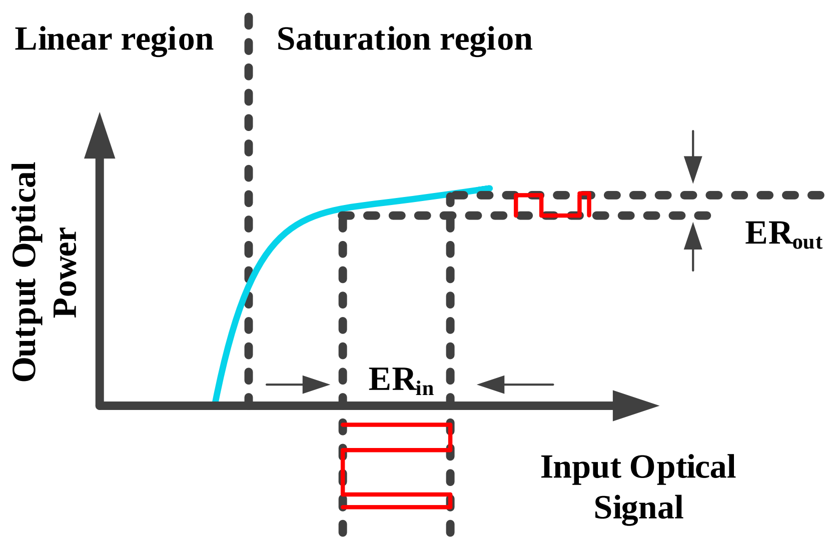

Fig. 2.8. Input-output characteristic of RSOA.

2.3.4. Comparison of different schemes for colorless ONUs

In order to have a better understanding of the characteristics of the proposed scheme, a comparison (complexity versus performance) is made between different schemes for colorless operation, which is shown in Table 2.1. We can see that different methods have their own advantages and disadvantages. To use a tunable laser at the ONU can provide the best performance, however, it is too expensive and very complex due to the need of wavelength assignment algorithm. The cheapest way is to use a spectrum slicing LED, but the performance is very poor. As far as cost, complexity and bit rate are concerned, injection locked FP-LD and RSOA with re-modulation are better than other two schemes.

TABLE 2.1. COMPARISON OF DIFFERENT SCHEMES FOR COLORLESS ONUS

Scheme	Bit rate	Advantages	Disadvantages	Complexity
Spectrum slicing LED [14]	<155 Mb/s	Cheap, on seed needed	Poor scalability and reach	Low
Injection locked FP-LD [22]	>2.5 Gb/s	Inexpensive, relatively high bit rate	Non-standard FP-LD may be needed, properly controlling the injected wavelength and power is necessary	Medium
RSOA with re-modulation [25]-[26]	>2.5 Gbit/s	Relatively high bit rate, no seed source	Downstream modulation index is limited, properly controlling the injected power is necessary	Medium
Tunable laser [83]	>10 Gbit/s	No seed needed, high bit rate	Too expensive, wavelength assignment algorithm is needed	Very complex

2.4. Centralized optical radio access network with MIMO

To support high data rate transmission for the next generation radio access networks, in particular for mobile fronthaul in which optical links that interconnect the centralized baseband unit (BBU) and the multiple remote radio heads (RRHs), we may transmit multiple signals over an optical link to enable MIMO [84-90]. Fig. 2.9 shows the schematic of a centralized optical radio access network with MIMO, which bridges wireless baseband units and remote radio units to support radio access network. For the downlink, at the CS, the electrical baseband signals are generated, aggregated and then converted to the optical domain by an optical transmitter. After a length of fiber transmission, at the BS, the electrical baseband signals are de-aggregated, up converted and sent to the corresponding antennas.

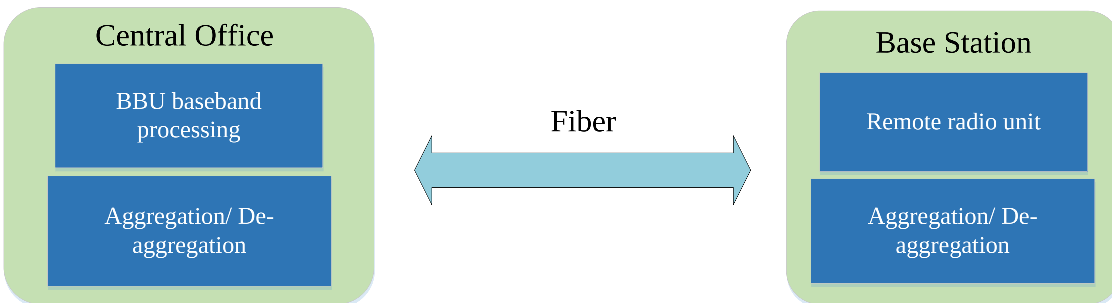

Fig. 2.9. Schematic of an optical radio access network with MIMO.

For the uplink, the received radio signals are down converted to baseband, aggregated and then transmitted back to the central office over the fiber. At the central station, the signals are de-aggregated and sent to the BBU baseband processing. In the following three sections, three ways to transmit multiple signals over an optical link are introduced.

2.4.1. Frequency-division aggregation of AxC signals in aggregated RoF

Fig. 2.10. TDM of the digitized I/Q bits of antenna-carriers (AxCs) in CPRI.

The first way is based on the common public radio interface (CPRI) [91]. The digitized in-phase and quadrature waveforms of multiple wireless signals as well as the control words (CWs) used for equipment control and management purpose are transmitted over the fiber in a binary sequence via time-division multiplexing (TDM). Fig. 2.10 defines the common public radio interface (CPRI) frame structure which contains CWs, I and Q samples (Each sample is digitized to 15 bits.) resulting of radio signals digitization. The ratio between the bits used for CWs and the I/Q bits is 1:15. Although such a technique can offer excellent robustness against noise, the spectral efficiency is very low since ON-OFF-keying (OOK) modulation format is employed. For example, for a LTE (long term evolution) channel with 20-MHz bandwidth and 2×2 MIMO, the CPRI rate is 2.4576 Gbit/s. Thus, the 3-dB bandwidth of the transmitted optical signal should be more than 1.2 GHz. In addition, the use of TDM inherently limits the performance in terms of latency of the system.

2.4.2. TDM of the digitized I/Q bits of antenna-carriers in common public radio interface

To improve the spectral efficiency, transmission of multiple wireless signals via frequency-division multiplexing (FDM) in a single wavelength is proposed [92-95]. Fig. 2.11 shows the frequency domain of the aggregated RoF signals. For the downlink, at the CS, different complex signals for different antennas are up converted to different frequency bands (aggregation) and then transmitted together over a single wavelength. At the BS, the complex signals are firstly down converted to the baseband (de-aggregation) and then up converted to their corresponding frequencies and sent to the corresponding antennas. In this scheme, the time domain of wireless signals are not digitized. Instead, the optical light is directly modulated by the aggregated wireless signals. For a LTE channel with 20 MHz bandwidth and 2×2 MIMO, the bandwidth of the transmitted optical signal is around 50 MHz. Apparently, the spectral efficiency is higher than that by using CPRI.

Fig. 2.11. Frequency-division aggregation of AxC signals in aggregated RoF.

2.4.3. Frequency-division multiplexing of AxC signals and a QAM signal that contains the CWs

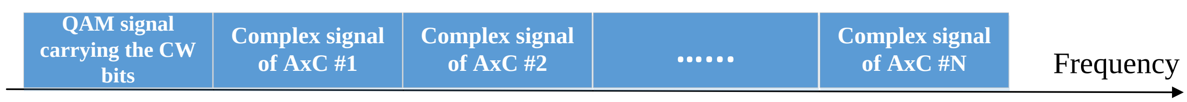

Fig. 2.12. FDM of AxC signals and a QAM signal that contains the CWs.

To make the aggregated RoF approach compatible with CPRI, it is necessary to transmit the CWs with the wireless signals [96]. Fig. 2.12 shows the FDM-based aggregated RoF/CW scheme. In this proposed scheme, a quadrature amplitude modulation (QAM) carrying the CW bits is multiplexed with the wireless signals via FDM and then transmitted over the fiber. The channel aggregation and de-aggregation can be realized by using efficient DSP based FFT and IFFT.

CHAPTER 3 RADIO OVER FIBER LINK BASED ON COHERENT DETECTION WITH PHASE NOISE CANCELLATION

RoF with coherent detection is considered one of the very promising technique to improve the performance of an RoF link, such as a superior receiver sensitivity compared with a conventional IM/DD RoF link. Due to its high receiver sensitivity, the optical power through the whole optical link can be controlled low, thus, the optical link becomes less sensitive to a variety of nonlinear effects. This feature is very attractive for WDM-PON or UDWDM-PON system. Since coherent detection can provide high receiver sensitivity, the optical power for each channel in PONs can be decreased dramatically while the performance is maintained. Thus, nonlinear effects in optical fiber which can affect the performance of the optical link may not occur. In addition, optical amplifiers for an RoF link with coherent detection may not be needed. Thus, the amplified spontaneous emission (ASE) noise from the optical amplifiers, which occupies a wide bandwidth and is hard to remove, can be avoided. On the other hand, an RoF link with coherent detection suffers from the performance degradation due to the phase noise introduced from both the transmitter and LO laser sources. Techniques to cancel the phase noise have to be employed. In this chapter, a phase noise cancellation technique is proposed. In addition, compared with an RoF link employing IM (optical double-sideband modulation) /DD which can only detect an intensity-modulated signal, an RoF link with coherent detection has much higher spectral efficiency, since coherent detection can detect both intensity- and phase-modulated signals. Therefore, a high spectral efficiency coherent RoF supporting amplitude and phase modulation with digital phase noise cancellation (PNC) is proposed.

3.1. Phase noise cancellation for an RoF link with coherent detection

A few solutions have been proposed to cancel the phase noise and the unstable frequency difference introduced from the transmitter laser source and LO laser source for RoF with coherent detection in recent years, such as the use of an optical phase-locked loop to lock the phase of the LO laser source [10, 11], a dual-mode local light source [12, 13], or a PNC circuit [97, 98]. Although the use of an optical phase-locked loop provides optimal performance of an IM/CD RoF link, it makes the implementation very complicated. The use of a PNC circuit can cancel the phase noise, but the LO laser source has to operate with an offset wavelength from the transmitter laser source by an intermediate frequency (IF) that is two to three times higher than the bandwidth of the RF input signal. Therefore, an automatic frequency control (AFC) loop or a tunable laser source (TLS) has to be used to guarantee that the frequency difference between the transmitter laser source and the LO laser source is two or three times higher than the bandwidth of the RF input signal.

In this section, a digital signal processing (DSP) assisted RoF link based on intensity modulation and coherent detection (IM/CD) for the transmission of a radio-frequency (RF) signal is proposed. The phase noise which is introduced by both the transmitter and LO laser sources can be, in principle, completely eliminated by summing the squared magnitudes of the in-phase and quadrature (I&Q) components from the coherent receiver. The proposed DSP-assisted RoF link can support both optical heterodyne detection and optical homodyne detection and no AFC loop is needed. The proposed DSP-assisted IM/CD RoF link is studied theoretically and verified by an experiment. The transmission of a 1.25-Gbps RF signal with a center frequency of 1.6 GHz over 25-km SMF is achieved. The phase noise and the unstable frequency difference from both the transmitter laser source and the LO laser source are cancelled successfully by the DSP-based PNC module. For a RF signal with a bit rate of 834 Mbps, the receiver sensitivity can reach -24.5 dBm which is better than that based on an IM/DD RoF link.

3.1.1. Principle

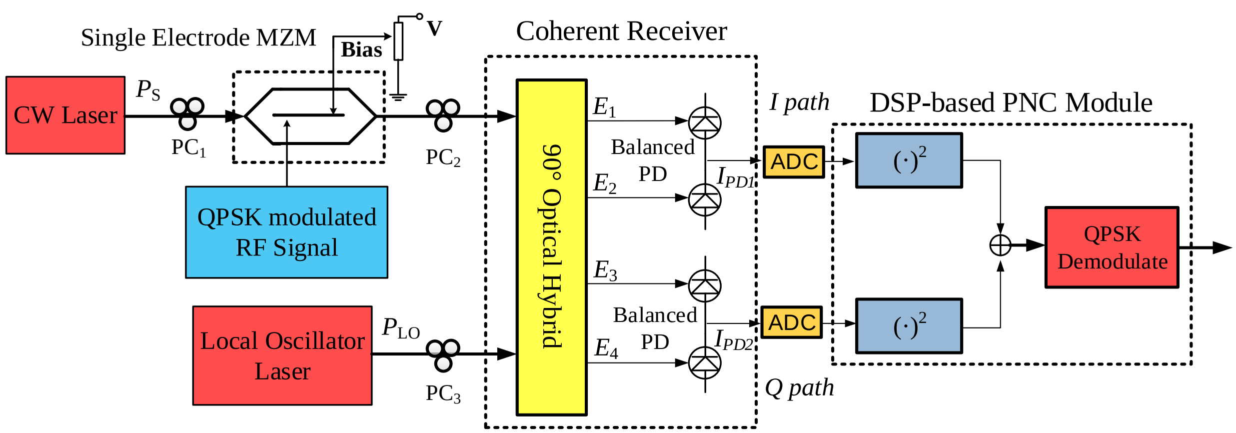

Fig. 3.1. Schematic diagram of the proposed RoF link with a DSP based PNC module. ADC: analog-to-digital converter, PC: polarization controller, CW laser: continuous-wave laser, Balanced PD: balanced photodetector, MZM: Mach-Zehnder modulator, QPSK: quadrature phase shift keying.

Fig. 3.1 shows the schematic of the proposed DSP-assisted IM/CD RoF link. An RF signal is directly modulated on an optical carrier at a chirp-free single-electrode Mach-Zehnder modulator (MZM). A phase-diversity coherent optical receiver is used to detect the intensity-modulated optical signal from the transmitter. At the outputs of the phase-diversity coherent optical receiver, two channels of signals corresponding to the I&Q components are obtained, which are then sent to the DSP-based PNC module. By summing the squared magnitudes of the

I&Q components, the phase noise is completely cancelled [99].

When the MZM is biased at the quadrature point, the optical field at the output of the MZM is given by

$$E_s(t) = \sqrt{2P_s L_s}\cos\left(\pi x(t)/2V_\pi + \pi/4\right)e^{j\left(\omega_c t + \varphi_c(t)\right)} \tag{3-1}$$

where P_s is the optical output power of the light wave from the transmitter laser source, ω_c is the angular frequency of the light wave, $x(t)$ is the RF input signal, $\varphi_c\left(t\right)$ is the phase term of the transmitter laser source, V_π is the half-wave voltage of the MZM, and L_s is the link loss between the coherent receiver and the transmitter.

Similarly, the optical field at the output of the LO laser source can be written as

$$E_{LO}(t) = \sqrt{2P_{LO}}e^{j\left(\omega_{LO} t + \varphi_{LO}(t)\right)} \tag{3-2}$$

where P_{LO} is the optical power of the light wave from the LO laser source, $\varphi_{LO}(t)$ is the phase term, and ω_{LO} is the angular frequency.

The optical signal from the transmitter and the light wave from the LO laser source are co-polarized and are applied to a 90^{o} optical hybrid. At the four outputs of the 90^{o} optical hybrid, we have four optical fields given by

$$E_1 = \sqrt{L}(E_s + E_{LO}) \tag{3-3}$$

$$E_2 = \sqrt{L}(E_s - E_{LO}) \tag{3-4}$$

$$E_3 = \sqrt{L}(E_s + E_{LO}e^{j\pi/2}) \tag{3-5}$$

$$E_4 = \sqrt{L}(E_s - E_{LO}e^{j\pi/2}) \tag{3-6}$$

where L is the link loss caused by the 90^{o} optical hybrid.

By applying E_1 and E_2, and E_3 and E_4 to two balanced photodetectors, we have two output photocurrents given by

$$I_{PD1} = 4RL\sqrt{P_s P_{LO} L_s}\left[\cos\left(\pi x(t)/2V_\pi + \pi/4\right)\cos\left(\left(\Delta\omega\right)t + \varphi(t)\right)\right] \tag{3-7}$$

$$I_{PD2} = 4RL\sqrt{P_s P_{LO} L_s}\left[\cos\left(\pi x(t)/2V_\pi + \pi/4\right)\sin\left(\left(\Delta\omega\right)t + \varphi(t)\right)\right] \tag{3-8}$$

where $\Delta\omega$ is the frequency difference between the transmitter laser source and the LO laser source, $\Delta\omega = \omega_c - \omega_{LO}$, $\varphi(t)$ is the phase noise introduced by both the transmitter laser source and the LO laser source, $\varphi(t) = \varphi_c(t) - \varphi_{LO}(t)$. Apparently, the two signals are affected by the phase noise and the unstable frequency introduced from the two laser sources. Then, the two signals, I_{PD1} and I_{PD2}, are separately sampled and digitized by two analog-to-digital converters (ADCs). Using the DSP, we can easily obtain

$$\begin{aligned} I_o^2 = I_{PD1}^2 + I_{PD2}^2 &= 8R^2L^2P_sP_{LO}L_s\left(1 - \sin\left(\pi x(t)/V_\pi\right)\right) \\ &\approx 8R^2L^2P_sP_{LO}L_s\left(1 - \left(\pi x(t)/V_\pi\right)\right) \end{aligned} \tag{3-9}$$

As can be seen, the RF signal is recovered, and it is independent of the phase noise.

3.1.2. Performance Evaluation

To verify that the proposed DSP-assisted IM/CD RoF link is effective in phase noise cancellation, an experiment is conducted based on the setup shown in Fig. 3.1 and a picture of the experimental setup is shown in Fig. 3.2. An optical wave at 1544.798 nm from a tunable laser source (TLS, Anritsu MG9638A) is sent to the single-electrode MZM (JDSU) via a polarization controller (PC_1). The MZM has a bandwidth of 10 GHz and a half-wave voltage of about 5 V. The linewidth and output power of the light wave from the TLS is 700 KHz and 7.8 dBm, respectively. A QPSK-modulated RF signal generated by an arbitrary waveform generator (Tektronix AWG7102) is applied to the MZM via the RF port. The MZM is biased at the quadrature point. Then, the optical signal from the output of the MZM, which is intensity modulated by the RF signal, is sent to the coherent receiver (Discovery Semiconductors DP-QPSK 40/100 Gbps Coherent Receiver Lab Buddy) via PC_2.

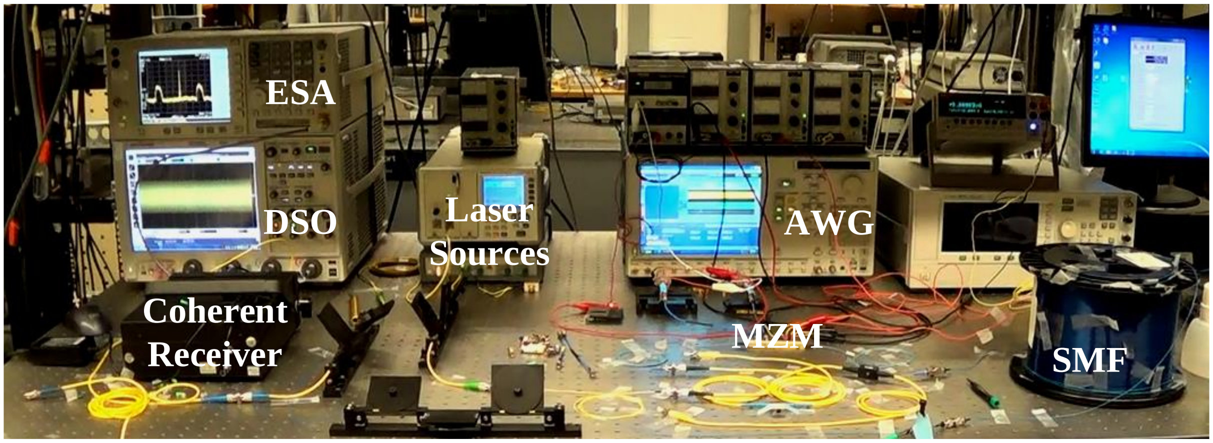

Fig. 3.2. Photograph showing the experimental setup of the proposed phase noise cancellation for an RoF link with coherent detection. AWG: arbitrary wave generator, ESA: electrical spectrum analyzer, DSO: digital storage oscilloscope, MZM: Mach-Zehnder modulator, SMF: single-mode fiber.

A second TLS (Yokogawa AQ2201) with a linewidth of about 1 MHz at a wavelength of 1544.788 nm and an optical power of 9 dBm is used as the LO laser source. The wavelength difference between the transmitter laser source and the LO laser source is 0.01 nm, corresponding to beat frequency of about 1.25 GHz. The light wave from the LO laser source is sent to the coherent receiver through PC_3 via the LO port (PC_3 can be replaced by a dynamic polarization controller in a practical system [100], since the dynamic polarization controller which is a mature commercial product can be used for coherent communication to make the optical signal from the transmitter and the light wave from the LO laser source be co-polarized [101]. Using a polarization diversity coherent receiver or the maximal-ratio combining method can also solve the polarization sensitivity of a coherent receiver [81].). A

Digital Storage Oscilloscope (Agilent DSO-X 93204A) is employed to perform the ADC with a sampling rate of 10 GSa/s. The sampled signals (in-phase and quadrature components, I_{PD1} and I_{PD2}) are processed off-line in a computer.

Firstly, we apply a QPSK-modulated RF signal to the MZM. The QPSK-modulated RF signal has a center frequency of 1.6 GHz and a symbol rate of 417 MSymbol/s. Fig. 3.3 shows the spectrum of the QPSK-modulated RF signal from the coherent receiver (in-phase component). It is seen that the RF signal is up converted to 2.85 GHz because of the wavelength difference of about 0.01 nm corresponding to a frequency of 1.25 GHz. The RF carrier in Fig. 3.3 is noisy, which is caused by the phase noise from the transmitter laser source and LO laser source. After processing at the DSP-based PNC module, the RF QPSK-modulated signal is down converted to its original frequency of 1.6 GHz. Fig. 3.4 shows the spectrum of the RF signal at the output of the DSP-based PNC module.

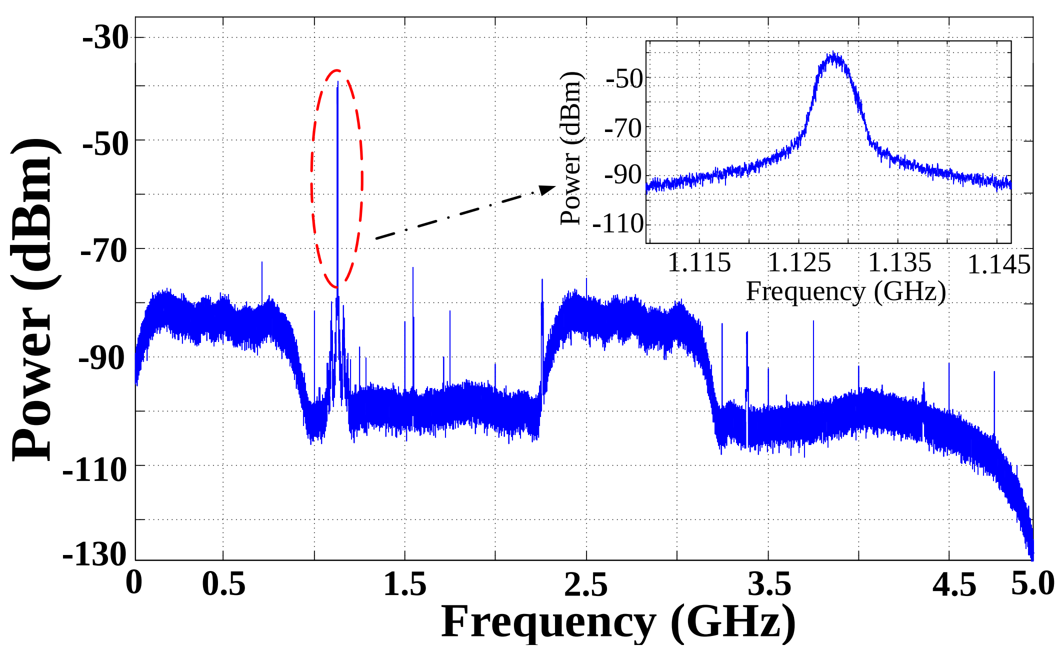

Fig. 3.3. Spectrum of the signal at the output of the coherent receiver (in-phase component).

Then, to further study the performance of the proposed DSP-assisted IM/CD RoF link, we also measure the error vector magnitude (EVM) versus the received optical power, which is compared with that of a conventional IM/DD RoF link. The conventional IM/DD RoF link consists of a laser source, a chirp-free MZM which is biased at the quadrature point, a 25-km SMF and a PD.

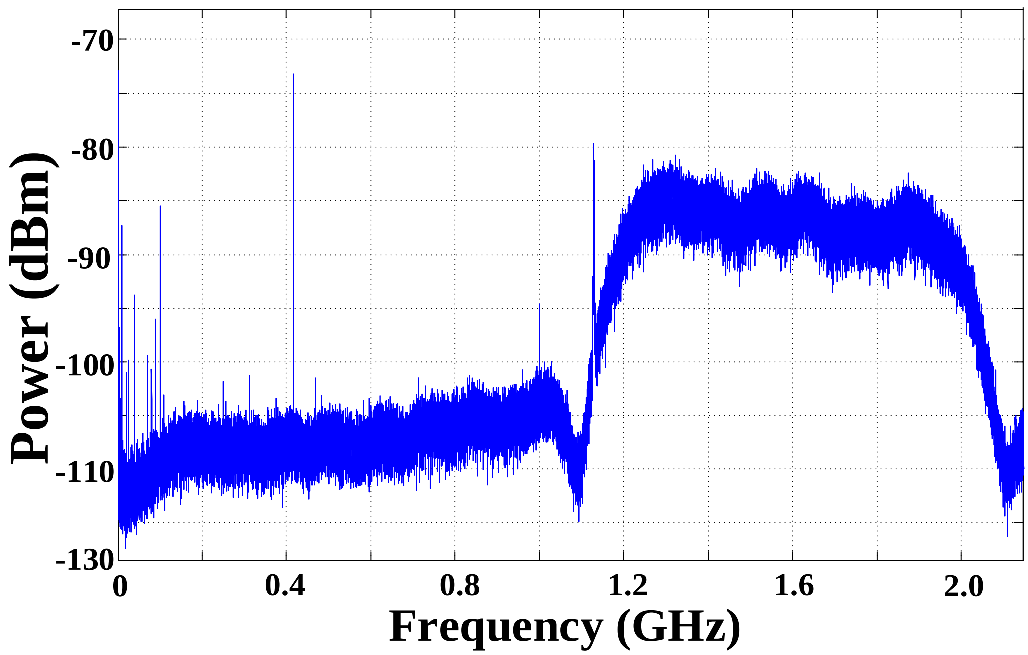

Fig. 3.4. Spectrum of the recovered RF signal at the output of the DSP-based PNC module.

Fig. 3.5 shows the measured EVM as a function of the received optical power for the transmission of a QPSK-modulated RF signal at 417 MSymbol/s, 625 MSymbol/s over a 25-km SMF with coherent detection using the DSP based PNC module and direct detection. The center frequency of the QPSK-modulated RF signal is 1.6 GHz. Then the BER is estimated based on the relationship between the EVM and the BER [102] (In [103], it is proved that the BER can be estimated by measured EVM even if BER < 10^{-2}.). Fig. 3.6 shows the corresponding estimated BER as a function of the received optical power. It can be seen that the receiver sensitivity for the transmission of the 417 MSymbol/s QPSK-modulated RF signal with the coherent detection using the DSP-based PNC module can reach -24.5 dBm, which is lower than that of the direct detection. Here, the receiver sensitivity is defined as the minimum average received optical power required to achieve a fixed BER of 10^{-9}. The corresponding constellation for the 417 MSymbol/s QPSK modulated RF signal with the coherent detection, when the received optical power is -24.5 dBm, is shown in Fig. 3.6, which is very clear. The receiver sensitivity for the transmission of the 625 MSymbol/s QPSK modulated RF signal with the coherent detection using the DSP-based PNC module is also measured, which is about -20 dBm.

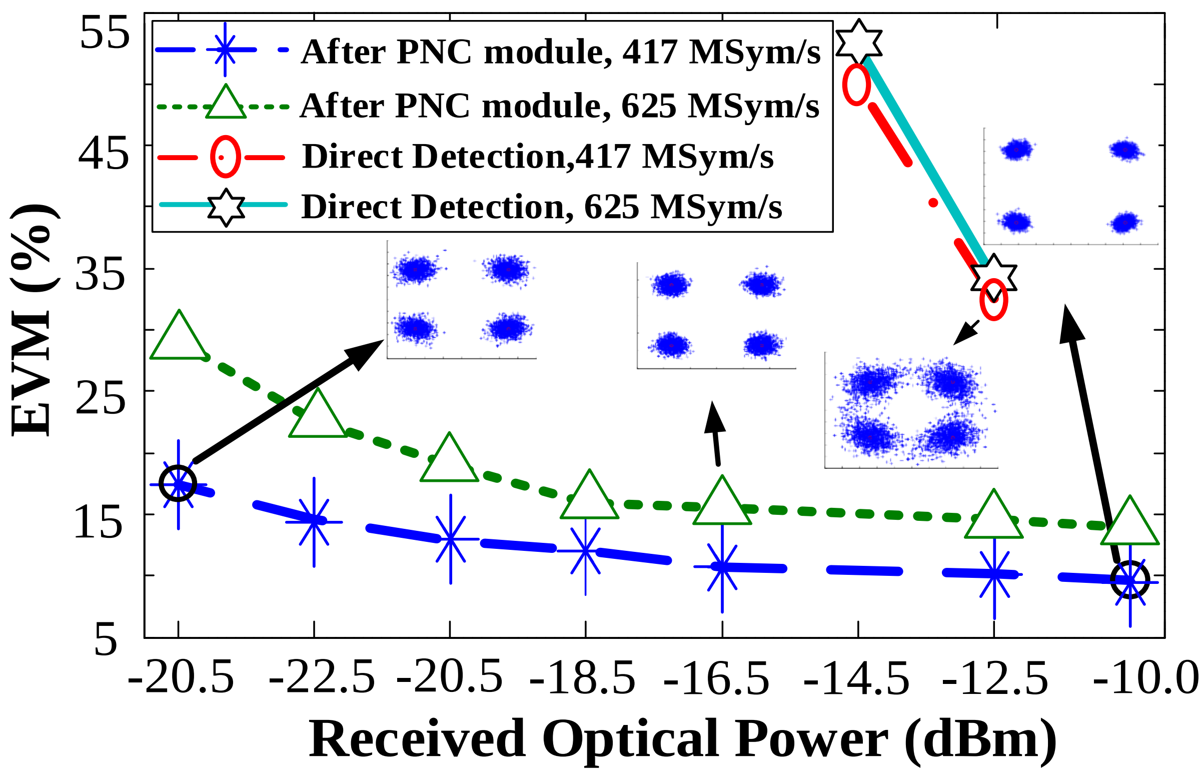

Fig. 3.5. Comparison of the EVMs for the transmission of a QPSK-modulated RF signal with a center frequency of 1.6 GHz over 25 km SMF based on coherent detection using the DSP-based PNC and based on direct detection.

To verify the effectiveness of the proposed phase noise cancellation technique which has been discussed in Chapter 3.1.1, we also measure the constellations of the detected signals for an intensity-modulation coherent detection (IM/CD) link without a digital PNC module. The detected signal at the output of the coherent receiver is affected by the unstable frequency difference and the phase noise introduced by the two laser sources. The experiment setups are shown in Fig. 3.7 (The linewidth of the transmitter laser source is 100 kHz and the linewidth of the LO laser source is 700 kHz. The frequency stability for the transmitter laser source is ± 0.3 GHz/24 hours, and for the LO laser source it is ± 100 MHz/hour.). Here, the microwave vector signal is a standard 16 quadrature amplitude modulation (16-QAM) signal with a center frequency of 2.5 GHz and a symbol rate of 625 MSymbol/s.

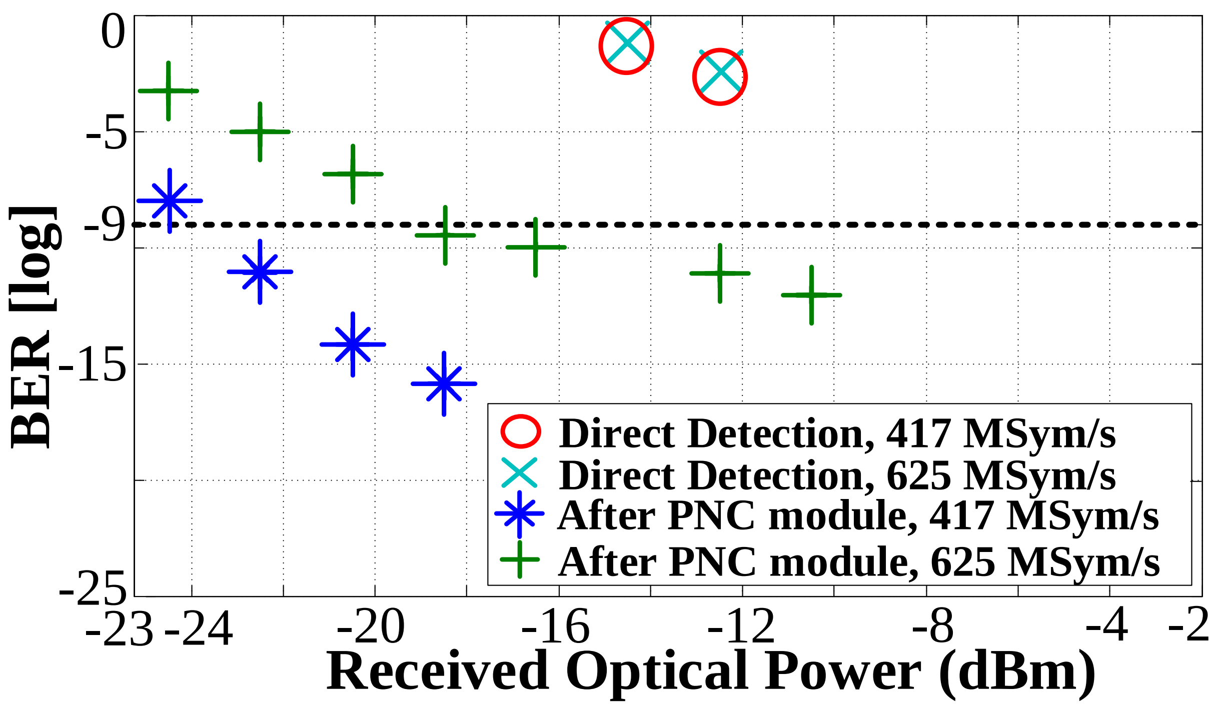

Fig. 3.6. The estimated BER for the transmission of a QPSK modulated RF signal with a center frequency of 1.6 GHz over 25 km SMF based on coherent detection using the DSP-based PNC and based on direct detection.

Fig. 3.8 shows the spectrum of the signal at the output of the coherent receiver. After coherent detection and sampling, two digital bandpass filters are used to select the upper sideband signal and lower sideband signal. Then, the two signals are demodulated in the DSP unit. The constellations of the 16-QAM microwave signals (upper and lower sidebands) are shown in Fig.

3.9. As can be seen, the recovered 16-QAM microwave vector signals are strongly affected by the phase noise and the unstable frequency difference introduced by the two laser sources.

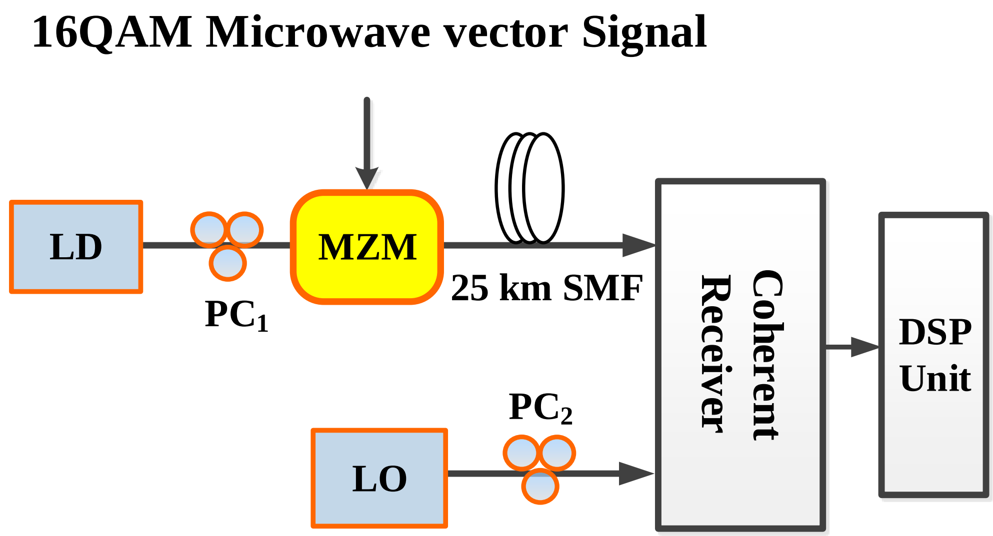

Fig. 3.7. Schematic diagram of an IM/CD RoF link without a PNC module.

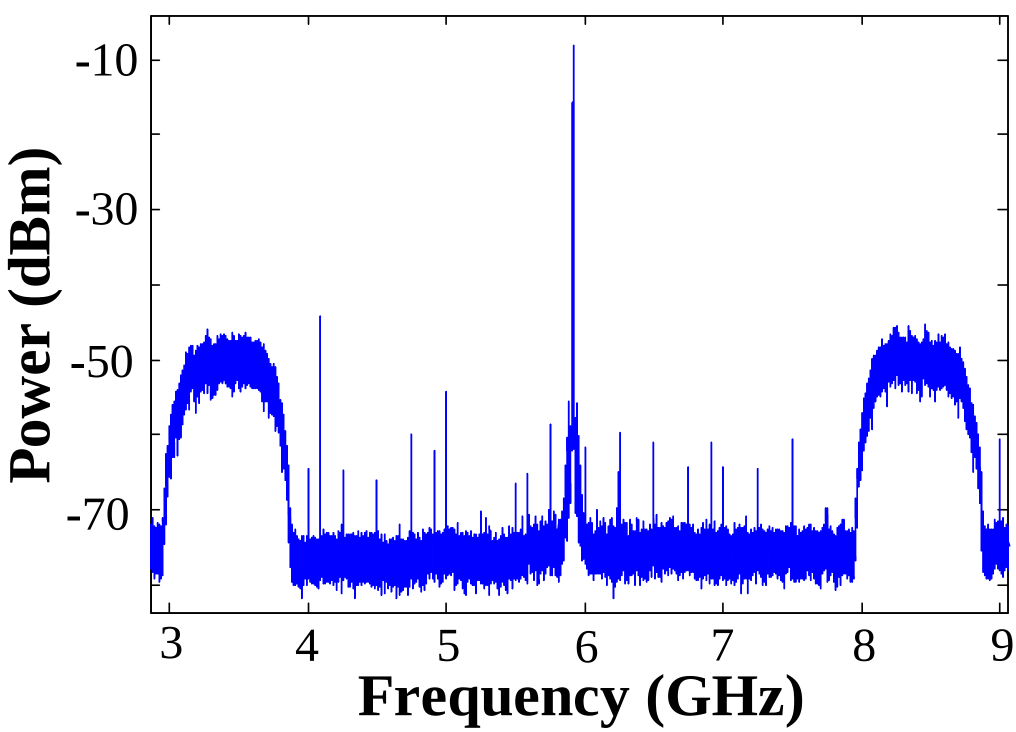

Fig. 3.8. Spectrum of the signal at the output of the coherent receiver for the IM/CD RoF link.

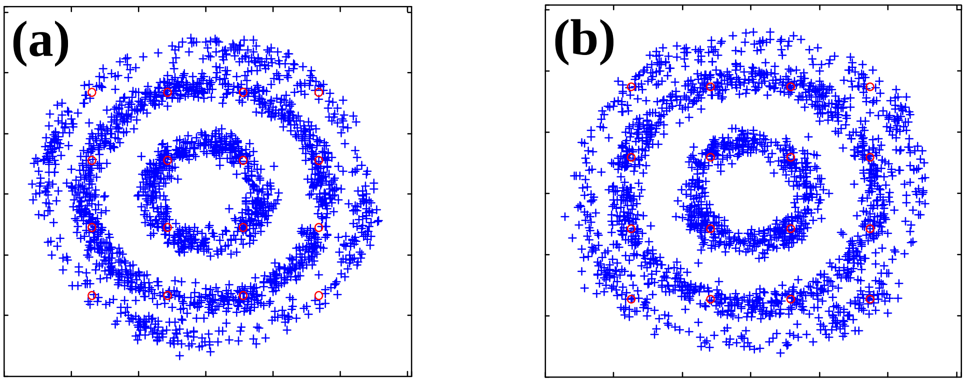

Fig. 3.9. The measured constellations of the signals at the output of the coherent receiver for an IM/CD RoF link. (a) The upper sideband signal, and (b) the lower sideband signal.

In addition, to evaluate the effectiveness of the PNC module under different bandwidth of the phase noise, we also measure the EVMs of the signal after the PNC module for different bandwidth of the phase noise. The experimental setup is shown in Fig. 3.10.

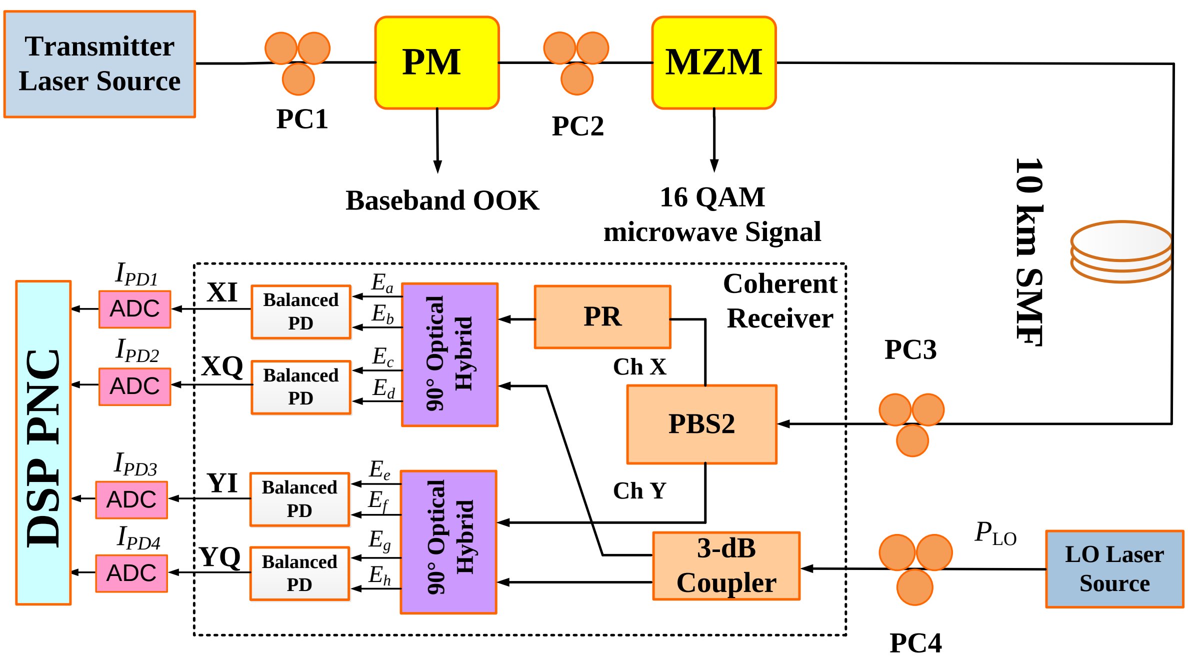

Fig. 3.10. Experimental setup for evaluating the effectiveness of the PNC module under different bandwidth of phase noise.

In Fig. 3.10, in order to simulate different bandwidth of the phase noise, the optical carrier is first phase-modulated by a baseband OOK (The peak to peak voltage is around 3 V, the half wave voltage for the phase modulator is around 5V.), then it is intensity-modulated by a 16-QAM microwave vector signal (The electrical power of the 16-QAM microwave signal is 7 dBm. The half-wave voltage of the phase modulator is around 5V). The linewidth of two laser sources (the transmitter laser source and the LO laser source) is 100 KHz. The wavelength difference between the two laser sources is 0.051 nm. The center frequency of the transmitted 16-QAM microwave vector signal is 2.5 GHz and the symbol rate is 625 MSymbol/s (2.5 Gbps). Fig. 3.11 shows the spectra at the output of coherent receiver (I_{PD1}) for different bandwidth of the phase noise. Fig. 3.12 shows the constellations for the recovered 16-QAM microwave vector signals with different bandwidth of phase noise after PNC module when the received optical power is -12 dBm and the optical power of the LO is 9 dBm. As can be seen in Fig. 3.12 (c), even the baseband OOK signal is 2000 Mbits/s, the constellation at the output of the PNC module for the 16-QAM microwave vector signal is still very clear which proves the effectiveness of the proposed PNC module.

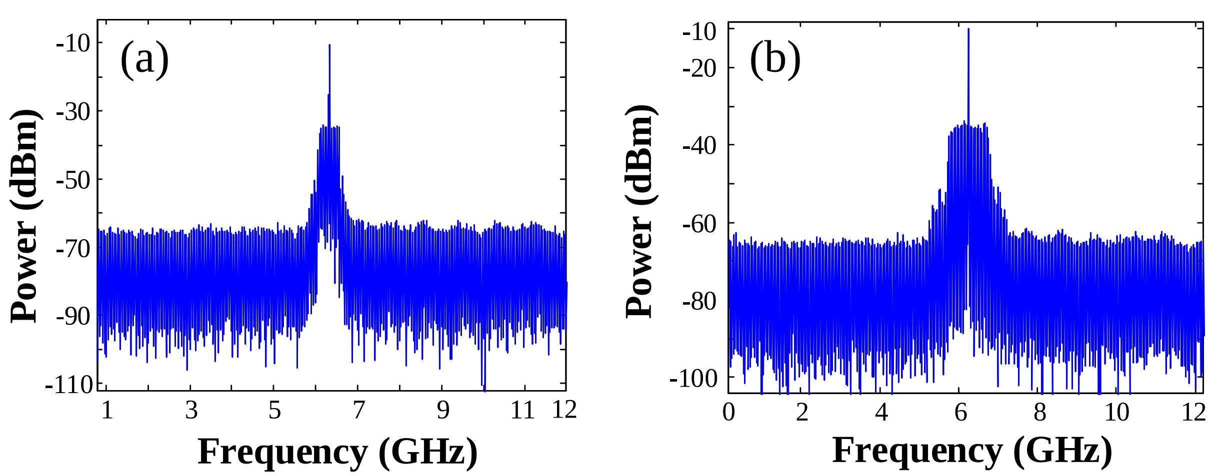

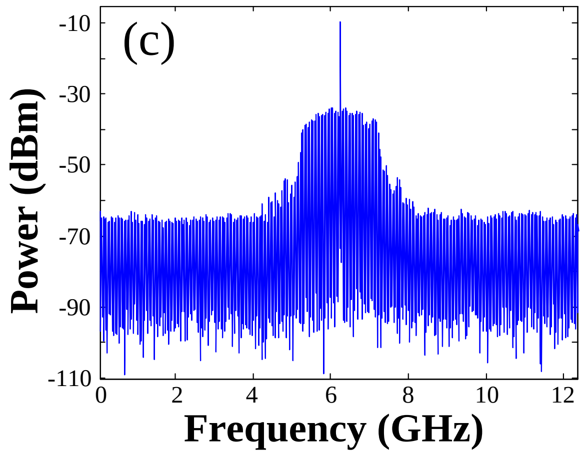

Fig. 3.11. The spectra at the output of the coherent receiver when the optical carrier is only phase-modulated by a baseband OOK signal. (a) Baseband OOK: 500 Mbits/s, (b) Baseband OOK: 1000 Mbits/s, (c) Baseband OOK: 2000 Mbits/s.

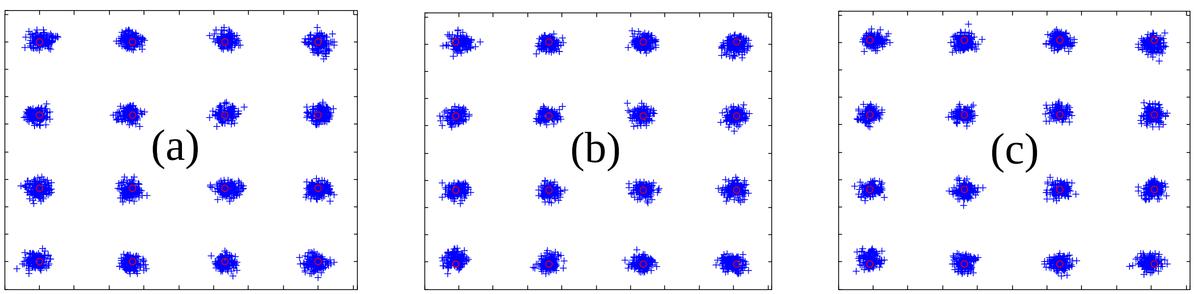

Fig. 3.12. Constellations for the recovered 16-QAM microwave vector signals with different bandwidth of phase noise after PNC module. (a) Baseband OOK: 500 Mbits/s, (b) Baseband OOK: 1000 Mbits/s, (c) Baseband OOK: 2000 Mbits/s.

Finally, in the experiment, the delay of the I path and the Q path should be equal. However, in a practical system, the delay of the two paths cannot be perfectly matched. Thus, I also study the performance impact due to the mismatch of the delay between the two paths. A simulation is performed. In the simulation, the center frequency of the transmitted microwave vector is 2.5 GHz and the symbol rate is 625 MSymbol/s. The linewidth of each of the two laser sources is 1

MHz. Two different situations are considered. 1) The delay of the two paths (I path and Q path) is equal; 2) the relative delay between the two paths is 2.5×10^{-11} s (The corresponding length difference between the two paths is around 5 mm.). For the first situation, the EVM of the recovered microwave vector signal is 9.99%. For the second situation, the EVM is 10.03%. The two EVMs are very close which proves the PNC module can tolerate such delay mismatch and can cancel the phase noise completely (For a commercial optical coherent receiver, the delay mismatch between the two paths can be controlled less than 2.5×10^{-11} s.).

3.2. A high spectral efficiency coherent RoF link employing both amplitude and phase modulation

In a conventional RoF link, IM/DD is usually employed which has an advantage of implementation simplicity. However, compared with a coherent RoF which can detect both intensity- and phase-modulated signals, an RoF employing IM/DD has a much lower spectral efficiency, since direct detection can only detect an intensity-modulated signal. For broadband wireless access networks, high spectral efficiency is always needed. In addition, a coherent RoF has a high receiver sensitivity, which provides an added advantage to a coherent RoF [104]. Numerous solutions have been proposed to implement coherent RoF link recently [99], [105-111]. In [109], [110], a phase-modulation and coherent-detection (PM/CD) RoF link was proposed. In [99], [111], two intensity-modulation and coherent-detection (IM/CD) RoF links were proposed. The limitation of the schemes is that only the phase [109], [110] or amplitude [99], [111] information on the optical carrier can be detected, thus the spectral efficiency is still limited. In this section, a high spectral efficiency coherent RoF supporting amplitude and phase modulation with digital PNC is proposed and experimentally demonstrated. At the transmitter, a light wave from a laser source is split into two channels. In the upper channel, the light wave is first intensity modulated by a 16-QAM microwave vector signal and then phase modulated by a QPSK microwave vector signal. The light wave in the lower channel is not modulated. Then, the two light waves from the two channels are polarization multiplexed at the polarization beam splitter (PBS) and sent to a receiver over a SMF. At the receiver, the two orthogonally polarized light waves are de-multiplexed by a second PBS and then detected by a coherent optical receiver, to generate four currents which contain the information of the 16-QAM and QPSK signals. An algorithm is developed to recover the 16-QAM and the QPSK microwave vector signals while cancelling the phase noise introduced by both the transmitter laser source and LO laser source. The proposed technique is validated by an experiment. The transmission of a 2.5-Gbps 16-QAM and a 1.25-Gbps QPSK microwave vector signals over a 25-km SMF is demonstrated. The transmission performance is evaluated by measuring the EVMs. The EVM of the recovered 16-QAM microwave vector signal can reach 8.05% and that of the recovered QPSK microwave vector signal can reach 8.23%. The BERs calculated from the measured EVMs are also evaluated. Compared with coherent-detection RoF links based only on phase [109], [110], or amplitude modulation [99], [111], the spectral efficiency of the proposed scheme is significantly increased while maintaining the same transmission performance.

3.2.1. Principle

Fig. 3.13 shows the schematic diagram of the proposed high spectral efficiency coherent RoF. At the transmitter, a light wave from a CW laser source is split by an optical coupler (OC) (95% and 5% optical powers for Channel 1 and Channel 2, respectively) into two channels. In Channel 1, the light wave is amplitude- and phase-modulated by a 16-QAM and a QPSK microwave vector signal, respectively, at a chirp-free single-electrode Mach-Zehnder modulator (MZM) and a phase modulator (PM) while the light wave in Channel 2 is not modulated. The two light waves from the two channels are then polarization multiplexed at a PBS (PBS1) and sent to a receiver via a 25-km SMF. At the receiver, a second PBS (PBS2) which is incorporated in the polarization- and phase-diversity coherent optical receiver (Discovery Semiconductors DP-QPSK 40/100 Gbps Coherent Receiver) is used to de-multiplex the two orthogonally polarized light waves (Channel X and Channel Y), which are then sent to two 90^o optical hybrids inside the coherent optical receiver. An LO signal from a second laser source is split into two channels and also sent to the two hybrids. After balanced detection in the coherent optical receiver, four channels (XI, XQ, YI and YQ) of signals corresponding to the in-phase and quadrature (I&Q) components of the two orthogonally polarized signals from the PBS2 are obtained, which are then sent to a DSP-based PNC module. An algorithm is developed to recover the 16-QAM microwave vector signal and the QPSK microwave vector signal while cancelling the phase noise introduced by both the transmitter and LO laser sources.

At the transmitter, for Channel 1, the MZM is biased at the quadrature point and 16-QAM microwave vector signal is applied to the MZM via the RF port. The optical field at the output of the MZM is given by

$$E_0\left(t\right)=\sqrt{2P_{s1}L_{s1}}\cos\left[\frac{\pi S_{RF-16QAM}(t)}{2V_{\pi IM}}+\frac{\pi}{4}\right]\times\exp\left\{j\left[\omega_c t+\varphi_{c1}\left(t\right)\right]\right\} \tag{3-10}$$

where P_{s1} is the optical power at the input of Channel 1, ω_c is the angular frequency of the light wave, $S_{RF-16QAM}(t)$ is the microwave vector signal applied to the MZM, the modulation format is 16-QAM, $\varphi_{c1}(t)$ is the phase term of the transmitter laser source for Channel 1, $V_{\pi IM}$ is the half-wave voltage of the MZM, and L_{s1} is the link loss between the OC and PBS1 for Channel 1.

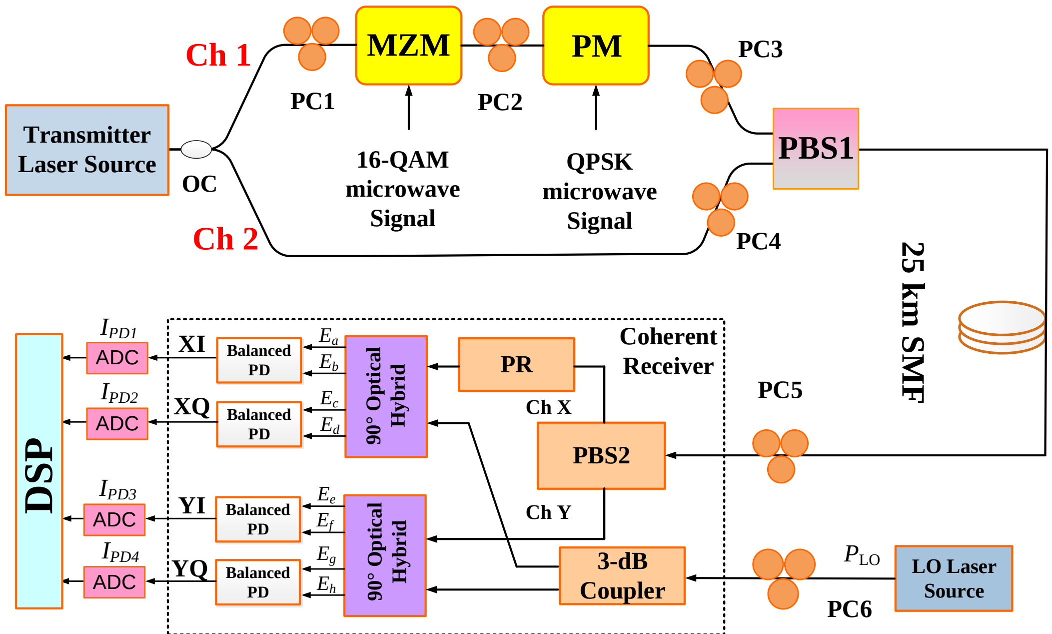

Fig. 3.13. Schematic of the proposed coherent RoF link with a DSP-based PNC module. ADC: analog-to-digital converter, OC: optical coupler, PC: polarization controller, CW laser: continuous-wave laser, Balanced PD: balanced photodetector, MZM: Mach-Zehnder modulator, QPSK: quadrature phase shift keying, PM: phase modulator, PBS: polarization beam splitter, PR: polarization rotator, 16-QAM: 16 quadrature amplitude modulation, SMF: single mode fiber.

Then, the amplitude-modulated optical signal is phase-modulated by a QPSK microwave vector signal. The optical field at the output of the PM is given by

$$E_1(t) = \sqrt{2P_{s1}L_{s1}} \cos\left[\frac{\pi S_{RF-16QAM}(t)}{2V_{\pi IM}} + \frac{\pi}{4}\right] \times \exp\left\{ j\left[\omega_c t + \varphi_{c1}(t) + \frac{\pi S_{RF-QPSK}(t)}{V_{\pi PM}}\right]\right\} \tag{3-11}$$

where $S_{RF-QPSK}(t)$ is the QPSK microwave vector signal applied to the PM, the modulation format is QPSK and $V_{\pi PM}$ is the half-wave voltage of the PM.

For Channel 2, the light wave is not modulated. The optical field at the output of Channel 2 is given by

$$E_2(t) = \sqrt{2P_{s2}L_{s2}} \exp\{j[\omega_c t + \varphi_{c2}(t)]\} \tag{3-12}$$

where P_{s2} is the optical power at the input of Channel 2, $\varphi_{c2}(t)$ is the phase term of the transmitter laser source for Channel 2, and L_{s2} is the link loss between the OC and PBS1 for Channel 2. Note, $\varphi_{c1}(t)$ and $\varphi_{c2}(t)$ are different, since the optical signals from the transmitter laser source are split by an OC and transmitted through two fibers.

Then, the two light waves from the two channels are polarization multiplexed at PBS1 and transmitted over the SMF. At the receiver, the two orthogonally polarized light waves are de-multiplexed by PBS2 into two channels (Channel X and Channel Y).

The optical fields at the outputs of PBS2 for Channel X and Channel Y are given by

$$E_x(t) = E_1(t) \tag{3-13}$$

$$E_y(t) = E_2(t) \tag{3-14}$$

On the other hand, the optical field at the output of the LO laser source can be written as

$$E_{LO}(t) = \sqrt{2P_{LO}} \exp\{j[\omega_{LO} t + \varphi_{LO}(t)]\} \tag{3-15}$$

Through tuning PC6, with the help of the polarization rotator in Fig. 3.13, the light wave from the LO laser source is co-polarized with the other optical signals at the inputs of the two 90^{o} optical hybrids. At the outputs of the two 90^{o} optical hybrids, eight optical fields are obtained, given by

$$\begin{pmatrix} E_a(t) & E_b(t) & E_c(t) & E_d(t) \\ E_e(t) & E_f(t) & E_g(t) & E_h(t) \end{pmatrix} = \sqrt{L_h} \begin{pmatrix} \sqrt{L_f} E_x(t) & E_{LO}(t) e^{j\varphi_x} / \sqrt{2} \\ \sqrt{L_f} E_y(t) & E_{LO}(t) e^{j\varphi_y} / \sqrt{2} \end{pmatrix} \cdot \begin{pmatrix} 1 & 1 & 1 & 1 \\ 1 & e^{j\pi} & e^{j\pi/2} & e^{-j\pi/2} \end{pmatrix} \tag{3-16}$$

where L_h is the link loss caused by the two 90° optical hybrids, L_f is the link loss caused by the SMF, and φ_x, φ_y are the phase terms arising from the polarization mismatch between the signal and the light wave from the LO laser source.

By applying (E_a, E_b), (E_c, E_d), (E_e, E_f), (E_g, E_h) to four balanced PDs which are terminated with 50-ohm resistors, four output photocurrents are obtained, which are given by

$$\begin{aligned} I_{PD1} &= 2RL_h\sqrt{2P_{s1}P_{LO}L_f L_{s1}} \cos\left(\pi S_{RF-16QAM}(t)/2V_{\pi IM} + \pi/4\right) \\ &\quad \times\cos\left(\Delta\omega t + \varphi_1(t) - \varphi_x + \pi S_{RF-QPSK}(t)/V_{\pi PM}\right) \end{aligned} \tag{3-17}$$

$$\begin{aligned} I_{PD2} &= 2RL_h\sqrt{2P_{s1}P_{LO}L_f L_{s1}} \cos\left(\pi S_{RF-16QAM}(t)/2V_{\pi IM} + \pi/4\right) \\ &\quad \times\sin\left(\Delta\omega t + \varphi_1(t) - \varphi_x + \pi S_{RF-QPSK}(t)/V_{\pi PM}\right) \end{aligned} \tag{3-18}$$

$$I_{PD3} = 2RL_h\sqrt{2P_{s2}P_{LO}L_f L_{s2}} \cos\left(\Delta\omega t + \varphi_2(t) - \varphi_y\right) \tag{3-19}$$

$$I_{PD4} = 2RL_h\sqrt{2P_{s2}P_{LO}L_f L_{s2}} \sin\left(\Delta\omega t + \varphi_2(t) - \varphi_y\right) \tag{3-20}$$

with

$$\Delta\omega = \omega_c - \omega_{LO}, \qquad \varphi_1(t) = \varphi_{c1}(t) - \varphi_{LO}(t), \qquad \varphi_2(t) = \varphi_{c2}(t) - \varphi_{LO}(t)$$

where $\Delta\omega$ is the frequency difference between the transmitter laser source and the LO laser source, $\varphi_1(t)$, $\varphi_2(t)$ are the phase noise introduced by the transmitter laser source and the LO laser source. Before we explain the method to recover the 16-QAM microwave vector signal and the QPSK microwave vector signal, it is important to investigate how the phase noise affects the 16-QAM microwave vector signal and the QPSK microwave vector signal. First, an ideal situation is considered, where $\Delta\omega = 0$ and no signal is sent to the PM ($S_{RF-QPSK}(t) = 0$). Then, (3-17) can be rewritten as

$$I_{PD1} = 2RL_h\sqrt{2P_{s1}P_{LO}L_f L_{s1}}\cos\left(\pi S_{RF-16QAM}(t)/2V_{\pi IM} + \pi/4\right) \times\cos\left(\varphi_1(t) - \varphi_x\right) \tag{3-21}$$

From (3-21), it can be seen that the phase noise $\varphi_1(t)$ is converted to an amplitude noise given by $\cos\left(\varphi_1(t) - \varphi_x\right)$ at the output of the coherent receiver.

If $\Delta\omega = 0$ and no signal is sent to the MZM, (3-21) can be expressed as

$$I_{PD1} = 2RL_h\sqrt{2P_{s1}P_{LO}L_f L_{s1}}\cos\left(\pi/4\right) \times\begin{bmatrix}\cos\left(\varphi_1(t)-\varphi_x\right)\cos\left(\pi S_{RF-QPSK}(t)/V_{\pi PM}\right) \\ -\sin\left(\varphi_1(t)-\varphi_x\right)\sin\left(\pi S_{RF-QPSK}(t)/V_{\pi PM}\right)\end{bmatrix} \tag{3-22}$$

As can be seen, the phase noise $\varphi_1(t)$ is also converted to an amplitude noise given by $\sin\left(\varphi_1(t) - \varphi_x\right)$.

Then, a more realistic situation is considered where $\Delta\omega \neq 0$ and both the intensity and phase of the optical light are modulated. Equations (3-17) and (3-18) can be further expanded as

$$I_{PD1} = 2RL_h\sqrt{2P_{s1}P_{LO}L_f L_{s1}} \times\left[\left(A\times C - A\times D\right) - \left(B\times C - B\times D\right)\right] \tag{3-23}$$

$$I_{PD2} = 2RL_h\sqrt{2P_{s1}P_{LO}L_fL_{s1}} \times \left[\left(A\times E + A\times F\right) - \left(B\times E + B\times F\right)\right] \tag{3-24}$$

with

$$\begin{aligned}
A &= \cos\left(\pi S_{RF-16QAM}\left(t\right)/2V_{\pi IM}\right)\cos\left(\pi/4\right)\\
B &= \sin\left(\pi S_{RF-16QAM}\left(t\right)/2V_{\pi IM}\right)\sin\left(\pi/4\right)\\
C &= \cos\left(\Delta\omega t + \varphi_1(t) - \varphi_x\right)\cos\left(\pi S_{RF-QPSK}(t)/V_{\pi PM}\right)\\
D &= \sin\left(\Delta\omega t + \varphi_1(t) - \varphi_x\right)\sin\left(\pi S_{RF-QPSK}(t)/V_{\pi PM}\right)\\
E &= \cos\left(\Delta\omega t + \varphi_1(t) - \varphi_x\right)\sin\left(\pi S_{RF-QPSK}(t)/V_{\pi PM}\right)\\
F &= \sin\left(\Delta\omega t + \varphi_1(t) - \varphi_x\right)\cos\left(\pi S_{RF-QPSK}(t)/V_{\pi PM}\right)
\end{aligned}$$

In (3-23) and (3-24), if we assume that both the QPSK and the 16-QAM microwave vector signals are small signals, then A×D and A×E represent the detected QPSK microwave vector signals at the outputs of the coherent receiver (I_{PD1} and I_{PD2}). The frequencies of the detected QPSK microwave vector signals are up converted because of the frequency difference between the transmitter laser source and LO laser source. And B×C, B×F represent the detected 16-QAM microwave vector signals and their frequencies are also up converted due to the same reason. If the center frequencies and bandwidths of the QPSK microwave vector signal and the 16-QAM microwave vector signal are identical, for each output of the coherent receiver (I_{PD1} and I_{PD2}), the spectra of the detected 16-QAM signal and the detected QPSK signal are completely overlapped. In addition, both the detected QPSK and 16-QAM microwave vector signals are affected by the phase noise introduced by both the transmitter laser source and LO laser source. Apparently, it is impossible to recover and demodulate the two microwave vector signals directly from the outputs of the coherent receiver. To demodulate the 16-QAM microwave vector signal and the QPSK microwave vector signal, DSP algorithms are employed to cancel the phase noise, eliminate the frequency shift and recover the signals from the overlapped spectra.

First, the four signals, I_{PD1}, I_{PD2}, I_{PD3} and I_{PD4} are separately sampled and digitized by four ADCs. Then, the DSP algorithm is employed [99]. By summing the squared magnitudes of I_{PD1} and I_{PD2}, we can obtain

$$\begin{aligned} I_1 &= I_{PD1}^2 + I_{PD2}^2 \\ &= 4R^2 L_h^2 L_f P_{s1} P_{LO} L_{s1} \left[1 - \sin\left(\pi S_{RF-16QAM}(t)/V_{\pi IM}\right)\right] \\ &\approx 4R^2 L_h^2 L_f P_{s1} P_{LO} L_{s1} \left[1 - \pi S_{RF-16QAM}(t)/V_{\pi IM}\right] \end{aligned} \tag{3-25}$$

As can be seen, the QPSK microwave vector signal is not present in the expression and the phase noise is cancelled, thus a recovery of the 16-QAM microwave vector signal free from phase noise is realized.

Also, through DSP, we can obtain

$$\begin{aligned} I_2 &= \operatorname{atan}\left[\frac{\left(I_{PD2} \times I_{PD3} - I_{PD1} \times I_{PD4}\right)}{\left(I_{PD1} \times I_{PD3} + I_{PD2} \times I_{PD4}\right)}\right] \\ &= \operatorname{atan}\left\{\frac{\sin\left[\pi S_{RF-QPSK}(t)/V_{\pi PM} + \varphi_{c1}(t) - \varphi_{c2}(t) - \varphi_x + \varphi_y\right]}{\cos\left[\pi S_{RF-QPSK}(t)/V_{\pi PM} + \varphi_{c1}(t) - \varphi_{c2}(t) - \varphi_x + \varphi_y\right]}\right\} \\ &= \pi S_{RF-QPSK}(t)/V_{\pi PM} + \varphi(t) \end{aligned} \tag{3-26}$$

with

$$\varphi(t) = \varphi_{c1}(t) - \varphi_{c2}(t) - \varphi_x + \varphi_y$$

In (3-26), the maximum frequency of $\varphi(t)$ is determined by the linewidth of the transmitter laser source. So, if the lower frequency of the QPSK microwave vector signal is higher than the maximum frequency of $\varphi(t)$, the QPSK microwave vector signal can be simply selected by a digital bandpass filter. The signal at the output of the digital band-pass filter is then expressed as

$$I_2 \approx \frac{\pi S_{RF-QPSK}(t)}{V_{\pi PM}} \tag{3-27}$$

Similarly, the 16-QAM microwave vector signal is not present in the expression and the phase noise is cancelled, thus a recovery of the QPSK microwave vector signal free from phase noise is also realized.

3.2.2. Experiment

An experiment based on the setup shown in Fig. 3.13 is performed and a picture of the experimental setup is shown in Fig. 3.14.

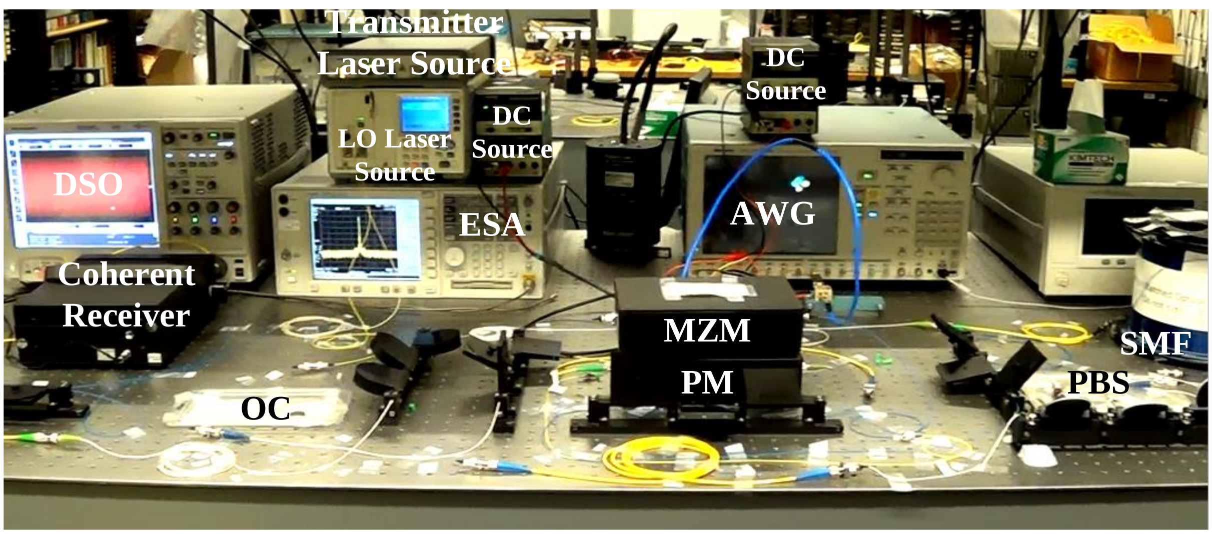

Fig. 3.14. Photograph showing the experiment setup of the proposed high spectral efficiency RoF link. AWG: arbitrary wave generator, ESA: electrical spectrum analyzer, DSO: digital storage oscilloscope, MZM: Mach-Zehnder modulator, PM: phase modulator, OC: optical coupler, PBS: polarization beam splitter, SMF: single mode fiber, DC Source: direct current source, LO laser source: local oscillator laser source.

A tunable laser source (TLS) operating at 1550.57 nm with a linewidth of about 100 kHz and an output power of 16 dBm is utilized as the transmitter laser source. The light wave from the

TLS is split into two channels by an OC with a splitting ratio of 95:5 (95% optical power for Channel 1 and 5% optical power for Channel 2). In Channel 1, the light wave is sent via a polarization controller (PC1) to a chirp-free single-electrode MZM (JDS-Uniphase) that is biased at the quadrature point, and is modulated by a 16-QAM microwave vector signal. Then, the amplitude-modulated light wave is sent to a PM (JDS-Uniphase) via a second PC (PC2), and is phase-modulated by a QPSK microwave vector signal. The optical signal at the output of the PM is then sent to PBS1 via PC3. The polarization extinction ratio of PBS1 is 20 dB. Both the 16-QAM microwave vector signal and the QPSK microwave vector signal are generated by an arbitrary waveform generator (Tektronix AWG7102) with a carrier frequency at 2.5 GHz. The symbol rate for each of the digital modulated microwave signals is 625 MSymbol/s, or the bit rate for the 16-QAM microwave vector signal is 2.5 Gbps and for the QPSK microwave vector signal is 1.25 Gbps, and the total bit rate for the whole system is 3.75 Gbps. The MZM has a bandwidth of 10 GHz, a half-wave voltage of about 5.5 V and a insertion loss of 4.5 dB, and the PM has a bandwidth of 20 GHz ,a half-wave voltage of 5 V and a insertion loss of 4.5 dB. In Channel 2, the light wave is not modulated, which is sent to PBS1 via PC4. PC3 and PC4 are used to make the polarization directions of the two signals align with the two principal axes of PBS1, thus the two light waves are polarization multiplexed, which are transmitted over a 25-km SMF and sent to a coherent receiver (Discovery Semiconductors DP-QPSK 40/100 Gbps Coherent Receiver Lab Buddy) via PC5. Through tuning PC5, the two polarization multiplexed light waves can be de-multiplexed by PBS2, which is inside the coherent receiver (Here, PC5 can be replaced by a dynamic polarization controller in a practical system since the dynamic polarization can be used to realize polarization demuliplexing [100, 101].). On the other hand, a second TLS (Yokogawa

AQ2201) operating at 1550.619 nm with a linewidth of about 1 MHz and an output power of 9.3 dBm is used as the LO laser source. The wavelength difference between the transmitter laser source and the LO laser source is 0.048 nm, corresponding to a beat frequency of about 6 GHz. The light wave from the LO laser source is sent to the LO port of the coherent receiver through PC6. A Digital Storage Oscilloscope (Agilent DSO-X 93204A) is employed to perform the analog-to-digital conversion at a sampling rate of 40 GSa/s. The sampled signals (I_{PD1}, I_{PD2}, I_{PD3} and I_{PD4}) are processed off-line in a computer with the proposed DSP algorithms developed to recover the 16-QAM and the QPSK microwave vector signals while cancelling the phase noises from the transmitter and LO laser sources.

In order to recover the 16-QAM and the QPSK microwave vector signals free from the phase noise, the lengths of the four paths for the in-phase and the quadrature components of the two orthogonally polarized signals from PBS2 should be precisely matched. In the experiment, the length differences of the cables at the outputs of the coherent receiver between the four paths are controlled within 1 mm, and the four paths inside the coherent receiver are well matched. Thus, the proposed DSP-based PNC algorithm is applicable for a coherent system using any commercial laser sources that are designed for optical communications applications. Fig. 3.15 shows the spectrum at the first output port of the coherent receiver (I_{PD1}), which contains the 16-QAM and the QPSK microwave vector signals. As can be seen, the detected microwave vector signals (the signals with the center frequencies of 3.5 GHz and 8.5 GHz) in Fig. 3.15 are just the mixing products of the 2.5-GHz transmitted microwave vector signals and the 6-GHz electrical carrier whose frequency is just the frequency difference between the two laser sources. In addition, the spectra of the 16-QAM microwave vector signal and QPSK microwave vector signal are completely overlapped, as mentioned in Chapter 3.2.1.

Fig. 3.16 shows the spectrum at the third output port of the coherent receiver (I_{PD3}). As can be seen, the microwave vector signals contains a strong phase noise which is introduced from both the transmitter laser source and LO laser source. Fig. 3.17 and Fig. 3.18 show the spectra of the recovered 16-QAM and QPSK microwave vector signals at the output of the DSP-based PNC module. Apparently, the signals are frequency translated back to the exact radio frequencies of the original signals after the digital processing. Then, we evaluate the performance of the system in terms of EVMs for the recovered microwave vector signals as a function of the received optical power. The results are shown in Fig. 3.19. As can be seen when the received optical power is -21.5 dBm, the constellations of the 16-QAM microwave vector signal and the QPSK microwave vector signal are clear and well separated.

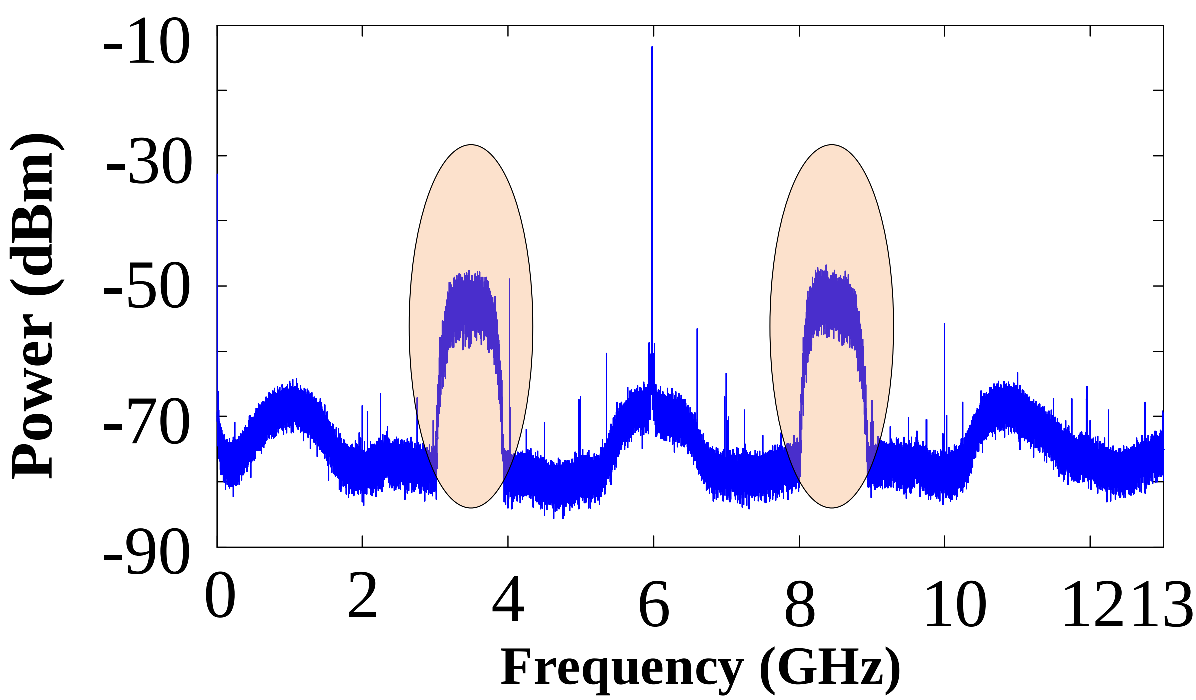

Fig. 3.15. Spectrum of the signals at the first output port of the coherent receiver (I_{PD1}).

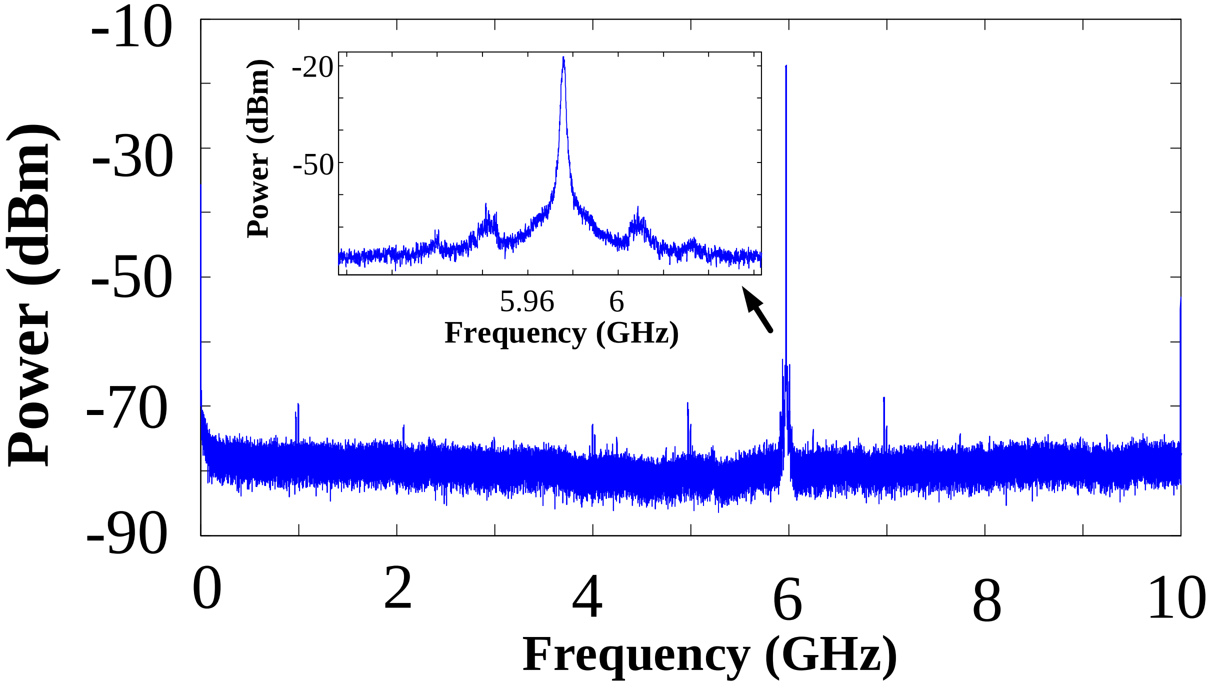

Fig. 3.16. Spectrum of the signal at the third output port of the coherent receiver (I_{PD3}).

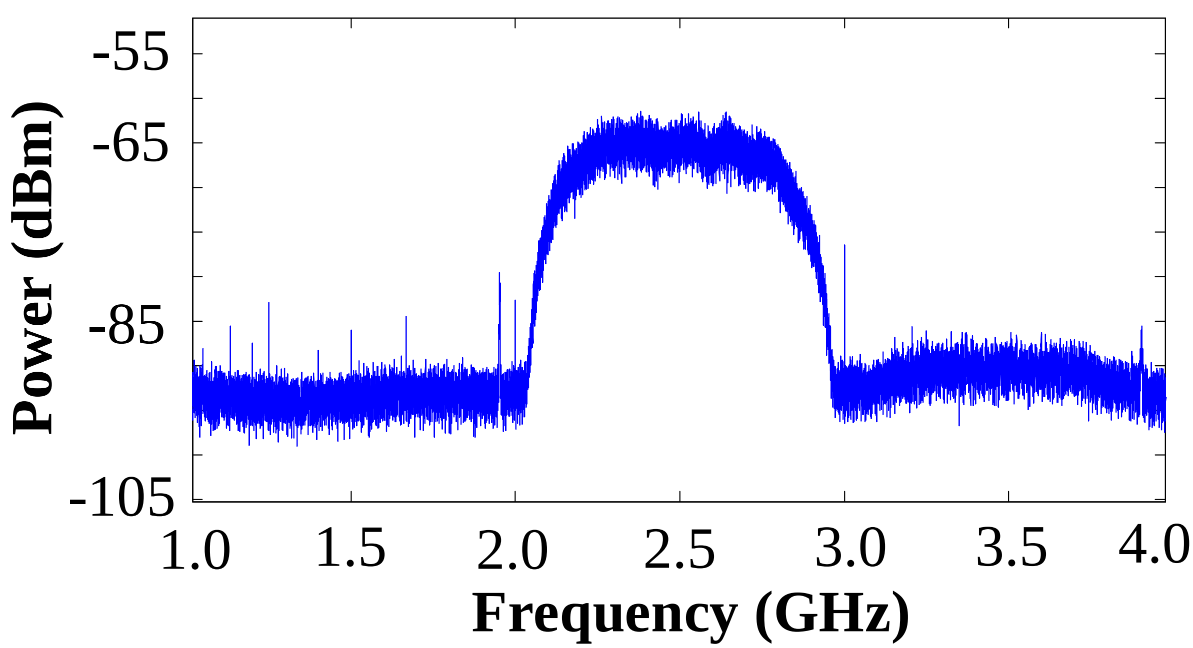

Fig. 3.17. Spectrum of the recovered 16-QAM microwave vector signal at the output of the DSP-based PNC module.

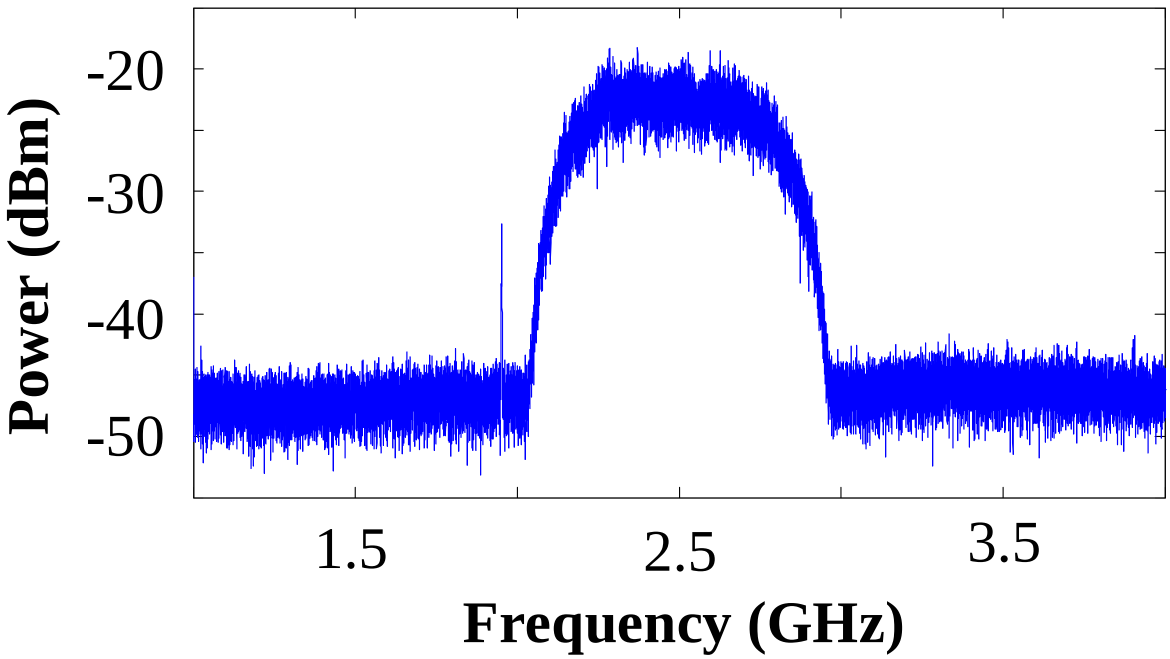

Fig. 3.18. Spectrum of the recovered QPSK microwave vector signal at the output of the DSP-based PNC module.

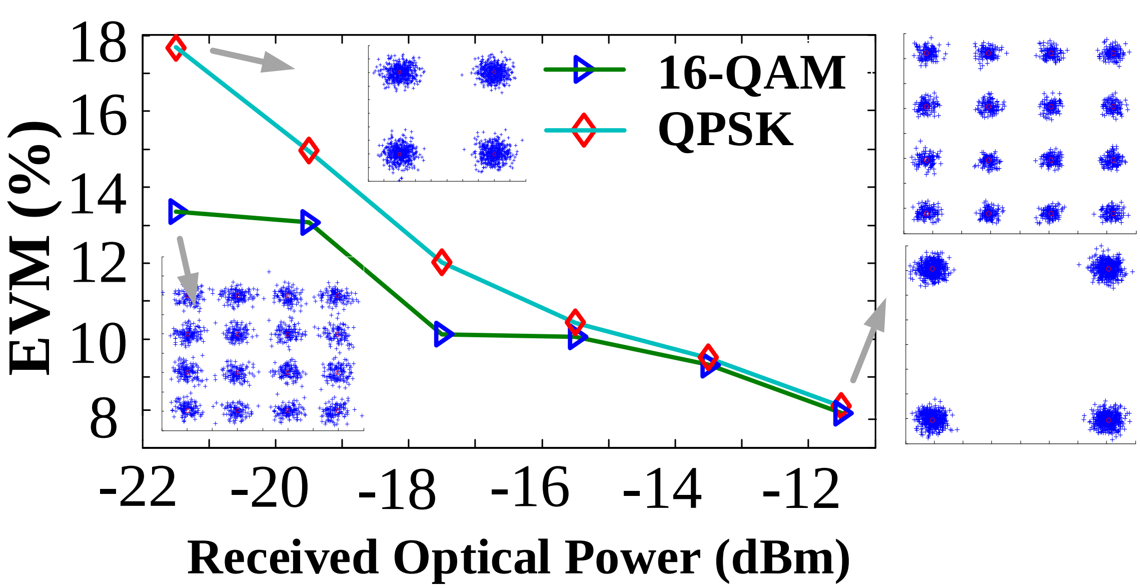

Fig. 3.19. EVM measurements at different received optical power levels for the QPSK and the 16-QAM signal transmitted over the 25-km SMF.

$$\overline{P}_{M-QAM} = \frac{2}{\log_2 M}\left(1-\frac{1}{\sqrt{M}}\right) \times erfc\left(\sqrt{\frac{3}{2(M-1)} \times SNR}\right) \tag{3-28}$$

with $$SNR = 1/EVM^2$$

where $erfc(\ )$ is the complementary error function and SNR is the signal-to-noise ratio [102], [112]-[114]. The BERs as a function of the received optical power calculated from the measured EVMs are shown in Fig. 3.20.

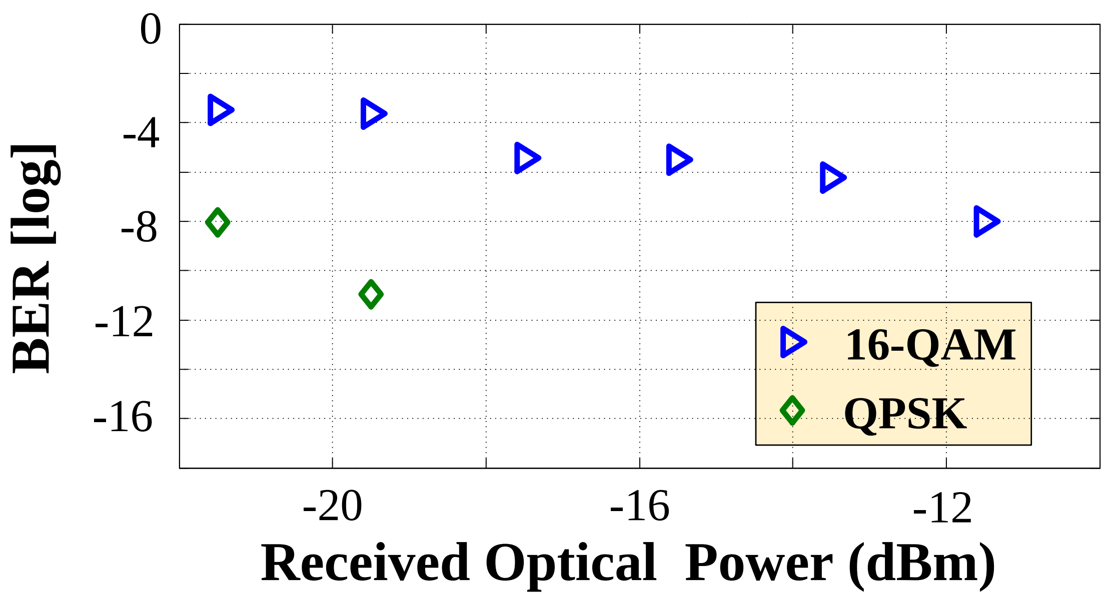

Fig. 3.20. BERs at different received optical power levels for the QPSK and the 16-QAM microwave vector signals transmitted over 25-km SMF.

Again, when the received optical power is -21.5 dBm, the BER is 10^{-8} for the QPSK signal, which is sufficiently small to recover the original signal. The BER for the 16-QAM signal is 10^{-4}, which is poorer than that of the QPSK signal. By using a state-of-the-art forward error correction (FEC) technique, the recovered signal would have a signal quality that is still suitable for error-free transmission [115, 116]. When the received optical power is -13.5 dBm, according to (3-28), the estimated signal-to-noise ratios of the QPSK and 16-QAM microwave vector signals after the PNC module are 20.45 dB and 20.61 dB, respectively. For such signal-to-noise ratios, error-free detection with higher-order modulation formats can be achieved by using the FEC techniques. Considering the FEC limit, for a signal with a signal-to-noise ratio of 20.45 dB, the highest-order modulation format for error-free detection is 64-QAM. So the sub-band spectrum efficiency of the proposed scheme can reach 10 bit/s/Hz if the FEC overhead (overhead 15%) is taken into account.

3.3. Conclusions

Firstly, a DSP-assisted IM/CD RoF link was proposed and experimentally demonstrated. The fundamental concept of the approach to phase noise cancellation was to sum the squared magnitudes of the in-phase and quadrature components from the coherent receiver by using a DSP-based PNC module. The phase noise terms from both the transmitter laser source and the LO laser source were completely cancelled. The effectiveness of the proposed technique for noise cancellation was verified by an experiment. Error-free transmission of a 1.25-Gbps RF signal with a center frequency of 1.6 GHz over 25 km SMF was achieved. The main advantages of the DSP-based PNC technique include: 1) It can support both optical heterodyne detection and optical homodyne detection; 2) It does not need any complicated AFC loop or phase locked loop. For a signal with a bit rate of 834 Mbps, the receiver sensitivity was -24.5 dBm. Compared with a conventional IM/DD RoF link, the receiver sensitivity of the proposed RoF link was improved.

Secondly, a high spectral efficiency coherent RoF link supporting simultaneous amplitude and phase modulation with digital phase noise cancellation was proposed and experimentally demonstrated. Through advanced DSP, amplitude- and phase-modulated microwave vector signals could be recovered and the phase noise introduced by both the transmitter laser source and LO laser source could be effectively cancelled. The proposed technique was evaluated experimentally. Two microwave vector signals with one being a 16-QAM microwave vector signal at 2.5 Gbps and another being a QPSK microwave vector signal at 1.25 Gbps were transmitted over a 25-km SMF link and recovered at the receiver. The EVMs for the recovered 16-QAM and QPSK microwave vector signals were measured to be 8.05% and 8.23%, respectively, which are good enough to achieve error-free transmission with FEC.

CHAPTER 4 RADIO OVER COLORLESS WDM-PON WITH WAVELENGTH REUSE BASED ON COHERENT DETECION INCORPORATING PHASE NOISE CANCELLATION

The ever-increasing demand for high data rate that is beyond what is provided by the present wireless and wired access networks (e.g., TDM based PONs with WiFi technology) will urge the use of radio over WDM-PONs to provide dedicated wide bandwidth to the client. In addition, the access network environment is very sensitive to variations in capital and operational costs because of its low cost-sharing characteristic, therefore colorless ONUs are essential. In this chapter, two approaches to realize radio over colorless WDM-PON with wavelength reuse based on coherent detection incorporating digital phase noise cancellation are proposed. Firstly, a wavelength reuse in a bidirectional radio over a colorless WDM-PON based on polarization multiplexing and coherent detection with digital phase noise cancellation is discussed [117]. A DSP algorithm, which supports both the optical homodyne and heterodyne detection, is developed to cancel the phase noise at the output of the coherent receiver. Error-free transmission of 5 Gbps 16-QAM downstream microwave signals and 2.5 Gbps 16-QAM upstream microwave signal over 10.5-km SMF is achieved. However, the system is not symmetrical, since the polarization multiplexing can be only applied for the downlink but not for the uplink, which results in that the data rate for the downlink is twice of that for the uplink. Thus, in the second approach, a symmetrical radio over a colorless WDM-PON with wavelength reuse based on polarization multiplexing and coherent detection incorporating digital phase noise cancellation is given in the second part [118]. The transmission of two 2.5-Gbps 16-QAM downstream microwave vector signals and two 2.5-Gbps 16-QAM upstream microwave vector signals over a 10.5-km single-mode fiber (SMF) is experimentally demonstrated. The total data rate is 5 Gbps. The error vector magnitudes (EVMs) for the recovered 16-QAM downstream microwave vector signals and the recovered 16-QAM upstream microwave vector signals can reach 7.3% and 8.65%, respectively, which are good enough to achieve error-free transmission with FEC. In addition, compared with the RSOA-based or the FP-LD based colorless ONUs, proper controlling the optical power and wavelength into the ONUs and the ER of the downstream signal are not necessary in these two proposed schemes.

4.1. Radio over colorless WDM-PON with wavelength reuse based on polarization multiplexing and coherent detection incorporating phase noise cancellation

Fig. 4.1 shows the proposed radio over WDM-PON with wavelength reuse based on polarization multiplexing and coherent detection incorporating digital phase noise cancellation. At a transmitter, a light wave from a CW laser source is split into two channels by a 3-dB (OC1), with the light wave at each being intensity modulated by a 16-QAM microwave signal for downstream transmission. The two intensity-modulated optical signals are then polarization multiplexed at a polarization beam combiner (PBC) and sent to a wavelength multiplexer (MUX), where all optical signals from all transmitters at the OLT are wavelength multiplexed and then transmitted over a SMF to a remote access node (RAN). At the RAN, a de-multiplexer (DEMUX) is used to de-multiplex the optical signals, which are then distributed to the corresponding ONUs. At each ONU, the two orthogonally polarized light waves are equally divided into two parts by another 50/50 coupler (OC2). The light wave at the upper channel is then polarization de-multiplexed at a polarization beam splitter (PBS1) and detected by two photodetectors (PDs). While the light wave at the lower channel is sent to a PolM, which is driven by a 16-QAM upstream microwave signal. The PolM is a special phase modulator that supports phase modulation along the two principal axes with opposite phase modulation indices.

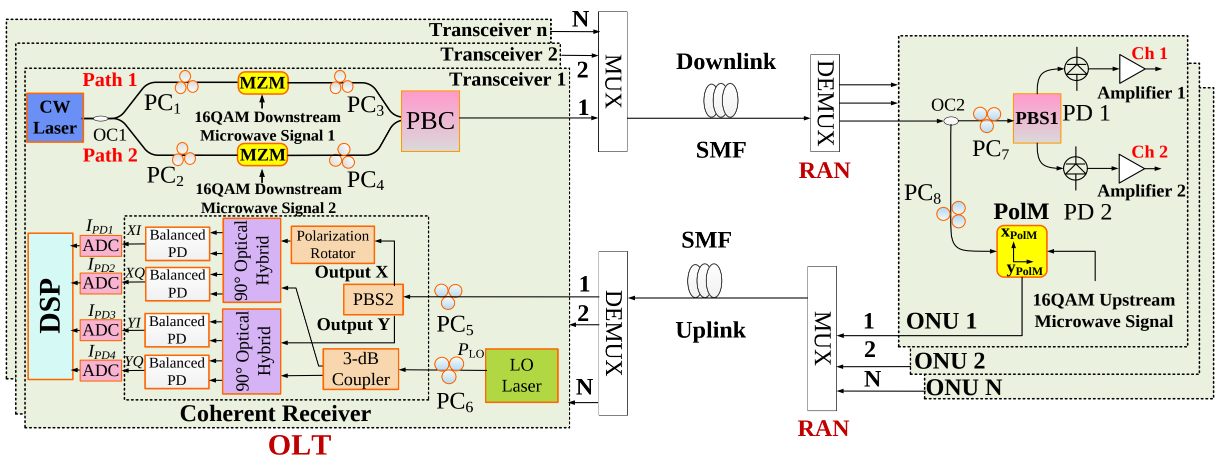

Fig. 4.1. A radio over WDM-PON with wavelength reuse based on polarization multiplexing and coherent detection.

By tuning a polarization controller (PC8) before the PolM, the polarization directions of the two orthogonally polarized light waves are adjusted to be parallel to the principle axes of the PolM. At the output of the PolM, the two orthogonally polarized light waves are phase-modulated by a 16-QAM microwave signal for upstream transmission. Then, the optical signals from different ONUs are wavelength multiplexed at a MUX and transmitted over an SMF to the OLT where a DEMUX is used to deliver a different optical wavelength to its corresponding receiver. At each receiver, a polarization- and phase-diversity coherent optical receiver is used to detect the optical upstream signal which is polarization de-multiplexed through a PC (PC5) and the second

PBS (PBS2). Four signals (I_{PD1} , I_{PD2} , I_{PD3} and I_{PD4}) at the four outputs of the coherent receiver are then sent to a DSP-based phase noise cancellation (PNC) module. An algorithm is developed to recover the 16-QAM upstream microwave signal while cancelling the phase noise introduced by both the transmitter and LO laser sources. Error-free transmission of two 2.5-Gbps 16-QAM downstream microwave signals and a 2.5-Gbps 16-QAM upstream microwave signal over a 10.5-km SMF is demonstrated.

4.1.1. Principle

The two orthogonally polarized optical signals at the output of the PBC for upstream transmission can be expressed as

$$\begin{bmatrix} E_x(t) \\ E_y(t) \end{bmatrix} = \sqrt{P_s} \begin{bmatrix} \sqrt{L_{s1}} \cos\left(\pi S_{RFdownstream1-16QAM}(t)/2V_{\pi IM1} + \pi/4\right) e^{j\left(\omega_c t + \varphi_{c1}(t)\right)} \\ \sqrt{L_{s2}} \cos\left(\pi S_{RFdownlstream2-16QAM}(t)/2V_{\pi IM2} + \pi/4\right) e^{j\left(\omega_c t + \varphi_{c2}(t)\right)} \end{bmatrix} \tag{4-1}$$

where P_s is the output optical power of the transmitter laser source, ω_c is the angular frequency of the light wave, $S_{RFdownstream1\text{-}16QAM}(t)$ and $S_{RFdownstream2\text{-}16QAM}(t)$ are the 16-QAM downstream microwave vector signals applied to the two MZMs, $V_{\pi IM1}$ and $V_{\pi IM2}$ are the half-wave voltages of the two MZMs, $\varphi_{c1}(t)$ and $\varphi_{c2}(t)$ are the phase terms of the transmitter laser source for path 1 and path 2, respectively, and L_{s1} and L_{s2} are the link losses for the two paths. Both the MZMs are biased at the quadrature point.

At an ONU, the electric fields of the optical signals at the output of the PolM along the two principle axes are given by

$$\begin{bmatrix} E_{x-PolM}(t) \\ E_{y-PolM}(t) \end{bmatrix} = \begin{bmatrix} \sqrt{L_{s1}P_s} \cos\left(\pi S_{RFdownstream1-16QAM}(t)/2V_{\pi IM1} + \pi/4\right) e^{j\left(\omega_c t + \pi S_{RFupstream}(t)/2V_{\pi PolM} + \varphi_{c1}(t)\right)} \\ \sqrt{L_{s2}P_s} \cos\left(\pi S_{RFdownstream2-16QAM}(t)/2V_{\pi IM2} + \pi/4\right) e^{j\left(\omega_c t - \pi S_{RFupstream}(t)/2V_{\pi PolM} + \varphi_{c2}(t)\right)} \end{bmatrix} \tag{4-2}$$

where $S_{RFupstream}(t)$ is the upstream microwave vector signal, the modulation format is 16-QAM, $V_{\pi PolM}$ is the half-wave voltage of the PolM. Then, the reused two orthogonally polarized light waves carrying the upstream data are transmitted over the uplink SMF and sent to the OLT. At the OLT, the two orthogonally polarized light waves are de-multiplexed by PBS2 and coherently detected at a coherent receiver. After the coherent detection, four photocurrents (I_{PD1}, I_{PD2}, I_{PD3} and I_{PD4}) at the output of the coherent receiver are obtained, which are sent to a DSP-based phase noise cancellation module. Using the DSP, we have

$$I_0 = arc\tan\left[\frac{(I_{PD2}\times I_{PD3} - I_{PD1}\times I_{PD4})}{(I_{PD1}\times I_{PD3} + I_{PD2}\times I_{PD4})}\right] = \frac{\pi S_{RFupstream}(t)}{V_{\pi PolM}} + \varphi(t) \tag{4-3}$$
$$with \qquad \varphi(t) = \varphi_{c1}(t) - \varphi_{c2}(t) - \varphi_x + \varphi_y$$

where φ_x and φ_y are the phase terms arising from the polarization mismatch between the upstream optical signal and the light wave from LO laser source. In (4-3), the maximum frequency of $\varphi(t)$ is determined by the linewidth of the transmitter laser source. Usually, it is less than 1 MHz. So, the upstream microwave vector signal can be simply selected by a digital bandpass filter if the spectrum of the vector signal does not overlap with the spectrum of $\varphi(t)$.

4.1.2. Experiment

An experiment based on the setup shown in Fig. 4.1 is performed. A picture of the experimental setup is shown in Fig. 4.2. The transmitter laser source operates at 1550.578 nm with a linewidth of about 100 kHz and an output power of 16 dBm. The LO laser source operates at 1550.527 with a linewidth of about 1 MHz and an output power of 8.8 dBm. PC_7

and PC_8 can be replaced with a dynamic polarization controller in a practical system (A dynamic polarization controller can be used for polarization demultiplexing for the downlink and polarization stabilization for the uplink [100, 101].). The center frequencies of the 16-QAM downstream microwave signals and the 16-QAM upstream microwave signal are all 2.5 GHz. The symbol rates are all 625 MSymbol/s. The total bit rates for the downstream data and the upstream data are 2 × 2.5 Gbps, and 2.5 Gbps, respectively. The length of the fiber between the transceiver and the ONU is 10.5 km.

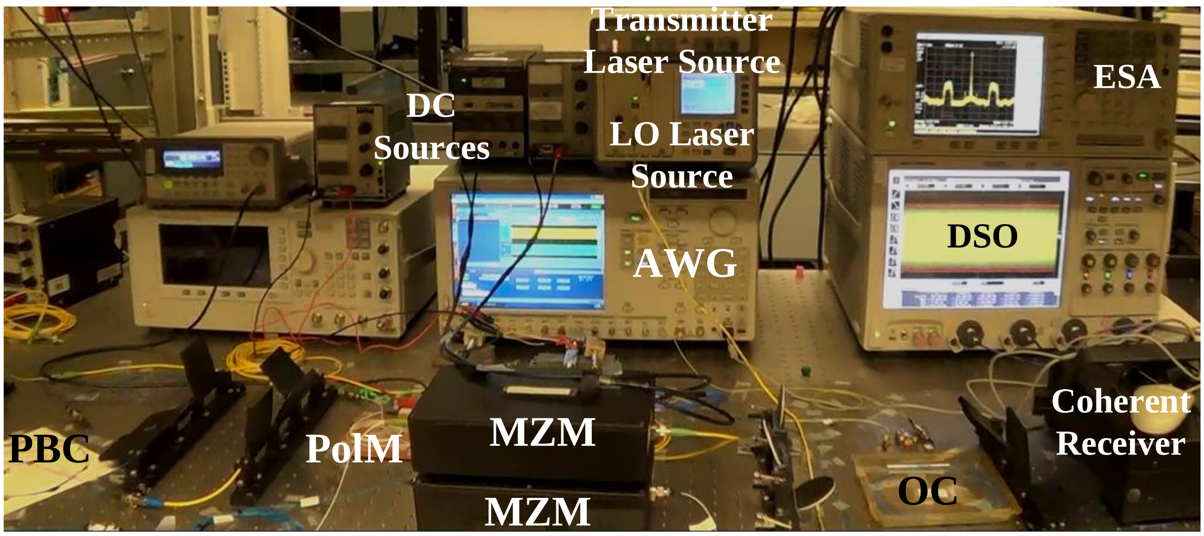

Fig. 4.2. Photograph showing the experimental setup of the proposed radio over colorless WDM based on wavelength reuse. AWG: arbitrary wave generator, MZM: Mach-Zehnder modulator, PolM: polarization modulator, PBC: polarization beam combiner, ESA: electrical spectrum analyzer, DSO: digital storage oscilloscope, DC Sources: direct current sources, LO laser source: local oscillator laser source.

As can be seen, the detected microwave signal (I_{PD1}) from the coherent receiver in Fig. 4.3 is frequency up converted from 2.5 GHz to 3.5 GHz and 8.5 GHz because of the wavelength difference between the two laser sources. In addition, the RF carrier in Fig. 4.3 is very noisy, which is caused by the phase noise from the transmitter laser source and LO laser source. Fig. 4.4 shows the spectrum of the recovered 16-QAM upstream microwave signal at the output of the DSP-based PNC module. Apparently, the 16-QAM upstream microwave signal is converted to its original frequency at 2.5 GHz.

The transmissions performance of the down and upstream in terms of EVMs is evaluated. First, the EVM of the transmission of the 16-QAM upstream microwave signal is measured, which is shown in Fig. 4.5. Two different situations are considered: 1) the optical carrier is pure; 2) the optical carrier is intensity-modulated by two 16-QAM downstream microwave signals. As can be seen, the power penalty caused by the wavelength reuse is about 2 dB. The BERs as a function of the received optical power calculated from the measured EVMs are shown in Fig. 4.6.

Then, the EVMs and the estimated BERs of the transmission of the two 16-QAM downstream microwave signals are measured, which are also shown in Fig. 4.5 and Fig. 4.6. Compared with the receiver sensitivity of the downlink, the receiver sensitivity of the uplink is much better than that of the downlink.

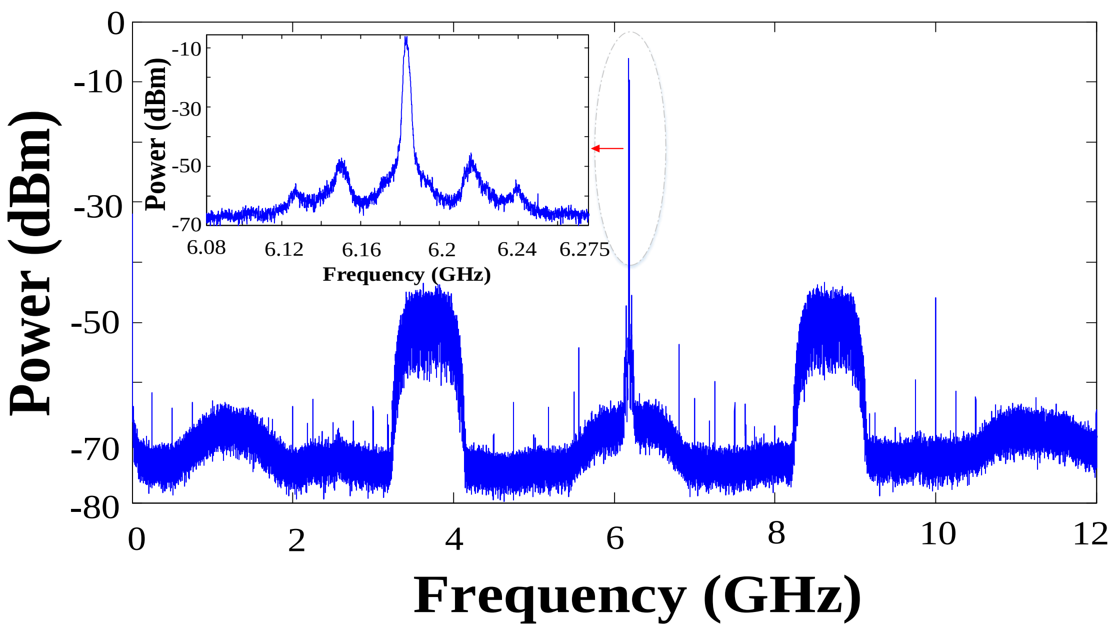

Fig. 4.3. Spectrum of the signal at the first output port of the coherent receiver (I_{PD1}).

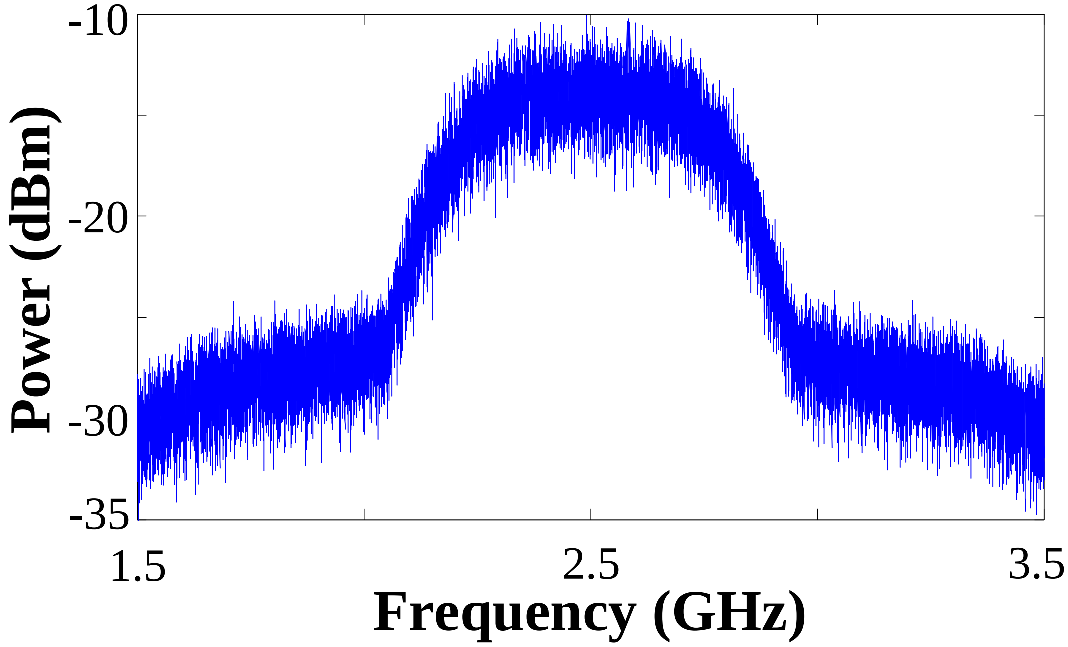

Fig. 4.4. Spectrum of the recovered 16-QAM upstream microwave signal at the output of the DSP-based PNC module.

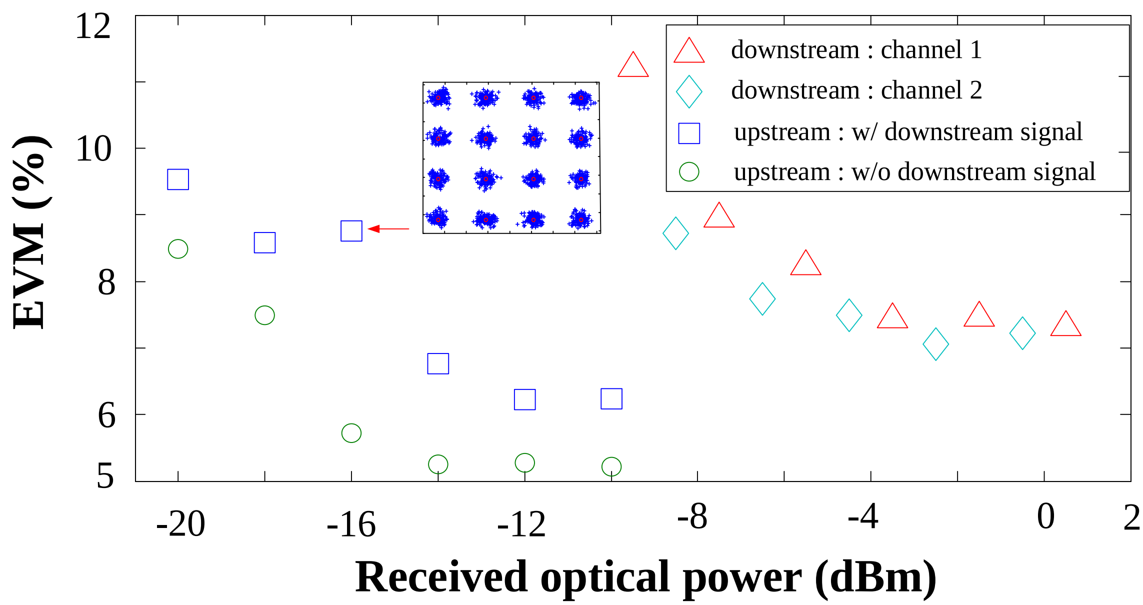

Fig. 4.5. EVMs at different received optical power levels for the two 16-QAM downstream signals and the 16-QAM upstream signal.

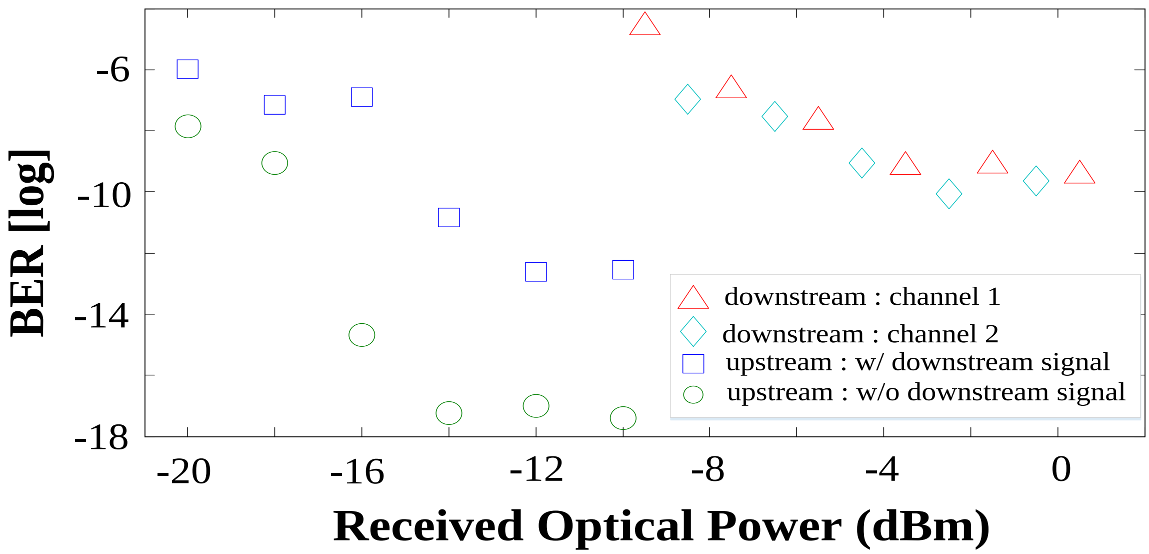

Fig. 4.6. The estimated BERs at different received optical power levels for the two 16-QAM downstream signals and the 16-QAM upstream signal.

4.2. Wavelength reuse in a symmetrical radio over WDM-PON based on polarization multiplexing and coherent detection

In the former section, the proposed network is not symmetrical, since the polarization multiplexing can be only applied for the downlink but not for the uplink, which results in that the data rate for the downlink is twice of that for the uplink. To overcome this drawback, in this section, a symmetrical radio over a colorless WDM-PON with wavelength reuse based on polarization multiplexing and coherent detection incorporating digital phase noise cancellation is proposed and demonstrated. In the optical line terminal (OLT), polarization multiplexing is employed to double the spectral efficiency and the data rate. In addition, coherent detection is used for the uplink, to improve the receiver sensitivity and also to compensate for the degraded data transmission performance due to the utilization of a wavelength-reused downstream optical signal. Two digital signal processing (DSP) algorithms for the recovery of two 16-QAM upstream microwave vector signals from the upstream signals, which contain the downstream signals and the phase noises from the transmitter laser source and the local oscillator (LO) laser source, are proposed. In the ONUs, no wavelength selective components are used, making the ONUs colorless. In addition, polarization multiplexing is also employed. Therefore, a symmetrical radio over WDM-PON is implemented. The proposed scheme is experimentally demonstrated. The transmission of two 2.5-Gbps 16-QAM downstream microwave vector signals and two 2.5-Gbps 16-QAM upstream microwave vector signals over a 10.5-km single-mode fiber (SMF) is experimentally demonstrated. The error vector magnitudes (EVMs) for the recovered 16-QAM downstream microwave vector signals and the recovered 16-QAM upstream microwave vector signals can reach 7.3% and 8.65%, respectively, which are good enough to achieve error-free transmission with forward error correction (FEC) [118].

4.2.1. Principle

The schematic of the proposed symmetrical radio over colorless WDM-PON based on polarization multiplexing and coherent detection incorporating digital phase noise cancellation is shown in Fig. 4.7. At a transceiver in the OLT, a continuous-wave (CW) light wave from a laser diode (LD) is equally divided into two channels by a 3-dB coupler (OC1) and sent to two Mach-Zehnder modulators (MZM1 and MZM2) via two polarization controllers (PC1 and PC2). In each path, the CW light wave is intensity-modulated by a 16-QAM microwave vector signal. Both the MZMs are biased at the quadrature point. The two intensity-modulated optical signals are sent via two PCs (PC3 and PC4) and polarization multiplexed at a polarization beam combiner (PBC1) and sent to a wavelength division multiplexer (MUX). At the MUX, all the optical intensity-modulated signals with different center wavelengths from different transmitters are multiplexed and transmitted to a remote access node (RAN) over a single-mode fiber (SMF).

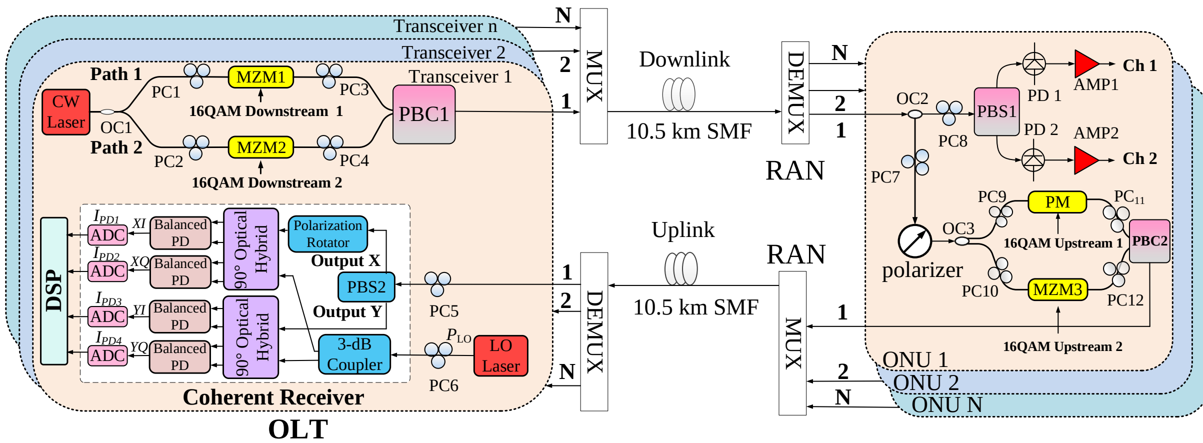

Fig. 4.7. Schematic diagram of the proposed symmetrical radio over WDM-PON with wavelength reuse based on polarization multiplexing and coherent detection. ADC: analog-to-digital converter, AMP: amplifier, PC: polarization controller, CW laser: continuous- wave laser, Balanced PD: balanced photodetector, PBS: polarization bema splitter, PBC: polarization beam combiner, OC: optical coupler, PM: phase modulator, MZM: Mach-Zehnder modulator, SMF: single-mode fiber, DSP: digital signal processing, DSP: digital signal processing, OLT: optical line terminal, ONU: optical network unit, LO laser: local oscillator laser, MUX: multiplexer, DEMUX: de-multiplexer.

At the RAN, all the optical intensity-modulated signals are wavelength de-multiplexed via a wavelength division de-multiplexer (DEMUX) and then distributed to the corresponding ONUs. At each ONU, the intensity-modulated light wave is equally divided into two channels by another 3-dB coupler (OC2). The light wave at the upper channel is then polarization de-multiplexed at a polarization beam splitter (PBS1) and detected by two photodetectors (PDs). While the optical signals at the lower channel is sent to a polarizer which is used to select one of the two orthogonally polarized intensity-modulated optical signals. Then the selected intensity-modulated optical signal is split into two portions by a third 3-dB coupler (OC3). One portion is phase-modulated by a 16-QAM upstream microwave vector signal via a phase modulator (PM), while the other portion is intensity-modulated by another 16-QAM upstream microwave vector signal via the third MZM. The two optical signals are polarization multiplexed again at PBC2 and sent to the RAN, where all optical signals from all ONUs are wavelength multiplexed and transmitted over another SMF to the OLT where a DEMUX is used to deliver a different optical wavelength to its corresponding receiver. At each receiver, a polarization- and phase-diversity coherent optical receiver is used to detect the two orthogonally polarized optical upstream signals which are polarization de-multiplexed through a PC (PC5) and the second PBS (PBS2). Four sampled signals ($I_{PD1}, I_{PD2}, I_{PD3}$ and I_{PD4}) at the output of the coherent receiver are sent to a DSP unit which is used to cancel the phase noise and recover the two 16-QAM upstream microwave vector signals.

Mathematically, the two orthogonally polarized intensity-modulated optical signals at the output of PBC1 in the transmitter can be expressed as

$$\begin{bmatrix} E_{d1}(t) \\ E_{d2}(t) \end{bmatrix} = \sqrt{P_s} \begin{bmatrix} \sqrt{L_{d1}} \cos\left(\dfrac{\pi S_{RFd1-16QAM}(t)}{2V_{\pi IM1}} + \dfrac{\pi}{4} \right) e^{j(\omega_c t + \varphi_{c1}(t))} \\ \sqrt{L_{d2}} \cos\left(\dfrac{\pi S_{RFd2-16QAM}(t)}{2V_{\pi IM2}} + \dfrac{\pi}{4} \right) e^{j(\omega_c t + \varphi_{c2}(t))} \end{bmatrix} \tag{4-4}$$

where P_s is the optical output power of the light wave from the transmitter laser source, ω_c is the angular frequency of the optical carrier, $S_{RFd1-16QAM}(t)$ and $S_{RFd2-16QAM}(t)$ are the input microwave vector signals for MZM1 and MZM2, $V_{\pi IM1}$ and $V_{\pi IM2}$ are the half-wave voltages of MZM1 and MZM2, and $\varphi_{c1}(t)$ and $\varphi_{c2}(t)$ are the phase terms of the transmitter laser source for Path 1 and Path 2. Note, $\varphi_{c1}(t)$ and $\varphi_{c2}(t)$ are different, since the optical signals from the transmitter laser source are split and transmitted through two different paths. L_{d1} and

L_{d2} are the link losses between OC1 and PBS1 for Path 1 and Path 2, respectively.

Then, the two intensity-modulated light waves from the two paths are polarization multiplexed at PBC1 and multiplexed with other wavelengths. After transmission over an SMF, the optical signals are wavelength de-multiplexed at the RAN and sent to the corresponding ONUs. At an ONU, the two received orthogonally polarized intensity-modulated light waves are divided into two parts by a 3-dB optical coupler. The upper part is polarization de-multiplexed at a polarization beam splitter (PBS1) and detected by two PDs. The photocurrents after the two PDs can be expressed as

$$\begin{aligned} I_{d1} &= R_1 \cdot \left[\sqrt{L_f} E_{d1}(t) / \sqrt{2} \right] \cdot \left[\sqrt{L_f} E_{d1}^*(t) / \sqrt{2} \right] / 2 \\ &= R_1 P_s L_{d1} L_f \left(1 - \sin\left(\frac{\pi S_{RFd1-16QAM}(t)}{V_{\pi IM1}} \right) \right) / 8 \\ &\approx R_1 P_s L_{d1} L_f \left(1 - \frac{\pi S_{RFd1-16QAM}(t)}{V_{\pi IM1}} \right) / 8 \end{aligned} \tag{4-5}$$

$$\begin{aligned} I_{d2} &= R_2 \cdot \left[\sqrt{L_f} E_{d2}(t) / \sqrt{2} \right] \cdot \left[\sqrt{L_f} E_{d2}^*(t) / \sqrt{2} \right] / 2 \\ &\approx R_2 P_s L_{d2} L_f \left(1 - \frac{\pi S_{RFd2-16QAM}(t)}{V_{\pi IM2}} \right) / 8 \end{aligned} \tag{4-6}$$

where R_1 and R_2 are the responsivities for PD1 and PD2, respectively. L_f is the link loss caused by the SMF.

The lower part is sent to a polarizer which is used to select one of the two orthogonally polarized intensity-modulated optical signals (Here, we suppose that the optical signal for Path 1 is selected.) and then the selected signal is split by a 3-dB optical coupler. One portion is phase modulated by a 16-QAM upstream microwave vector signal and the other is intensity-modulated by another 16-QAM upstream microwave vector signal. The two signals waves are then polarization multiplexed at PBC2. The optical fields of the two orthogonally polarized optical signals at the output of PBC2 are given by

$$\begin{bmatrix} E_{up1}(t) \\ E_{up2}(t) \end{bmatrix} = \begin{bmatrix} A \\ B \end{bmatrix} \tag{4-7}$$

with

$$A = \frac{\sqrt{P_s L_{d1} L_{up1} L_f}}{2} \cos\left[\frac{\pi S_{RFd1-16QAM}(t)}{2V_{\pi IM1}} + \frac{\pi}{4}\right] \times \exp\left\{ j\left[\omega_c t + \varphi_{c3}(t) + \pi S_{RFup1-16QAM}(t)/V_{\pi PM}\right]\right\}$$

$$B = \frac{\sqrt{P_s L_{d1} L_{up2} L_f}}{2} \cos\left[\frac{\pi S_{RFd1-16QAM}(t)}{2V_{\pi IM1}} + \frac{\pi}{4}\right] \times \cos\left[\frac{\pi S_{RFup2-16QAM}(t)}{2V_{\pi IM3}} + \frac{\pi}{4}\right] \exp\left\{ j\left[\omega_c t + \varphi_{c4}(t)\right]\right\}$$

where L_f is the link loss caused by the SMF, L_{up1} and L_{up2} are the link losses between OC3 and PBC2 for the upper channel and the lower channel. $\varphi_{c3}(t)$ and $\varphi_{c4}(t)$ are the phase terms of the transmitter laser source for the upper and the lower channels. Note again $\varphi_{c3}(t)$ and $\varphi_{c4}(t)$ are different. $V_{\pi IM3}$ and $V_{\pi PM}$ are the half-wave voltages of MZM3 and the phase modulator (PM), respectively.

The wavelength-reused two orthogonally polarized light waves carrying the upstream data are transmitted to the RAN and sent to the OLT over another SMF. At the OLT, the two orthogonally polarized light waves are polarization de-multiplexed by PBS2. The optical fields at the outputs of PBS2 for Output X and Output Y are given by

$$E_x(t) = \sqrt{L_f} E_{up1}(t) \tag{4-8}$$

$$E_y(t) = \sqrt{L_f} E_{up2}(t) \tag{4-9}$$

On the other hand, the optical field at the output of the LO laser source can be written as

$$E_{LO}(t) = \sqrt{2P_{LO}} e^{j[\omega_{LO}t + \varphi_{LO}(t)]} \tag{4-10}$$

where P_{LO} is the optical power of the light wave from the LO laser source, $\varphi_{LO}(t)$ is the phase term, and ω_{LO} is the angular frequency.

Through tuning PC6, with the help of the polarization rotator in Fig. 4.7, the light wave from the LO laser source is co-polarized with the other optical signals at the inputs of the two 90° optical hybrids. At the outputs of the two 90° optical hybrids, eight optical fields are obtained, given by

$$\begin{aligned} &\begin{pmatrix} E_1(t) & E_2(t) & E_3(t) & E_4(t) \\ E_5(t) & E_6(t) & E_7(t) & E_8(t) \end{pmatrix} \\ &= \sqrt{L_h} \begin{pmatrix} E_x(t) & E_{LO}(t) e^{j\varphi_x} / \sqrt{2} \\ E_y(t) & E_{LO}(t) e^{j\varphi_y} / \sqrt{2} \end{pmatrix} \cdot \begin{pmatrix} 1 & 1 & 1 & 1 \\ 1 & e^{j\pi} & e^{j\pi/2} & e^{-j\pi/2} \end{pmatrix} \end{aligned} \tag{4-11}$$

where φ_x and φ_y are the phase terms arising from the polarization mismatch between the upstream optical signal and the light wave from LO laser source. By applying (E_1, E_2), (E_3, E_4), (E_5, E_6), (E_7, E_8) to four identical balanced PDs which are terminated with 50-ohm resistors, four output photocurrents are obtained, which are given by

$$\begin{aligned} I_{PD1} = {} & RL_h L_f \sqrt{P_s P_{LO} L_{d1} L_{up1}} \cos\left[\pi S_{RFd1-16QAM}(t)/2V_{\pi IM1} + \pi/4\right] \\ & \times \cos\left[\Delta\omega t + \varphi_{c3}(t) + \pi S_{RFup1-16QAM}(t)/V_{\pi PM} - \varphi_x\right] \end{aligned} \tag{4-12}$$

$$\begin{aligned} I_{PD2} = {} & RL_h L_f \sqrt{P_s P_{LO} L_{d1} L_{up1}} \cos\left[\pi S_{RFd1-16QAM}(t)/2V_{\pi IM1} + \pi/4\right] \\ & \times \sin\left[\Delta\omega t + \varphi_{c3}(t) + \pi S_{RFup1-16QAM}(t)/V_{\pi PM} - \varphi_x\right] \end{aligned} \tag{4-13}$$

$$I_{PD3} = RL_h L_f \sqrt{P_s P_{LO} L_{d1} L_{up2}} \cos\left[\pi S_{RFd1-16QAM}(t)/2V_{\pi IM1} + \pi/4\right] \times\cos\left[\pi S_{RFup2-16QAM}(t)/2V_{\pi IM3} + \pi/4\right]\cos\left[\Delta\omega t + \varphi_{c4}(t) - \varphi_y\right] \quad (4\text{-}14)$$

$$I_{PD4} = RL_h L_f \sqrt{P_s P_{LO} L_{d1} L_{up2}} \cos\left[\pi S_{RFd1-16QAM}(t)/2V_{\pi IM1} + \pi/4\right] \times\cos\left[\pi S_{RFup2-16QAM}(t)/2V_{\pi IM3} + \pi/4\right]\sin\left[\Delta\omega t + \varphi_{c4}(t) - \varphi_y\right] \quad (4\text{-}15)$$

where R is the responsivity for the balanced PDs.

Through the DSP, we can have

$$\begin{aligned} I_1 &= \tan^{-1}\left[\frac{\left(I_{PD2}\times I_{PD3} - I_{PD1}\times I_{PD4}\right)}{\left(I_{PD1}\times I_{PD3} + I_{PD2}\times I_{PD4}\right)}\right] \\ &= \tan^{-1}\left\{\frac{\sin\left[\pi S_{RFup1-16QAM}(t)/V_{\pi PM} + \varphi(t)\right]}{\cos\left[\pi S_{RFup1-16QAM}(t)/V_{\pi PM} + \varphi(t)\right]}\right\} \\ &= \pi S_{RFup1-16QAM}(t)/V_{\pi PM} + \varphi(t) \end{aligned} \quad (4\text{-}16)$$

with $$\varphi(t) = \varphi_{c3}(t) - \varphi_{c4}(t) - \varphi_x + \varphi_y$$

In (4-16), the maximum frequency of $\varphi(t)$ is determined by the linewidth of the transmitter laser source. If the spectrum of $S_{RFup1-16QAM}(t)$ does not overlap with that of $\varphi(t)$, $S_{RFup1-16QAM}(t)$ can be selected via a digital bandpass filter, which is free from the phase noise.

Also, through DSP we can have,

$$\begin{aligned} I_2 &= \left(I_{PD3}^2 + I_{PD4}^2\right)/\left(I_{PD1}^2 + I_{PD2}^2\right) \\ &= L_{up2}/L_{up1}\times\left\{\cos\left[\pi S_{RFup2-16QAM}(t)/2V_{\pi IM3} + \pi/4\right]\right\}^2 \\ &= L_{up2}/L_{up1}\times\left\{1 - \sin\left[\pi S_{RFup2-16QAM}(t)/V_{\pi IM3}\right]\right\}/2 \\ &\approx L_{up2}/L_{up1}\times\left[1 - \pi S_{RFup2-16QAM}(t)/V_{\pi IM3}\right]/2 \end{aligned} \quad (4\text{-}17)$$

As can be seen, a recovery of the signal, $S_{RFup2-16QAM}(t)$, free from the phase noise, is realized.

4.2.2. Experiment

An experiment based on the setup shown in Fig. 4.7 is conducted. A picture of the experimental setup is shown in Fig. 4.8. A CW light wave from a tunable laser source (TLS, Agilent N7714A) operating at 1550.445 nm with a linewidth of 100 kHz and an optical power of 16.0 dBm is split into two paths by OC1. In each channel, the CW light is intensity-modulated by a 16-QAM downstream microwave vector signal via its corresponding MZM (MZM1 and MZM2). Note that PC1 and PC2 are used to minimize the polarization dependent loss at MZM1 (JDSU) and MZM2 (JDSU), and PC3 and PC4 are used to make the polarization directions of the two optical signals align with the two principal axes of PBC1, thus the two light waves are polarization multiplexed and transmitted to the ONU over a 10.5 km SMF. The bandwidth of the MZMs at the OLT is 10 GHz and the half-wave voltage is around 5.5 V. At the ONU, the two orthogonally polarized intensity-modulated signals are equally divided by OC2. The light wave at the upper channel is then polarization de-multiplexed at a polarization beam splitter (PBS1) and detected by two PDs (New Focus, Model: 1414-50) with a bandwidth of 20 GHz and a responsivity of 0.6 A/W. While the optical signal at the lower channel is sent to a polarizer via PC7 (PC7 and PC8 can be replaced by a dynamic polarization controller in a practical system [100]. A dynamic polarization controller can be used to realize polarization multiplexing for the downlink and polarization stabilization for the uplink [101].), which is used to select one of the two orthogonally polarized intensity-modulated optical signals. The selected intensity-modulated optical signal is split again by OC3 for wavelength reuse. One portion is phase modulated by a 16-QAM upstream microwave vector signal at the PM (JDSU) with a bandwidth of 20 GHz and a half-wave voltage of 5 V, while the other portion is intensity-modulated by another 16-QAM upstream microwave vector signal at MZM3 (JDSU) with a bandwidth of 10 GHz and a half-wave voltage of 5.5 V. All the downstream and upstream 16-QAM microwave vector signals are generated by an arbitrary waveform generator (Tektronix AWG7102). The symbol rates and the center frequencies for the 16-QAM microwave vector signals are all 2.5 Gbps and 2.5 GHz. Again, the two portions of optical signals are polarization multiplexed at PBC2 and transmitted to the OLT over another 10.5 km SMF.

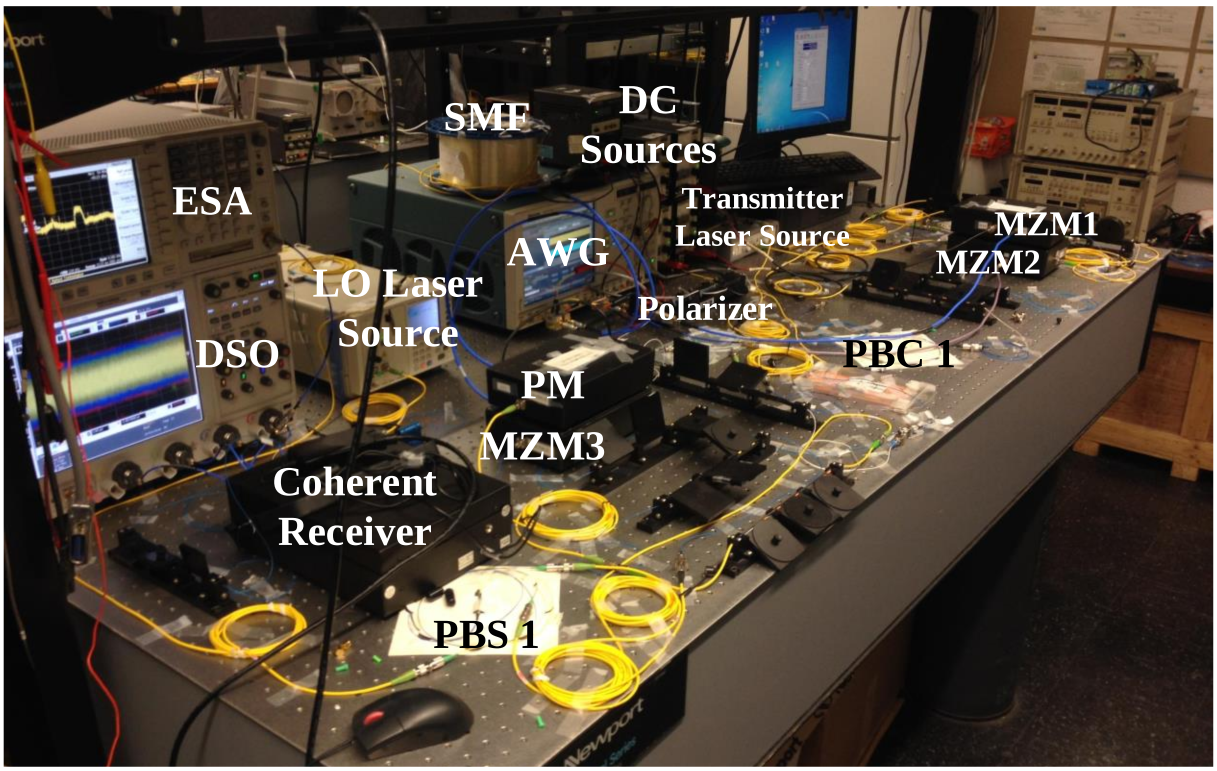

Fig. 4.8. Photograph showing the experimental setup of the proposed radio over colorless WDM based on wavelength reuse. AWG: arbitrary wave generator, MZM: Mach-Zehnder modulator, PBS: polarization beam splitter, PBC: polarization beam combiner, ESA: electrical spectrum analyzer, DSO: digital storage oscilloscope, DC Sources: direct current sources, LO laser source: local oscillator laser source, PM: phase modulator, SMF: single-mode fiber.

At the OLT, a coherent receiver (Discovery Semiconductors DP-QPSK 40/100 Gbps Coherent Receiver Lab Buddy) is used to detect the upstream optical signals. Through tuning PC5 (PC5 can be replaced by a dynamic polarization controller in a practical system [100, 101]. A dynamic polarization controller can be used to realize polarization demultiplexing [101].), the two polarization multiplexed light waves can be polarization de-multiplexed by PBS2, which is inside the coherent receiver.

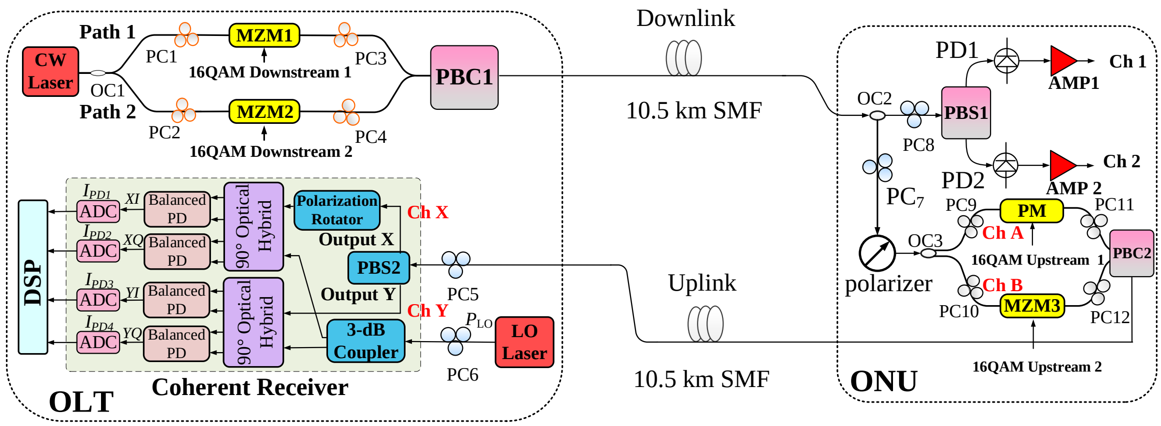

Fig. 4.9. Experimental setup of the proposed symmetrical radio over WDM-PON with wavelength reuse based on polarization multiplexing and coherent detection. ADC: analog-to-digital converter, PC: polarization controller, CW laser: continuous- wave laser, Balanced PD: balanced photodetector, PBS: polarization bema splitter, PBC: polarization beam combiner, OC: optical coupler, PM: phase modulator, MZM: Mach-Zehnder modulator, SMF: single mode fiber, DSP: digital signal processing, DSP: digital signal processing, OLT: optical line terminal, ONU: optical network unit, LO laser: local oscillator laser.

In the experiment, at the output X of PBS2, the optical signal for Channel A is obtained, while the optical signal for Channel B is obtained at the other output of PBS2. On the other hand, a second TLS (Yokogawa AQ2201) which has a center wavelength of 1550.476 nm, a linewidth of 1 MHz and an output optical power of 9 dBm is used as the LO laser source. The light wave from the LO laser source is sent to the LO port of the coherent receiver through PC6. Through tuning PC5 and PC6, with the help of the polarization rotator in Fig. 4.9, the light wave from the LO laser source is co-polarized with the other upstream optical signals at the inputs of the two

90^{o} optical hybrids. After coherent detection, at the output of the coherent receiver, a Digital Storage Oscilloscope (Agilent DSO-X 93204A) is employed to perform the analog-to-digital conversion at a sampling rate of 40 GSa/s. The sampled signals ($I_{PD1}, I_{PD2}, I_{PD3}$ and I_{PD4}) are processed off-line in a computer with the proposed DSP algorithms developed to recover the two 16-QAM upstream vector signals, which is discussed in Chapter 4.2.1. Note, the time delays of Channel A and Channel B should be equal. To evaluate the relative time delay between Channel A and Channel B, a CW light wave which is intensity modulated by an electrical pulse is divided into Channel A and Channel B. Then the light waves from the two channels are polarization multiplexed at the PBC, sent to a coherent receiver and polarization de-multiplexed at the PBS inside the coherent receiver. A DSO (Agilent DSO-X 93204A) is employed to monitor the four signals at the outputs of the coherent receiver.

Fig. 4.10 shows the temporal waveforms of the four signals. As can be seen, the relative time delays between XI and XQ, YI and YQ are small and can be ignored. However, the relative time delay between Channel A and Channel B is about 14.625 ns (585/40e9 s). In order to recover the two 16-QAM upstream microwave vector signals (signal 1 and signal 2), the relative time delay between Channel A and Channel B is controlled precisely identical by DSP. In addition, the length differences of the cables at the outputs of the coherent receiver between the four paths are controlled within 1 mm. Fig. 4.11 shows the spectrum at the second output of the coherent receiver (I_{PD2}), which contains 16-QAM upstream microwave vector signal 1 and 16-QAM downstream microwave vector signal 1. Due to the frequency difference between the transmitter laser source and the LO laser source, the center frequencies of the transmitted microwave vector signals are changed at the outputs of the coherent receiver. The detected microwave vector signals (the signals with the center frequencies of 1.375 GHz and 6.375 GHz) at the second output of the coherent receiver are the mixing products of the 2.5-GHz transmitted microwave vector signals and the 3.875-GHz electrical carrier whose frequency is just the frequency difference between the two laser sources.

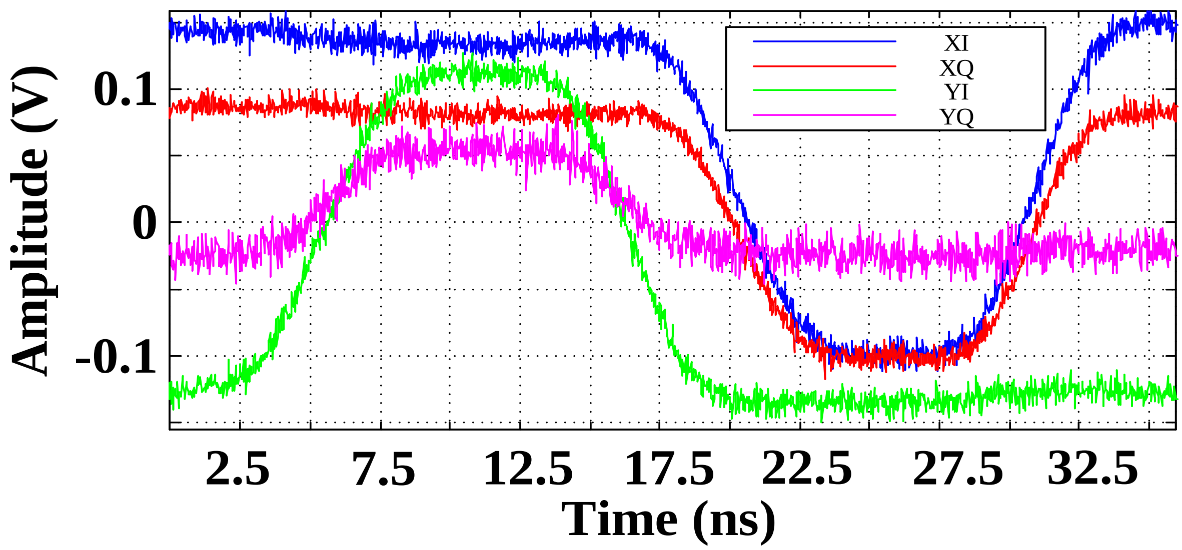

Fig. 4.10. Temporal waveforms at the outputs of the coherent receiver (XI, XQ, YI, YQ).

In addition, the spectra of 16-QAM upstream microwave vector signal 1 and 16-QAM downstream microwave vector signal 1 are completely overlapped.

Fig. 4.12 and Fig. 4.13 show the spectra of the recovered 16-QAM upstream microwave vector signal 1 and 16-QAM upstream microwave vector signal 2 at the output of the DSP unit. The center frequencies of the detected signals at the outputs of the coherent receiver are recovered to their original center frequencies (2.5 GHz) after the processing, which demonstrate that the DSP algorithm cancels the frequency difference successfully. To evaluate the transmission performance of the system, first we measure the EVMs for the recovered two 16-QAM upstream vector signals versus the received optical power which is shown in Fig. 4.14 (Here, the received optical power refers to the optical power at the output of PC5). Three different situations are considered: first, the reused optical light is a pure optical carrier (fiber length: 10.5 km); second, the reused optical light is intensity-modulated by a downstream microwave vector signal (fiber length: 0 km), and third, the reused optical light is intensity-modulated by a downstream microwave vector signal (fiber length: 10.5 km).

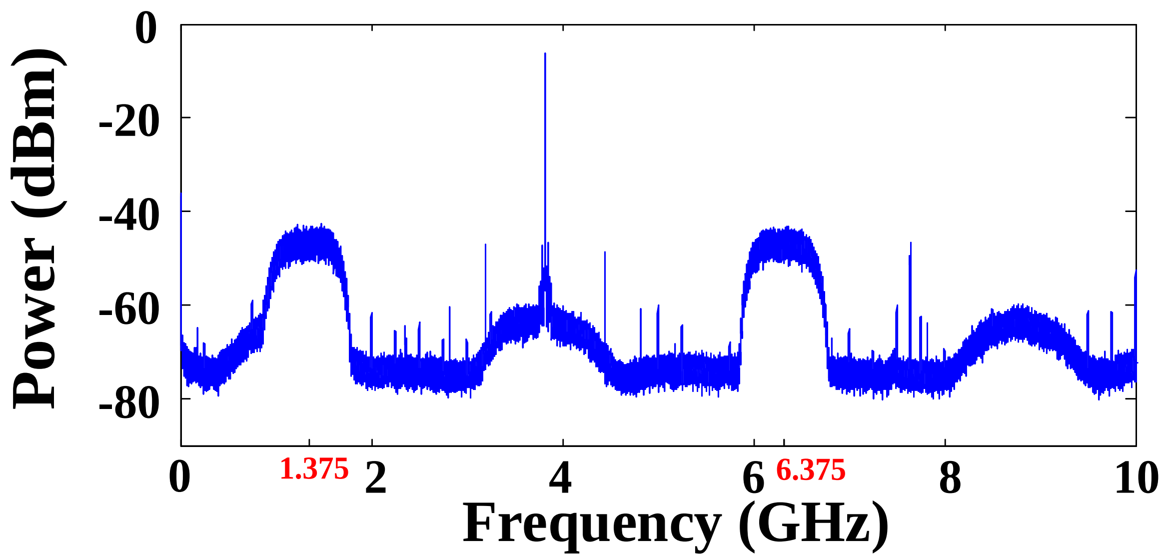

Fig. 4.11. Spectra of the signals at the second output of the coherent receiver (I_{PD2}).

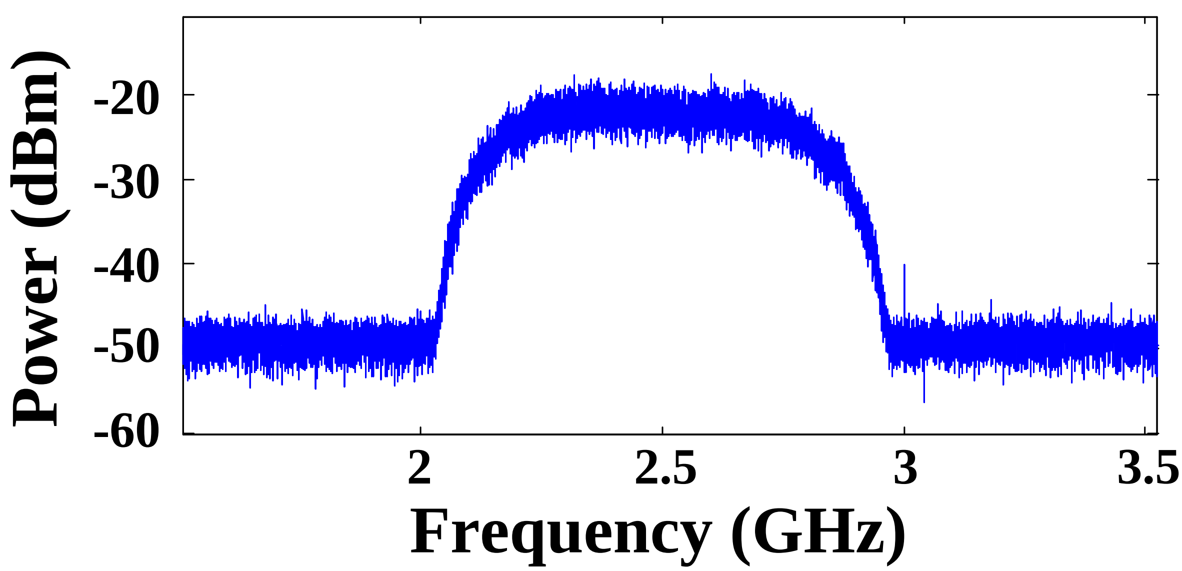

Fig. 4.12. Spectrum of the recovered 16-QAM upstream microwave vector signal 1 at the output of the DSP unit.

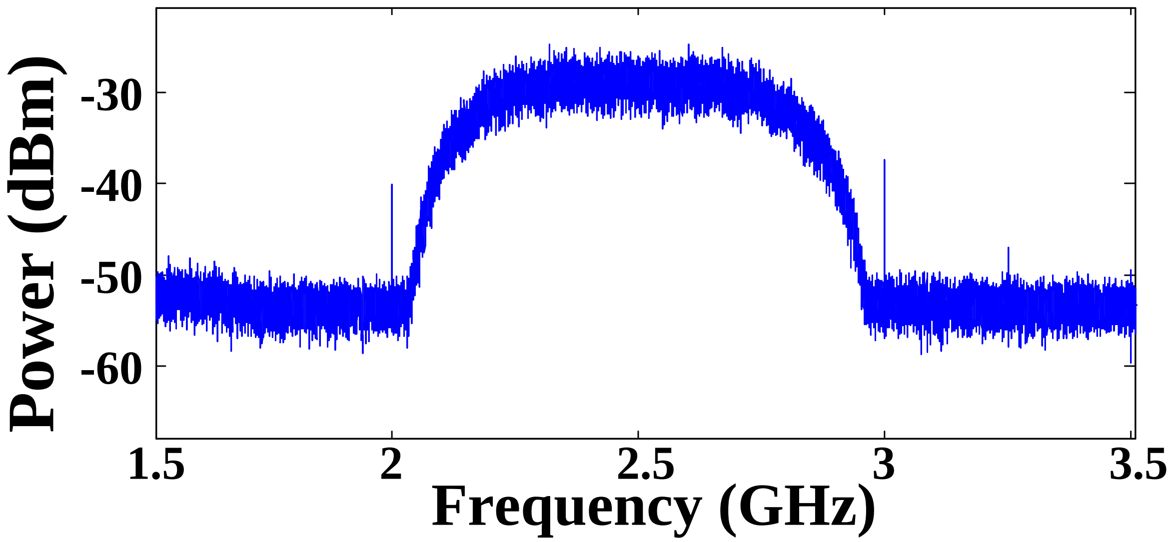

Fig. 4.13. Spectrum of the recovered 16-QAM upstream microwave vector signal 2 at the output of the DSP unit.

As can be seen in Fig. 4.14, the power penalty caused by the wavelength reuse is about 3.4 dB for upstream signal 1 and it is around 2 dB for upstream signal 2. While the power penalty caused by the fiber transmission is around 1 dB. For the third situation, the constellations of the two recovered 16-QAM microwave vector signals are shown in Fig. 4.15. It can be seen that when the received optical power (Here, the received optical power refers to the optical power at the output of PC5) is -11 dBm, the constellations are quite clear for both upstream signals. The corresponding estimated BERs as a function of the received optical power are also calculated, which are shown in Fig. 4.16. Here, the noise after the digital phase noise cancellation (PNC) module is assumed as a stationary random process with Gaussian statistics. Thus, we can calculate the BERs of M-ary QAM from the EVMs based on the relationship given by

$$\overline{P}_{M-QAM}=\frac{2}{\log_2 M}\left(1-\frac{1}{\sqrt{M}}\right)\times erfc\left(\sqrt{\frac{3}{2(M-1)}\times SNR}\right) \tag{4-18}$$

with

$$SNR = 1/EVM^2$$

where erfc ( ) denotes the complementary error function and SNR is signal-to-noise ratio [112]-[114]. When the received optical power is only -19 dBm, the BERs of the two recovered upstream signals are still less than 3×10^{-3}. By using the FEC technique, error-free transmission can be achieved [115-116]. As can be seen in Fig. 4.16, the transmission performance (BERs) of 16-QAM upstream microwave vector signal 1 is better than that of 16-QAM upstream microwave vector signal 2. The reason is that the link loss of Channel A is less than that of Channel B. Second, we measure the EVMs versus the received optical power for the two 16-QAM downstream signals, which is shown in Fig. 4.17. In Fig. 4.17, the received optical power for downstream signal 1 and downstream signal 2 refer to the optical power at the inputs of the corresponding PDs.

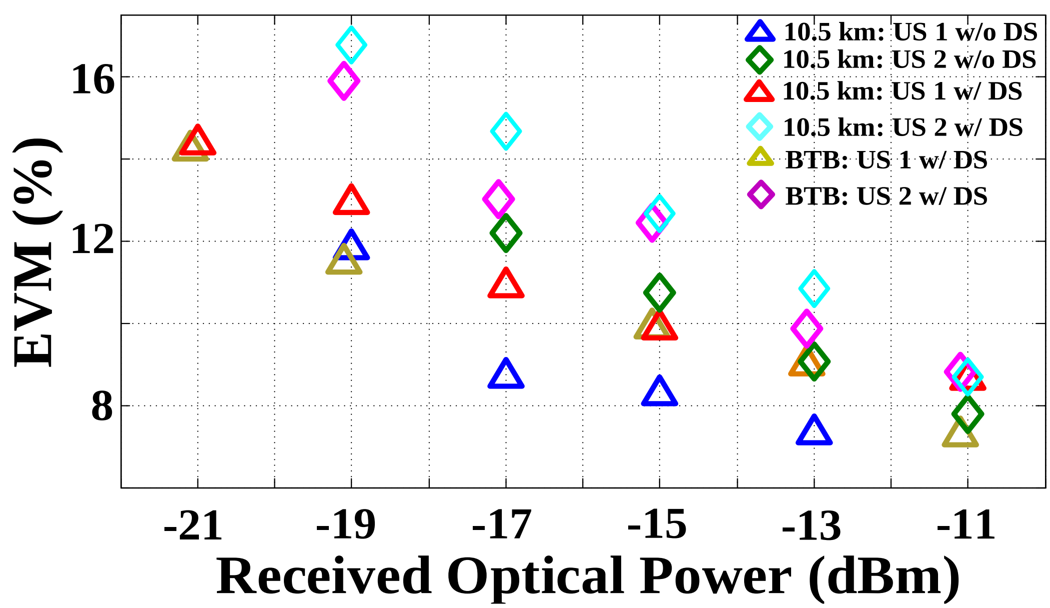

Fig. 4.14. EVM measurements at different received optical power levels for the 16-QAM upstream microwave vector signal 1 and the 16-QAM upstream microwave vector signal 2. US 1: upstream signal 1, US 2: upstream signal 2, DS: downstream signal, BTB: back to back.

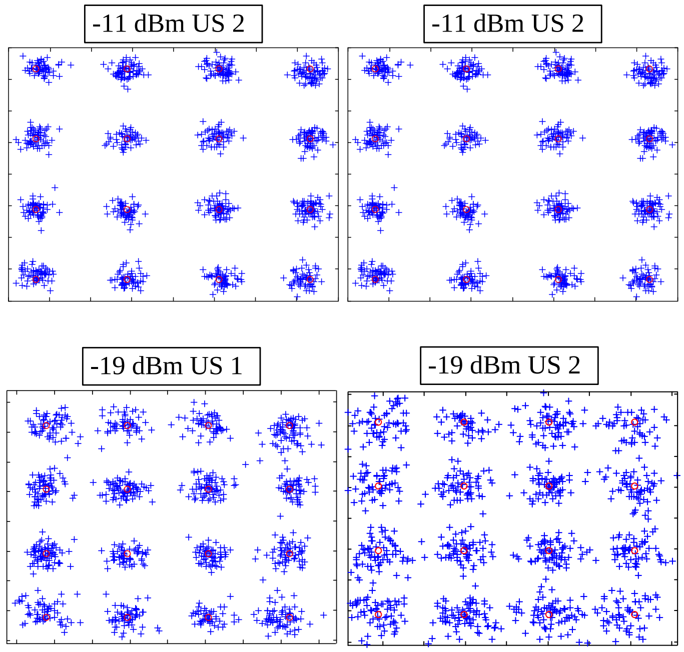

Fig. 4.15. Constellations diagrams of the two recovered 16-QAM upstream microwave vector signals at the output of the DSP unit. US 1: upstream signal 1, US 2: upstream signal 2.

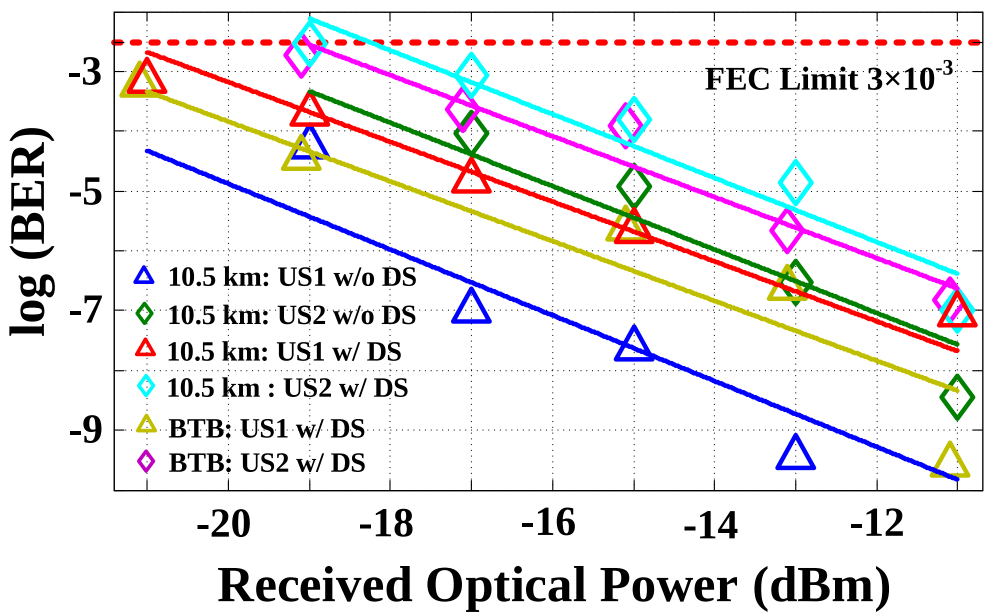

Fig. 4.16. Estimated BERs at different received optical power levels for the 16-QAM upstream microwave vector signal 1 and the 16-QAM upstream microwave vector signal 2. US 1: upstream signal 1, US 2: upstream signal 2, DS: downstream signal, BTB: back to back.

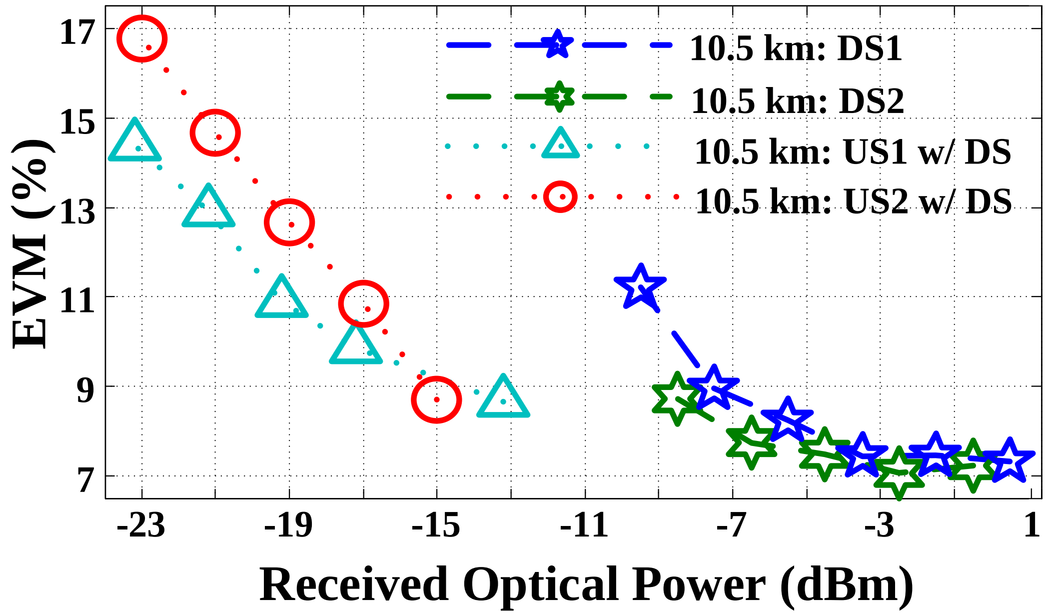

Fig. 4.17. EVMs at different received optical power levels for the two 16-QAM downstream signals and the two 16-QAM upstream signals. US 1: upstream signal 1, US 2: upstream signal 2, DS: downstream signal, DS 1: downstream signal 1, DS 2: downstream signal 2.

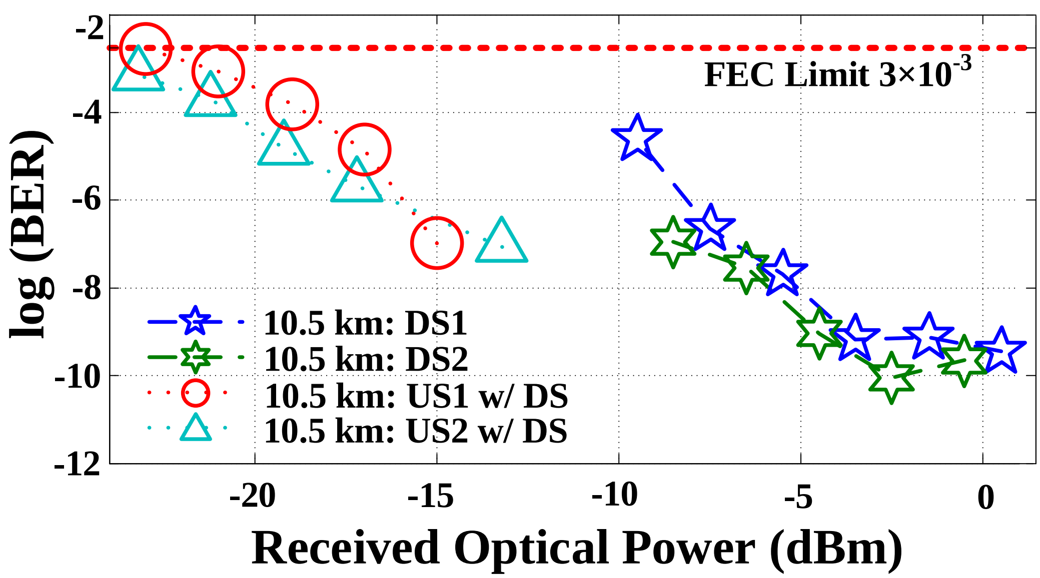

Fig. 4.18. Estimated BERs at different received optical power levels for the two 16-QAM downstream signals and the two 16-QAM upstream signals. US 1: upstream signal 1, US 2: upstream signal 2, DS: downstream signal, DS 1: downstream signal 1, DS 2: downstream signal 2.

While the received optical power for upstream signal 1 and upstream signal 2 refer to the received optical power after the PC5 from Channel A and Channel B, respectively. It can be seen in Fig. 4.17, since coherent detection is used for the upstream signals, the receiver sensitivity for the uplink is much better than that for the downlink. Fig. 4.18 shows the corresponding estimated BERs as a function of the received optical power.

4.3. Conclusions

Firstly, a bidirectional radio over a colorless WDM-PON with wavelength reuse based on polarization multiplexing and coherent detection incorporating digital phase noise cancellation was proposed and experimentally demonstrated. The polarization multiplexing was employed for the downlink to increase the spectral efficiency. Coherent detection with digital phase noise cancellation was used for the upstream transmission to compensate for the degraded transmission performance due to the reuse of the optical wavelength. Error-free transmission of two 2.5-Gbps 16-QAM downstream microwave signals and a 2.5-Gbps 16-QAM upstream microwave signal over a 10.5-km SMF was experimentally demonstrated.

Secondly, a symmetrical radio over colorless WDM-PON based on polarization multiplexing and coherent detection incorporating digital phase noise cancellation was proposed and experimentally demonstrated. For upstream transmission, wavelength reuse was employed, thus colorless WDM-PON was enabled. The wavelength reuse was achieved with the help of coherent detection, to eliminate the impact from the downstream signals. In addition, the symmetry of the network was achieved by using polarization multiplexing for both the downstream and upstream signals, thus the spectral efficiency was also increased. Furthermore, coherent detection with digital signal processing for upstream transmission also increased the receiver sensitivity. The proposed symmetrical radio over colorless WDM-PON was evaluated experimentally. With the proposed DSP algorithms, two 16-QAM upstream signals modulated on a reused wavelength carrying one of the two downstream signals and with phase noises from the transmitter laser source and the LO laser source were successfully recovered. In the experiment, the transmission of two 2.5-Gbps 16-QAM downstream microwave signals and two 2.5-Gbps 16-QAM upstream microwave signals over a 10.5-km SMF was experimentally demonstrated. The power penalty caused by the wavelength reuse is about 3.0 dB.

CHAPTER 5 HIGH SPECTRAL EFFICIENCY COHERENT ROF LINK BASED ON OSSB MODULATION WITH LOW-COST FREE-RUNNING LASER SOURCES FOR UDWDM-PONS

RoF links based on optical double-sideband with carrier (ODSB+C) modulation and direct detection has been widely studied, since it is easy to implement and is less costly [119]. But such an optical modulation scheme makes poor use of the optical spectrum resources, since the spectrum between the two sidebands (the lower and upper sidebands) cannot be utilized effectively. In addition, the information carried by the upper sideband and lower sideband is exactly identical, thus the spectrum of one of the two bandwidths is completely wasted. To solve the problem, RoF links based on the optical single-sideband with carrier (OSSB+C) modulation employing direct detection have been widely studied [120-126]. In addition to an increased spectral efficiency, the use of OSSB+C modulation can also avoid the power penalty resulted from the fiber chromatic dispersion. For direct detection of an OSSB+C-modulated RoF signal, the optical carrier has to be preserved. However, the optical carrier actually does not carry any information and around 90% of the optical power is occupied by the optical carrier, which would decrease significantly the energy efficiency. Thus, OSSB modulation with fully suppressed optical carrier (OSSB) [121] or partially suppressed optical carrier [127] has been proposed to increase the energy efficiency. An RoF signal with a partially suppressed optical carrier has an improved energy efficiency, but the spectral efficiency is still poor. In addition, with a fully suppressed optical carrier, an RoF link becomes much less sensitive to fiber nonlinear effects, which is extremely attractive for ultra-dense wavelength division multiplexing (WDM) RoF passive optical networks (PONs) (UDWDM-RoF-PONs), a potential solution for the next generation broadband wireless access networks (e.g., 5G). In a UDWDM-RoF-PON, however, the channels are very tightly spaced with a channel spacing of 6.25 GHz or less, thus an effective use of the limited spectrum is particularly important. In addition, due to the tightly spaced channels, the use of a WDM filter may not be able to demultiplex the ultradense channels, thus direct detection with a WDM filter is not a feasible solution. To demultiplex the ultradense channels without the use of a WDM filter, one potential solution is to use coherent detection. Through coherent detection, the channels can be separated electronically in a coherent receiver. Furthermore, coherent detection can also provide high receiver sensitivity [99], [111], [117, 118]. On the other hand, coherent detection is sensitive to the phase noise introduced by the transmitter and local oscillator (LO) laser sources. In addition, the unstable frequency difference between the transmitter laser source and LO laser source due to the frequency instability of the two laser sources must be cancelled, to effectively recover the OSSB RoF signal.

In this chapter, I proposed and demonstrate, for the first time to the best of my knowledge, a high spectral efficiency coherent RoF link based on OSSB modulation and phase noise cancellation with low-cost free-running laser sources. The system is transparent to the modulation format and the data rate and it is suitable for both the uplink and downlink transmission in a channel of a coherent UDWDM-RoF-PON. Specifically, at the transmitter, a light wave from a laser source is externally modulated by a real-valued pre-coded microwave vector signal via a dual-parallel Mach-Zehnder modulator (DP-MZM) to generate an OSSB RoF signal. At the output of the DP-MZM, the OSSB RoF signal is sent to a coherent receiver over a single-mode fiber (SMF), to detect the RoF signal, where an LO laser source is employed for coherent detection. A digital signal processing (DSP) algorithm is developed to recover the standard microwave vector signal from the real-valued pre-coded microwave vector signal while cancelling the phase noise and the unstable frequency difference introduced by both the transmitter laser source and LO laser source. The reason that the microwave vector signal is pre-coded is that the DSP algorithm will change the phase and amplitude of the microwave vector signal while cancelling the phase noise. To obtain a standard microwave vector signal, pre-coding the phase term and the amplitude term of the microwave vector signal is necessary. Conventional methods, such as the use of a complicated optical phase-locked loop (PLL) or the use of a digital PLL with an expensive narrow-linewidth laser source (usually < 100 kHz) are not used in the proposed scheme, since the system complexity and the cost would be increased. The proposed DSP-assisted coherent RoF link based on two free-running laser sources with OSSB modulation in a UDWDM-PON is verified by an experiment. In the experiment, a 2.5 Gbps OSSB RoF signal with a channel spacing as narrow as 3 GHz over a 25-km SMF link is demodulated. The channel selection is realized through coherent detection with a digital bandpass filter. For the transmission of a 2.5-Gbps 16 quadrature amplitude modulation (16-QAM) microwave vector signal, the optical sensitivity at the feed forward correction (FEC) level over a 25-km SMF link is -24.8 dBm, while for a 1.875-Gbps 8 phase shift keying (8-PSK) microwave vector signal, the optical sensitivity can reach -29.8 dBm which leaves enough margin to accommodate the splitting losses in the optical distribution network (ODN) [128].

5.1. Principle

Fig. 5.1 shows the schematic diagram of the proposed DSP-assisted RoF link with coherent detection employing OSSB modulation. A continuous-wavelength (CW) light from a laser diode with the power P_s and the angular frequency ω_c is sent via a polarization controller (PC1) to a DP-MZM where it is externally modulated by a real-valued pre-coded microwave vector signal. The real-valued pre-coded microwave vector signal is applied to the DP-MZM via the two RF electrodes with one channel having a $\pi/2$ phase shift. The DP-MZM consists of two sub-MZMs (sub-MZM1 and sub-MZM2). Both sub-MZM1 and the sub-MZM2 are biased at the null transmission point while the main MZM is biased at the quadrature point.

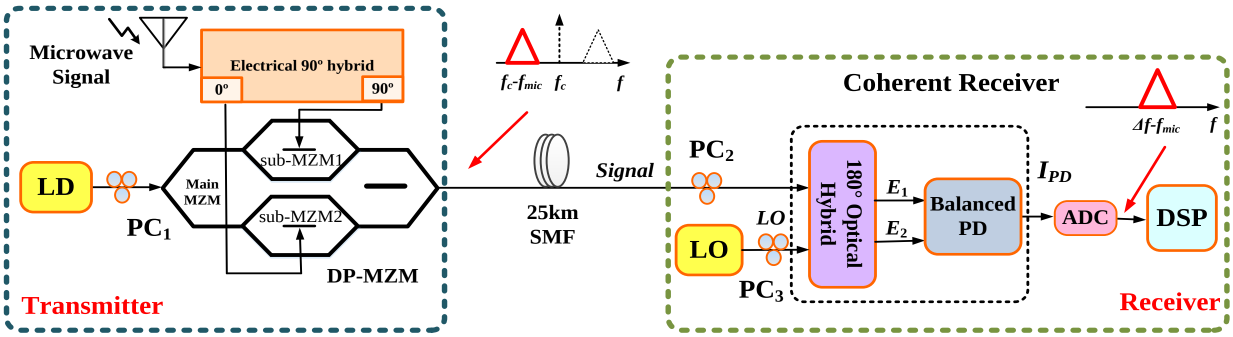

Fig. 5.1. Schematic diagram of the proposed RoF link based on OSSB modulation employing coherent detection incorporating digital frequency difference cancellation and phase noise cancellation. fc: the center frequency of the light from LD, fmic: the center frequency of the microwave signal, Δf: the frequency difference between the frequencies of the LD and the LO laser source.

At the output of the DP-MZM, an OSSB signal without optical carrier is obtained which then is sent to a coherent receiver over a 25-km SMF. At the coherent receiver, a free-running LO laser source is used as the LO laser source to detect the OSSB signal. A DSP algorithm is developed to recover the standard microwave vector signal from the real-valued pre-coded microwave vector signal while cancelling the phase noise and the frequency difference introduced by the transmitter laser source and LO laser source.

The optical field at the output of the DP-MZM can be written by

$$E_s\left(t\right)=\sqrt{2P_s}/2\begin{bmatrix}\sin\left(\pi S_{RF}(t)/2V_\pi\right)e^{j(\omega_c t+\phi_c(t)+\pi/4)}\\ +\sin\left(\pi\hat{S}_{RF}(t)/2V_\pi\right)e^{j(\omega_c t+\phi_c(t)-\pi/4)}\end{bmatrix} \quad (5\text{-}1)$$

where $S_{RF}(t)$ is the real-valued pre-coded microwave vector signal, $\hat{S}_{RF}(t)$ is the Hilbert transform of the signal $S_{RF}(t)$, ω_c is the angular frequency and $\phi_c\left(t\right)$ is the phase of the light wave from the transmitter laser source, and V_π is the half-wave voltage of the DP-MZM. Here, the real-valued pre-coded baseband vector signal is expressed as

$$\begin{aligned}&S_{real-valued-baseband}\left(t\right)=r_m\cos\left(\omega_s t+\theta_n\right)\\&m=1,2,...,\mathrm{M}_1;\quad n=1,2,...,\mathrm{M}_2\end{aligned} \quad (5\text{-}2).$$

The real-valued pre-coded baseband vector signal can be viewed as a signal with the combined amplitude (r_m) and phase (θ_n) modulation. {r_m, $1\leqslant m\leqslant M_1$} denotes the set of M_1 possible amplitudes while {θ_n, $1\leqslant n\leqslant M_2$} is the M_2 possible phases of the carrier that convey the transmitted information [129]. ω_s is equal to the value of the symbol rate for the pre-coded baseband vector signal. Then, the real-valued pre-coded baseband vector signal is up converted to the microwave band. The real-valued pre-coded microwave vector signal $S_{RF}(t)$ can be written by

$$\begin{aligned}&S_{RF}\left(t\right)=r_m\cos\left(\omega_s t+\theta_n\right)\cdot\cos\left(\omega_{RF}t\right)\\&m=1,2,...,\mathrm{M}_1;\quad n=1,2,...,\mathrm{M}_2\end{aligned} \quad (5\text{-}3)$$

and the Hilbert transform of the signal $S_{RF}(t)$ can be expressed as

$$\hat{S}_{RF}(t) = r_m \cos\left(\omega_s t + \theta_n\right) \cdot \sin\left(\omega_{RF} t\right)$$
$$m = 1, 2, ..., \mathrm{M}_1; \qquad n = 1, 2, ..., \mathrm{M}_2 \tag{5-4}$$

where ω_{RF} is the center frequency of the real-valued pre-coded microwave vector signal [130].

After the OSSB modulation, the optical signal at the output of the DP-MZM is sent to the receiver over an SMF. At the receiver side, a coherent receiver with a free-running LO laser source is used to coherently detect the OSSB RoF signal. The optical field of the light wave from the LO laser source is given by

$$E_{LO}(t) = \sqrt{2P_{LO}} e^{j(\omega_{LO} t + \phi_{LO}(t))} \tag{5-5}$$

where P_{LO} is the optical power and ω_{LO} is the angular frequency, and $\phi_{LO}(t)$ is the phase term. By tuning the two PCs (PC_2 and PC_3), the polarization direction of the OSSB RoF signal is adjusted to be parallel to the polarization direction of the light wave from the LO at the inputs of the 2 × 2 power splitter. At the two outputs of the 2 × 2 power splitter, the optical signals can be expressed as

$$E_1 = \sqrt{L_h}(\sqrt{L_s} E_s + E_{LO}) \tag{5-6}$$

$$E_2 = \sqrt{L_h}(\sqrt{L_s} E_s - E_{LO}) \tag{5-7}$$

where L_s is the link loss and L_h is the loss caused by the 2 x 2 power splitter.

Then, the two optical signals are applied to a balanced PD. The electrical signal at the output of the balanced PD can be written by

$$I_{PD} = R\left(E_1 \cdot E_1^* - E_2 \cdot E_2^*\right)/2$$
$$= 2RL_h\sqrt{P_s P_{LO} L_s}\begin{bmatrix} \sin\left(\pi S_{RF}(t)/2V_\pi\right) \\ \times\cos\left(\Delta\omega t + \varphi_c(t) - \varphi_{LO}(t) + \pi/4\right) \\ +\sin\left(\pi \hat{S}_{RF}(t)/2V_\pi\right) \\ \times\cos\left(\Delta\omega t + \varphi_c(t) - \varphi_{LO}(t) - \pi/4\right) \end{bmatrix} \tag{5-8}$$

where R is the responsivity of the balanced PD. If we assume that $S_{RF}(t)$ is a small signal, (5-8) can be rewritten as

$$I_{PD} \approx \frac{\pi RL_h\sqrt{P_s P_{LO} L_s}}{V_\pi}\begin{bmatrix} S_{RF}(t)\times\cos\begin{pmatrix} \Delta\omega t + \varphi_c(t) \\ -\varphi_{LO}(t) + \dfrac{\pi}{4} \end{pmatrix} \\ +\hat{S}_{RF}(t)\times\cos\begin{pmatrix} \Delta\omega t + \varphi_c(t) \\ -\varphi_{LO}(t) - \dfrac{\pi}{4} \end{pmatrix} \end{bmatrix} \tag{5-9}$$

where $\Delta\omega$ is the frequency difference between the transmitter laser source and the LO laser source, $\Delta\omega = \omega_c - \omega_{LO}$. Apparently, I_{PD} is an SSB signal [131]. Then, the electrical signal, I_{PD}, is sampled and digitized by an analog-to-digital converter (ADC). Using a DSP module, we can calculate the square of the sampled signal,

$$\begin{aligned} I_o &= I_{PD}^2 \\ &= \pi^2 R^2 L_h^2 P_s P_{LO} L_s / 4V_\pi^2 \times r_m^2 \cos\left(2\omega_s t + 2\theta_n\right) \\ &+\pi^2 R^2 L_h^2 P_s P_{LO} L_s / 4V_\pi^2 \times r_m^2 \\ &-\pi^2 R^2 L_h^2 P_s P_{LO} L_s / 2V_\pi^2 \times\left[r_m^2 \cos^2\left(\omega_s t + \theta_n\right)\right] \\ &\times\left[\sin\left(2\Delta\omega t - 2\omega_{RF} t + 2\varphi_c(t) - 2\varphi_{LO}(t)\right)\right] \end{aligned} \tag{5-10}$$

In (5-10), it can be seen that the first term is independent of both the phase noise and the frequency difference between the two laser sources, and it contains all the transmitted information. A digital bandpass filter can be used to extract the signal which is expressed as the first term in (5-10). Then, we have

$$I_1 = \pi^2 R^2 L_h^2 P_s P_{LO} L_s / 4V_\pi^2 \times r_m^2 \cos\left(2\omega_s t + 2\theta_n\right) \tag{5-11}$$

Here the amplitude and phase information in (5-11) are r_m^2 and $2\theta_n$, respectively. Thus, the amplitude r_m and phase θ_n of the driving signal $S_{RF}(t)$ must be pre-coded in order to obtain the standard vector signal at the receiver. Table 5.1 shows the possible amplitudes and phases for the pre-coded QPSK, 8-PSK and 16-QAM vector signals. Fig. 5.2 shows the constellations for the pre-coded vector signals (QPSK, 8-PSK and 16-QAM) and the standard vector signals (QPSK, 8-PSK and 16-QAM). The phases of the pre-coded QPSK, 8-PSK and 16-QAM signals are half of the generated standard QPSK, 8-PSK and 16-QAM signals at the output of the DSP module and the amplitudes of the generated standard 16-QAM signal at the output of the DSP module are the square of the amplitudes of the pre-coded 16-QAM signal. After the DSP module, the standard vector signal (QPSK, 8-PSK, 16-QAM) which is free from phase noise and unstable frequency difference introduced by the two laser sources is achieved.

TABLE 5.1. THE POSSIBLE AMPLITUDES AND PHASES FOR THE PRE-CODED QPSK, 8-PSK AND 16-QAM SIGNALS

	Amplitudes (r_m)	Phases (θ_n)
QPSK	1	$\pi/8, 5\pi/8, 11\pi/8, 15\pi/8$
8-PSK	1	$\pm\pi/16, \pm5\pi/16, \pm9\pi/16, \pm13\pi/16$
16-QAM	$1, \sqrt{2}$	$\pm\pi/16, \pm5\pi/16, \pm9\pi/16, \pm13\pi/16$

5.2. Experiment

An experiment based on the setup shown in Fig. 5.1 is conducted. A picture of the experimental setup is shown in Fig. 5.3.

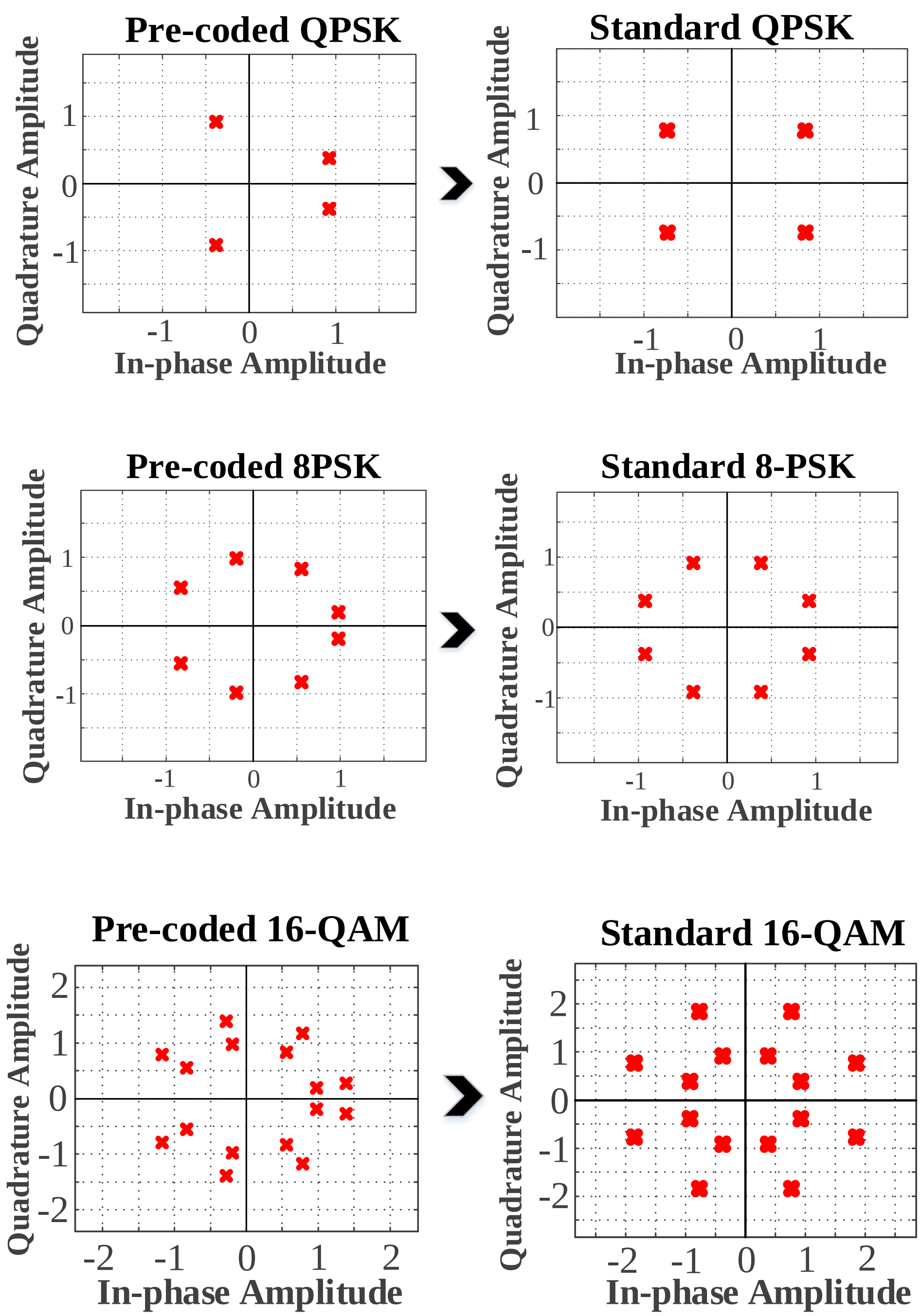

Fig. 5.2. The constellations for the pre-coded QPSK, 8-PSK, 16-QAM and the standard QPSK, 8-PSK, 16-QAM.

A CW light at 1549.947 nm from a tunable laser source (TLS, Agilent N7714A) with a linewidth of 100 KHz and an optical power of 16 dBm is sent to the DP-MZM (JDS-U) via

PC$_1$. (Note that the polarization controller can be replaced by a polarization maintaing fiber).

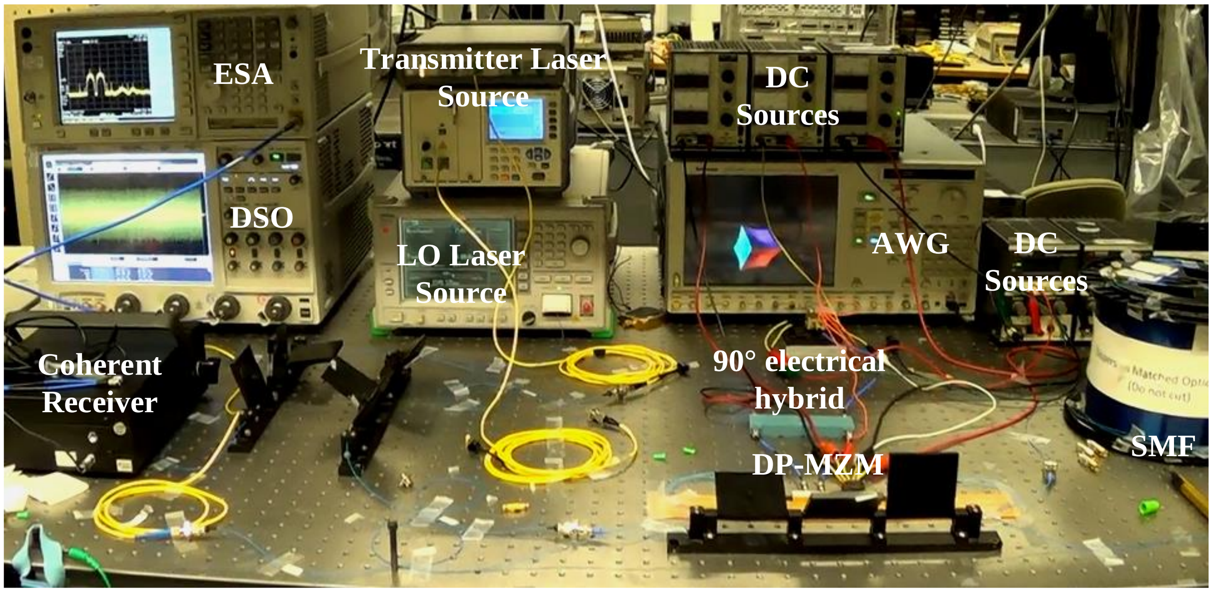

Fig. 5.3. Photograph showing the experimental setup of the proposed coherent RoF link based on OSSB modulation. AWG: arbitrary-wave generator, DP-MZM: dual-parallel Mach-Zehnder modulator, DSO: digital storage oscilloscope, DC Sources: direct current sources, ESA: electrical spectrum analyzer, LO laser source: local oscillator laser source, SMF: single-mode fiber.

The half-wave voltage of the DP-MZM is about 6.33 V and the bandwidth is 10 GHz. A real-valued pre-coded microwave vector signal with a center frequency of 2 GHz and a symbol rate of 625 MSymbol/s generated by an arbitrary waveform generator (Tektronix AWG7102) is used to drive the DP-MZM via the two RF ports. A broadband electrical 90^{o} hybrid (Crane Aerospace & Electronics, QHM-4R-9.5G) provides π/2 phase difference between the two drive signals. Both sub-MZM1 and sub-MZM2 in the DP-MZM are biased at the null transmission point while the main MZM is biased at the quadrature point. An OSSB RoF signal with no optical carrier is generated at the output of the DP-MZM (The suppression ratio for the optical carrier is about 30 dB, while the suppression ratio for the upper sideband is more than 20 dB), which is then transmitted over a 25 km SMF and coherently detected at the coherent receiver (Discovery Semiconductors DP-QPSK 40/100 Gbps Coherent Receiver Lab Buddy). A second CW light at 1549.988 nm with a linewidth of 700 KHz and an optical power of 7.8 dBm from a second TLS (Anritsu MG9638A) used as the LO laser source is applied to the coherent receiver via the LO port. The frequency difference between the transmitter laser source and the LO laser source is around 5.1 GHz. By tuning PC_2 and PC_3, the light wave from the LO laser source is co-polarized with the OSSB RoF signal. Note that in a practical system, we can use a polarization diversity receiver instead of tuning PC_2 and PC_3 [81]. An alternative solution is to use a dynamic polarization controller to make the optical signal from the transmitter and the light wave from the LO laser source be co-polarized [101]. At the output of the coherent receiver, a Digital Storage Oscilloscope (Agilent DSO-X 93204A) is employed to perform the analog-to-digital conversion with a sampling rate of 80 GSa/s to convert the electrical signal to a discrete-time signal. Then, the discret-time signal (I_{PD}) is processed offline in a computer (Since the function of the DSP unit is just like an analog bandpass filter plus an analog envelope detector and a microwave vector signal demodulator, in order to avoid using a high sampling-rate analog to digital converter (ADC), in a practical system, the ADC can be replaced with these analog circuits).

First, we apply a real-valued pre-coded 8-PSK microwave vector signal with its spectrum is shown in Fig. 5.4 to the DP-MZM. The real-valued pre-coded 8-PSK microwave vector signal has a center frequency of 2 GHz and a symbol rate of 625 MSymbol/s or a bit rate of 1.875 Gbps. Fig. 5.5 shows the spectrum at the output of the coherent receiver. It can be seen that the detected real-valued pre-coded 8-PSK microwave vector signal (the signal with a center frequency of 3.1 GHz) in Fig. 5.5 is just the mixing product of the 2 GHz transmitted microwave vector signal and the 5.1 GHz electrical carrier whose frequency is just the frequency difference between the two laser sources. In addition, the 5.1 GHz electrical carrier and the upper-sideband signal are suppressed by more than 20 dB, which proves that an OSSB RoF signal with a bandwidth of around 3 GHz is successfully generated (If a bias voltage controller is employed for the DP-MZM, the leakages from both the optical carrier and upper sideband signal can be below the noise floor. So they will not affect other signals in other channels). After being digitized and processed in the DSP module to cancel both the phase noise and frequency difference between the two laser sources, a standard 8-PSK signal is obtained. The measured constellation for the recovered standard 8-PSK signal is shown in Fig. 5.6(a), when the received optical power is -23.8 dBm.

Then, we also apply a real-valued pre-coded QPSK microwave vector signal with a bit rate of 1.25 Gbps and a real-valued pre-coded 16-QAM microwave vector signal with a bit rate of 2.5 Gbps to the DP-MZM, respectively. The symbol rates for the QPSK and 16-QAM signals are both 625 MSymbol/s and the center frequencies are 2 GHz. The measured constellations for the recovered standard vector signals are shown in Fig. 5.6(b) and (c). As can be seen, the constellations are very clear which again proves that the OSSB RoF signal is demodulated successfully. Since the function of the DSP module is just like the function of an envelope detector, the Gaussian white noise is higher for the vector signals that have larger amplitudes. That is the reason why in Fig. 5.6(c) the constellations at the outer circle are not as clear as those at the inner circle.

To verify the effectiveness of the proposed phase noise cancellation (PNC) technique, we also measure the constellations of the detected signal for an intensity-modulation and coherent-detection (IM/CD) RoF link without using precoding and a PNC module. The experimental setup is shown in Fig. 5.7. Here, the microwave vector signal is a standard 16 quadrature amplitude modulation (16-QAM) signal with a center frequency of 2.5 GHz and a symbol rate of 625 MSymbol/s.

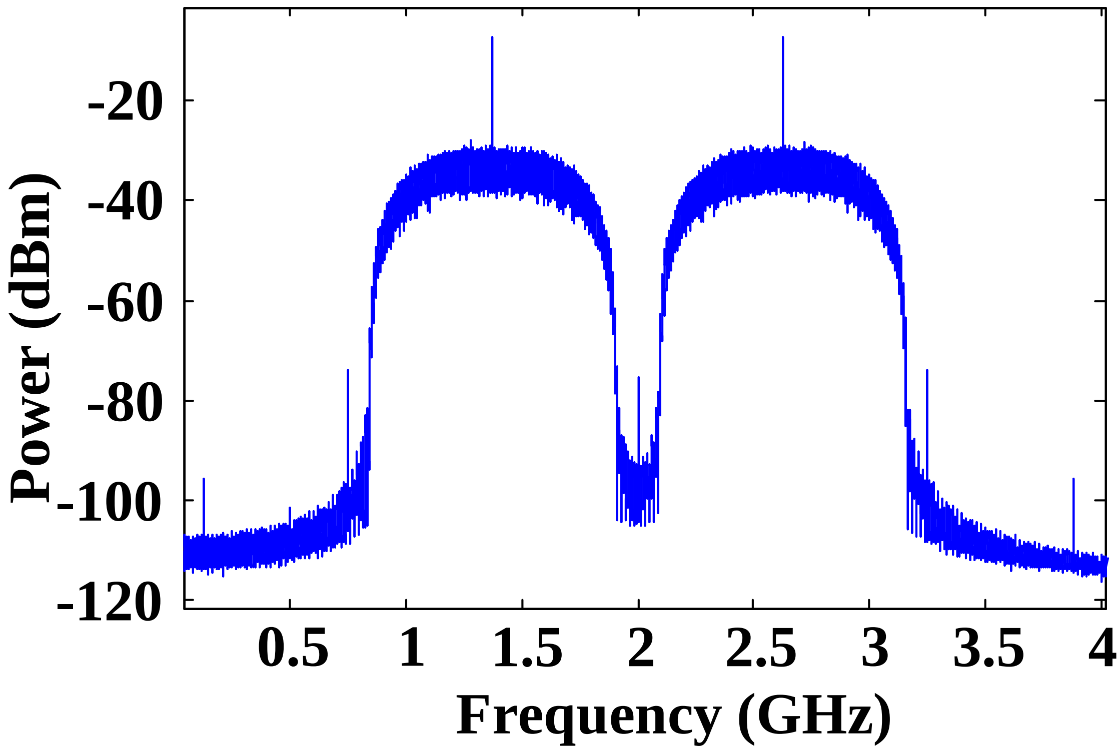

Fig. 5.4. Spectrum of the real-valued pre-coded 8-PSK microwave signal (Center frequency: 2GHz, Symbol rate: 625MSymbol/s, Bit rate: 1.875 Gbps).

The linewidth of the transmitter laser source is 100 kHz and the linewidth of the LO laser source is 700 kHz. The frequency stability for the transmitter laser source is ± 0.3 GHz/24 hours, and for the LO laser source it is ± 100 MHz/hour. The detected signal at the output of the coherent receiver is affected by the unstable frequency difference and the phase noise introduced by the two laser sources. A conventional digital phase lock loop is not able to track the unstable frequency difference between the two laser sources. Fig. 5.8 shows the spectrum of the signal at the output of the coherent receiver. After coherent detection and sampling, two digital bandpass filters are used to select the upper sideband signal and lower sideband signal. Then, the two signals are demodulated in the DSP unit. The constellations of the 16-QAM microwave signals (upper and lower sidebands) are shown in Fig. 5.9. As can be seen, the recovered 16-QAM microwave vector signals are strongly affected by the phase noise and the unstable frequency difference introduced by the two laser sources.

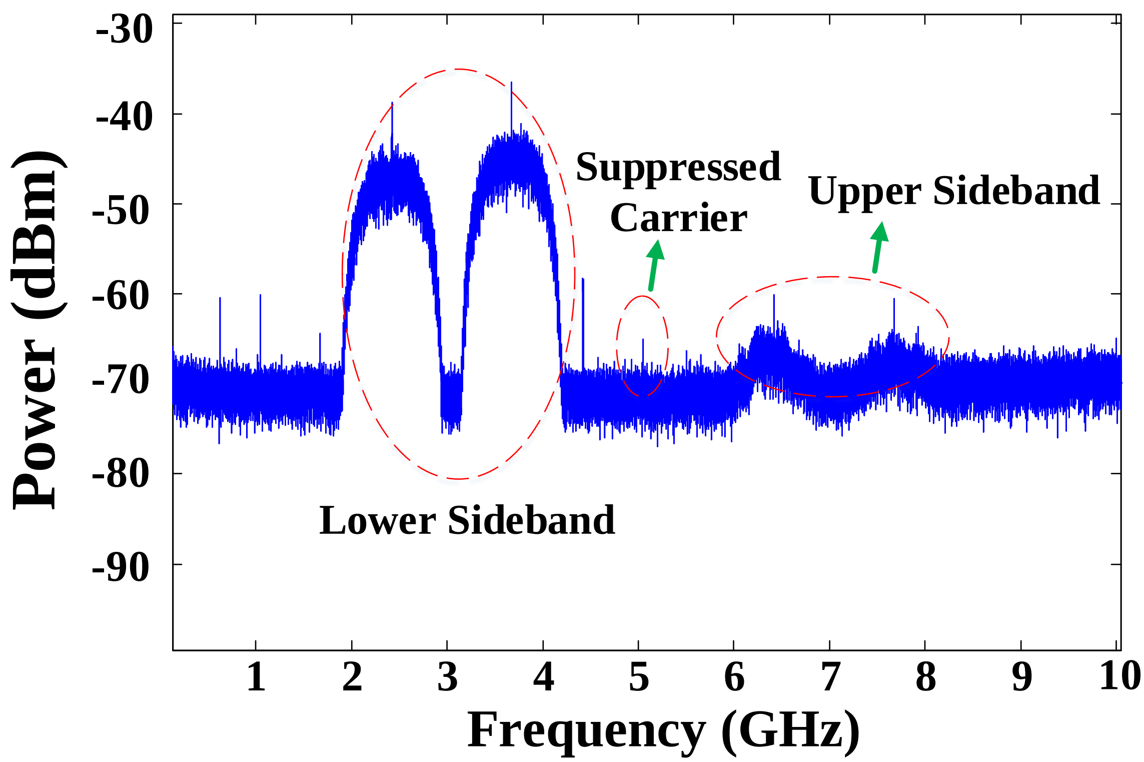

Fig. 5.5. Spectrum of the signal at the output of the coherent receiver.

To further study the performance of the whole system, error vector magnitudes (EVMs) for the recovered standard vector signals (QPSK, 8-PSK and 16-QAM) versus the received optical power levels are also measured, which are shown in Fig. 5.10. In Fig. 5.10, the symbol rates for the QPSK, 8-PSK and 16-QAM are all 625 MSymbol/s and the center frequencies for their corresponding real-valued pre-coded input microwave vector signals are 2 GHz. As can be seen, even the received optical power is only -31.8 dBm, the EVMs for the three different modulation-format vector signals can be still less than 21%.

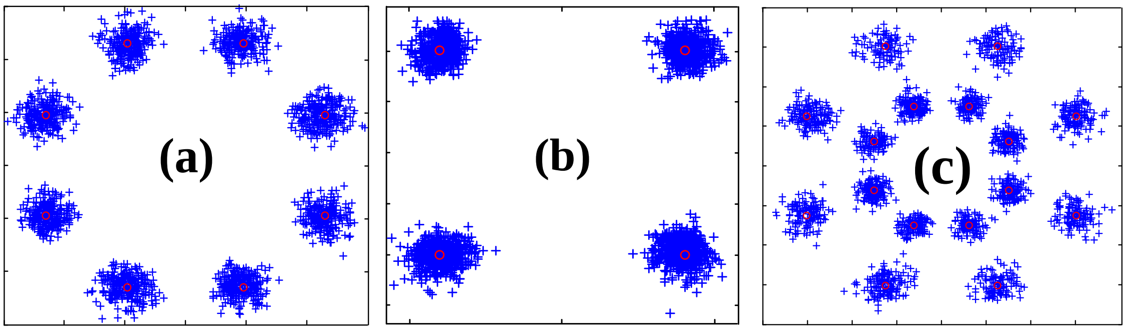

Fig. 5.6. The measured constellations for the recovered standard vector signals. (a) The standard 8-PSK signal (the received optical power: -23.8 dBm), (b) the standard QPSK signal (the received optical power: -23.8 dBm), (c) the standard 16-QAM signal (the received optical power: -24.9 dBm).

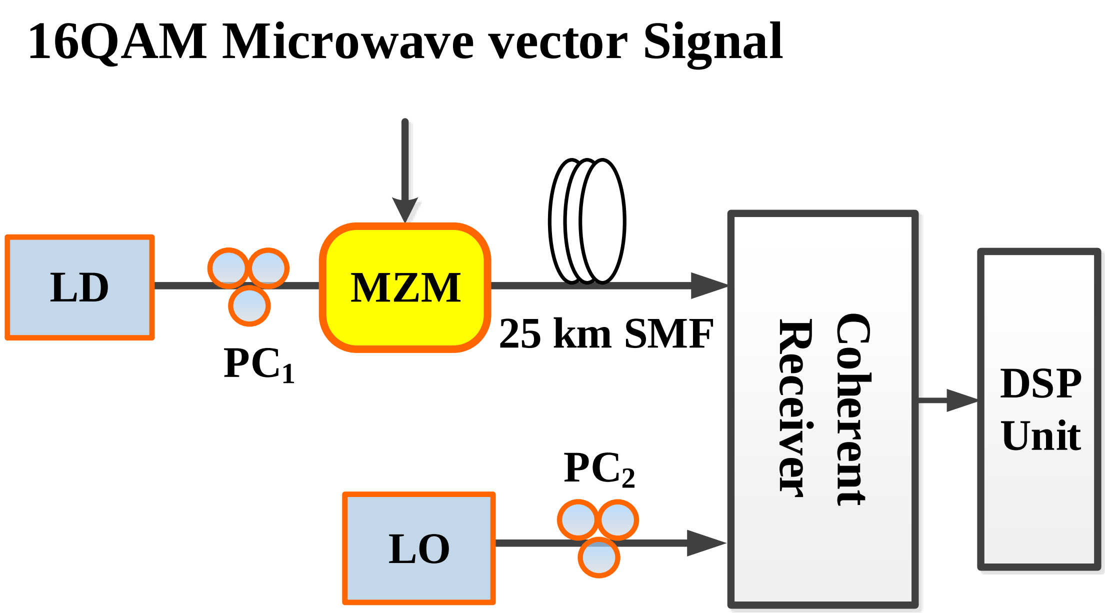

Fig. 5.7. Schematic diagram of an IM/CD RoF link without a PNC module and precoding.

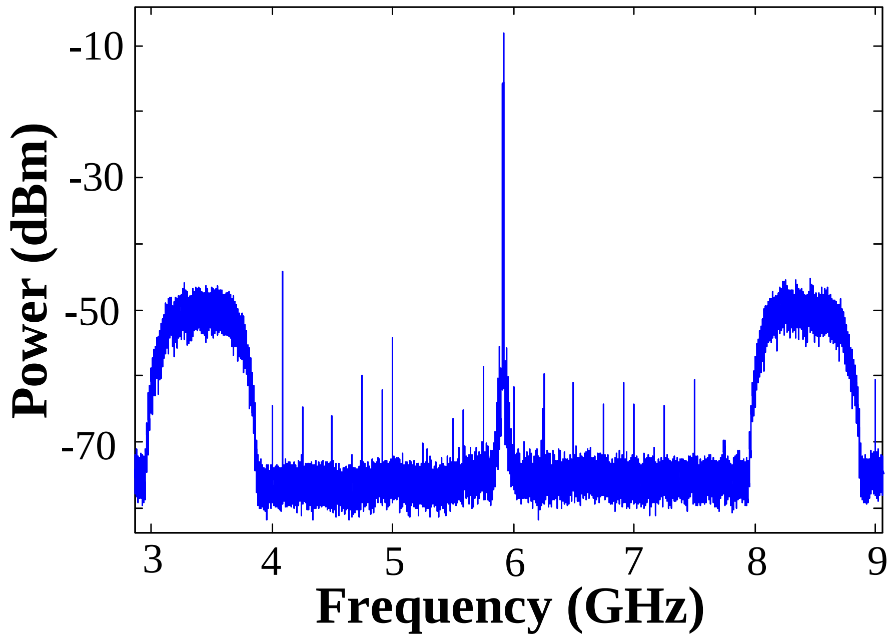

Fig. 5.8. Spectrum of the signal at the output of the coherent receiver for the IM/CD RoF link without precoding and a PNC module.

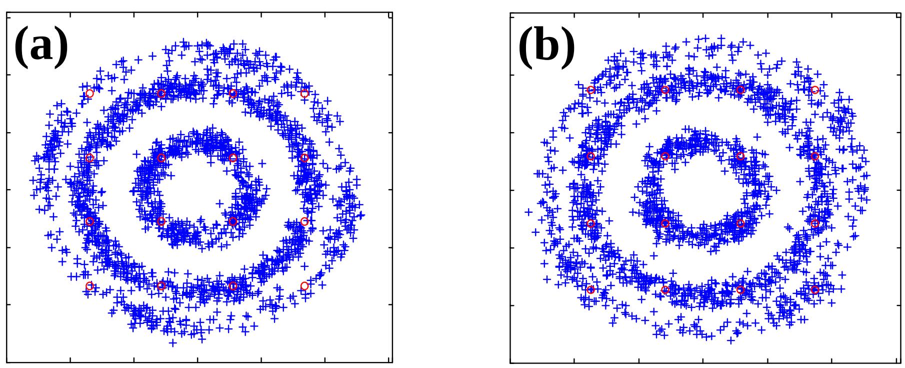

Fig. 5.9. The measured constellations of the signals at the output of the coherent receiver for an IM/CD RoF link. (a) The upper sideband signal, and (b) the lower sideband signal.

Then, the bit error rates (BERs) are estimated based on the relationship between an EVM and a BER [132], [133]. Here we assume that the noise after the DSP module is a stationary random process with Gaussian statistics. Fig. 5.11 shows BERs as a function of the received optical power calculated from the measured EVMs. For the recovered standard 8-PSK signal, when the received optical power is -29.8 dBm, the BER can reach 7.1×10^{-4}. When the received optical power is -24.9 dBm, for the 16-QAM signal, the BER is less than 1×10^{-3}. While for the QPSK signal, when the received optical is only -31.8 dBm, the BER is still less than 1×10^{-6}. By using a state-of-the-art FEC technique, error-free transmission can be achieved when a raw BER is less than 3×10^{-3}.

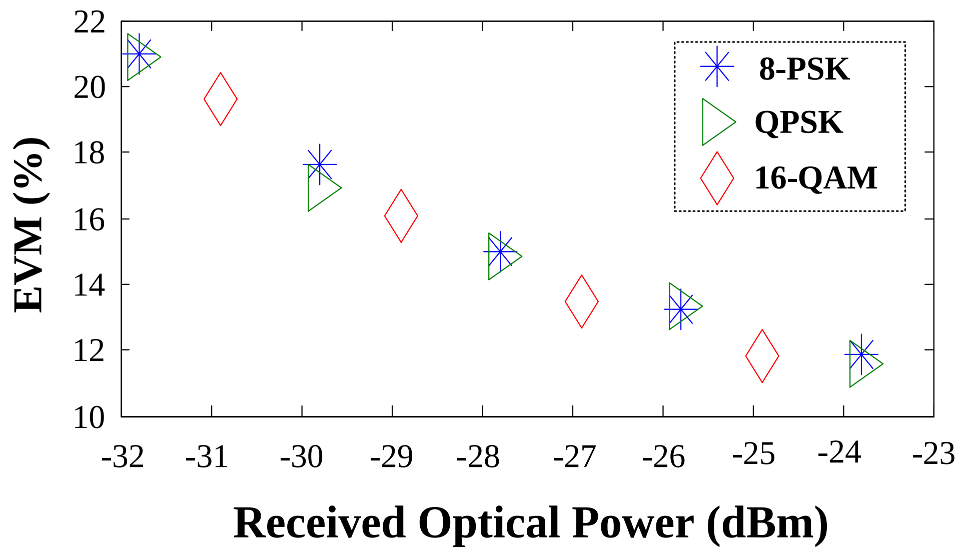

Fig. 5.10. EVM measurements at different received optical power levels for the recovered QPSK, 8-PSK and 16-QAM signals transmitted over a 25-km SMF.

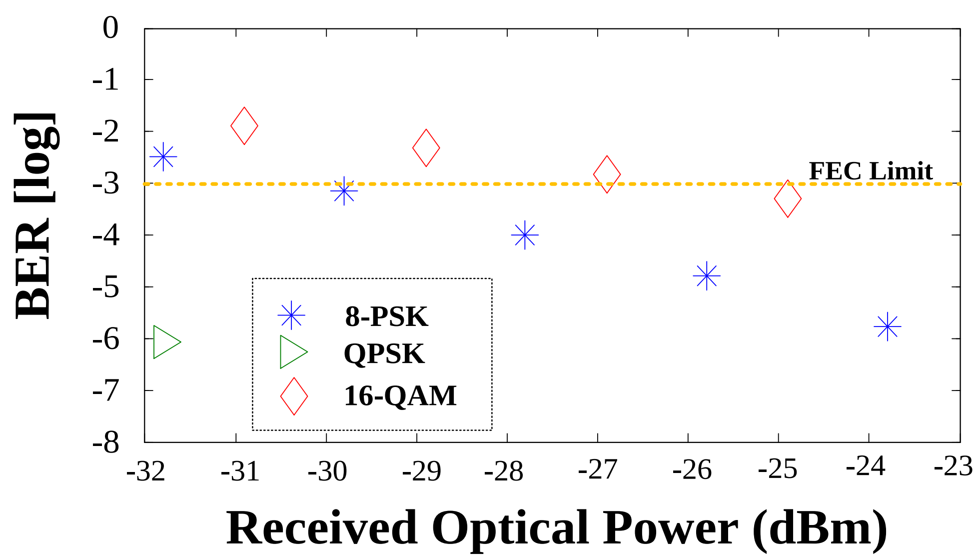

Fig. 5.11. BERs at different received optical power levels for the recovered QPSK, 8-PSK and 16-QAM signals transmitted over a 25-km SMF.

5.3. Conclusions

An OSSB RoF link based on coherent detection for UDWDM-PONs was proposed and experimentally demonstrated. By proper pre-coding the input real-valued microwave vector signals and using a DSP algorithm, the real-valued microwave vector signals could be recovered. In the experiment, the phase noise and the unstable frequency difference introduced by the two free-running laser sources (the transmitter laser source and LO laser source) was cancelled through the DSP algorithm. Different modulation-format real-valued pre-coded microwave vector signals (1.25-Gbps QPSK, 1.875-Gbps 8-PSK and 2.5-Gbps 16-QAM) with center frequencies of 2 GHz were transmitted over a 25-km SMF and recovered at the coherent receiver. The channel spacing could be as narrow as 3 GHz and the data rate for each channel could reach 2.5 Gbps. The proposed RoF link had a very high sensitivity. For the transmission of a 2.5-Gbps 16-QAM microwave vector signal over a 25-km SMF, the link had a sensitivity of -24.8 dBm (FEC level), while for a 1.875-Gbps 8-PSK microwave vector signal, the sensitivity could reach -29.8 dBm.

CHAPTER 6 4 × 4 MULTI-INPUT MULTI-OUTPUT MICROWAVE PHOTONIC LINK BASED ON COHERENT DETECTION

The transmission of microwave signals over an optical fiber, or an RoF link, has been considered as a simple, low cost and low-power-consumption solution for broadband wireless signal transmission [7, 8]. Such links also enable centralized radio access network (C-RAN) architecture which can reduce the network complexity and system cost, offering improved network performance via coordinated multi-points and improved network energy efficiency [134]-[138]. In addition, in a C-RAN the central stations (CSs) are located in physically secured locations thus IPsec for the links between CSs and the core network is no longer needed. On the other hand, to meet the requirement of huge amount of mobile and wireless local area network data and enable multiple-input multiple-output (MIMO) - a key technology for the fifth-generation (5G), RoF links are required to transmit multiple wireless signals over a single wavelength. One solution is to transmit digitized in-phase (I) and quadrature (Q) components of multiple wireless signals in a binary sequence via time-division multiplexing (TDM), which is widely used in today's mobile fronthaul [4, 139]. Although such a technique can offer excellent robustness against noise, the spectral efficiency is very low since ON-OFF-keying (OOK) modulation format is employed [139]. In addition, the use of TDM inherently limits the performance in terms of latency of the system. To improve the bandwidth efficiency and decrease the latency, the transmission of multiple wireless signals via frequency-division multiplexing (FDM) in a single wavelength has been proposed [140]. The main disadvantage of the two solutions [139, 140] is that at the remote radio head (RRH) electrical local oscillators

(ELOs) with different frequencies for different wireless signals used to realize frequency conversion, are required, making the RRH very costly. To avoid using ELSs at the RRH, several schemes have been proposed [141, 142]. In [141], a simple 2 × 2 MIMO orthogonal frequency division multiplex (OFDM) RoF link employing single-sideband modulation was proposed, which can tolerate the chromatic dispersion existing in the fiber link. To cancel the high peak-to-average-power ratio due to the OFDM modulation [141], single-sideband single-carrier modulation which has a lower peak-to-average-power ratio was employed [142]. For both schemes, to realize a 2 × 2 MIMO RoF link, multiple optical wavelengths to carry different wireless signals have to be employed [141, 142]. Thus, multiple optical wavelengths, multiple modulators, and multiple photodiodes (PDs) have to be used, which would make the system complicated and costly. In addition, the spectral efficiency for each channel (each wavelength) is very low. Thus, multiple optical wavelengths, multiple modulators, and multiple photodiodes (PDs) have to be used, which would make the system complicated and costly. In addition, the spectral efficiency for each channel (each wavelength) is very low. To simplify the system, increase the spectral efficiency and avoid using ELOs at the RRH, several MIMO optical-wireless integration systems have been proposed in which optical polarization multiplexing has to be employed. For example, a 2 × 2 MIMO RoF link implemented using two orthogonally polarized optical light waves to carry two microwave signals was reported [143]-[155]. The limitation in [143]-[154] is that only 2 × 2 MIMO can be employed. In this chapter, two coherent RoF links are proposed which enable 4 × 4 MIMO without using FDM. In addition, no ELO is needed in the RRHs. Both schemes are theoretically and experimentally demonstrated. For the first scheme, three 1 Gbps OFDM signals and a 1.5 Gbps OFDM signal all with 16 quadrature amplitude modulation (16-QAM) at an identical microwave carrier frequency of

2.91 GHz modulated on a single optical carrier are transmitted over a 10-km single-mode fiber (SMF). When the received optical power is only -20.3 dBm, the raw bit error rates of the four wireless signals are still less than 3×10^{-3} which enables error-free transmission if the state-of-the-art forward error correction (FEC) technique is employed. However, the center frequency of the transmitted wireless signals is not transparent to the RoF link due to the need of two bandpass filters to eliminate the two pilot tones. For future optical-wireless systems, the center frequency and the data rate should be transparent to the optical link. Thus, a novel high spectral efficiency RoF link based on coherent detection and DSP to transmit four microwave signals over a single optical carrier is proposed. The proposed scheme is validated by an experiment. The transmission of four 2.5-Gbps 16 quadrature amplitude modulation (16-QAM) microwave signals with an identical center frequency of 2.5 GHz over 10-km SMF with a total data rate of 10 Gbps is achieved. The error vector magnitudes (EVMs) are measured to be 9.5%.

6.1. A 4 × 4 MIMO coherent microwave photonic link with optical independent sideband and optical orthogonal modulation

In this section, an RoF link to transmit four wireless signals with an identical microwave center frequency without using FDM over a single optical wavelength based on optical independent sideband (OISB) modulation and optical orthogonal modulation incorporating optical coherent detection and digital signal processing (DSP) is proposed and experimentally demonstrated. In the proposed scheme, four independent microwave signals are transmitted to the receiver, which enables 4 × 4 MIMO and no ELOs are needed at the RRH for frequency conversion. Compared with the schemes in [139, 140], due to the use of OISB modulation, optical orthogonal modulation and coherent detection which can detect both the phase and intensity information of optical signals are employed, the spectral efficiency and the number of the transmitted wireless signals for each channel (or wavelength) is increased. In addition, the LO is not from the transmitter, no optical amplifier is needed and no additional noise from the optical amplifier will be introduced. Furthermore, since the remote LO is replaced by a LO at the receiver side, polarization multiplexing can be employed which would enable 8 × 8 MIMO. In addition, since the four microwave signals are with an identical microwave center frequency, more microwave signals using FDM could be transmitted, thus the data rate could be further increased. Finally, the phase noise and unstable frequency difference introduced by the transmitter laser source and the LO laser source are cancelled by a DSP-based phase noise cancellation unit. A proof-of-concept experiment is performed. Three 1 Gbps OFDM signals and a 1.5 Gbps OFDM signal all with 16 quadrature amplitude modulation (16-QAM) at an identical microwave carrier frequency of 2.91 GHz modulated on a single optical carrier are transmitted over a 10-km single-mode fiber (SMF). When the received optical power is only -20.3 dBm, the raw bit error rates of the four wireless signals are still less than 3×10^{-3} which enables error-free transmission if the state-of-the-art forward error correction (FEC) technique is employed.

6.1.1. Principle

Fig. 6.1 shows the schematic of the proposed coherent RoF link based on OISB modulation and optical orthogonal modulation. A continues-wave (CW) light from a laser diode (LD) is sent to a dual-parallel Mach-Zehnder modulator (DP-MZM) which consists of three MZMs (two sub-MZMs, sub-MZM1 and sub-MZM2, and one main MZM). The main MZM is biased at the quadrature point and sub-MZM2 is biased at the null point while sub-MZM1 is low biased. Two microwave signals are applied to the DP-MZM via the two electrodes. At the output of the DP-MZM, two optical pilot tones, an optical carrier and an OISB signal which contains four microwave OFDM signals are generated. Each sideband carries two OFDM signals whose optical subcarriers are orthogonal. After 10-km SMF transmission, the OISB signal is coherently detected at the receiver. After DSP, the four microwave OFDM signals are separated and the phase noise and unstable frequency difference between the transmitter laser source and LO laser source are cancelled. In the signal processing unit, no ELOs are needed.

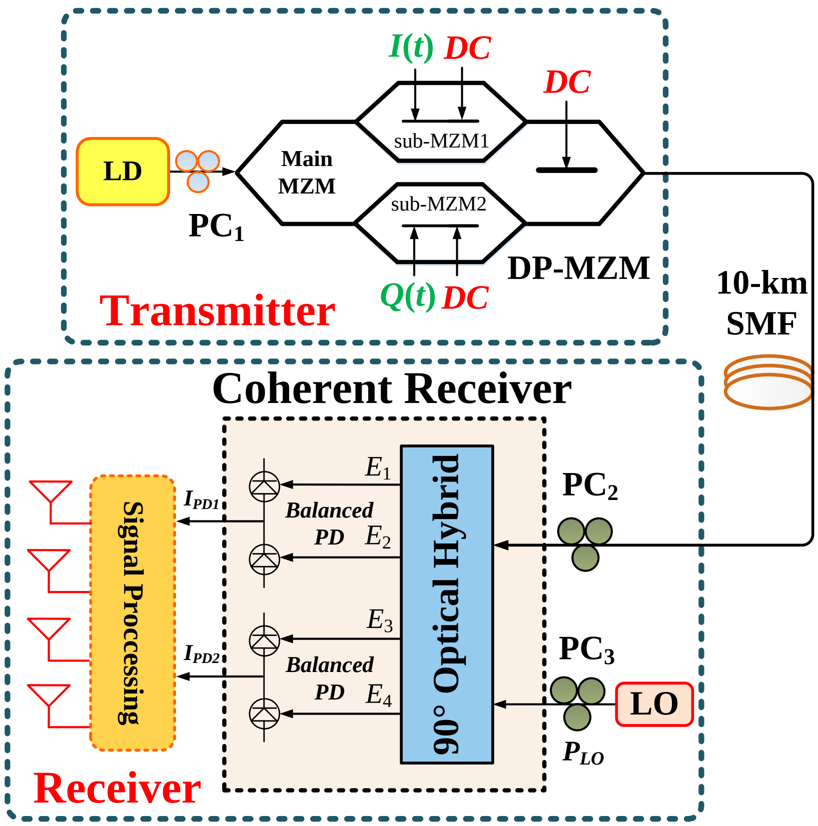

Fig. 6.1. Schematic diagram of the proposed coherent RoF link based on OISB modulation and optical orthogonal modulation. PC: polarization controller, CW laser: continuous-wave laser, Balanced PD: balanced photodetector, DP-MZM: dual parallel Mach-Zehnder modulator, LD: laser diode, SMF: single-mode fiber.

Fig. 6.2 shows the principle of the dual independent sideband generation with four real OFDM signals. Firstly, four baseband real OFDM signals, which are individually vector mapped, are generated. Note, the modulation format, the symbol rate, the bandwidth and the number of subcarriers of each real OFDM signal can be different.

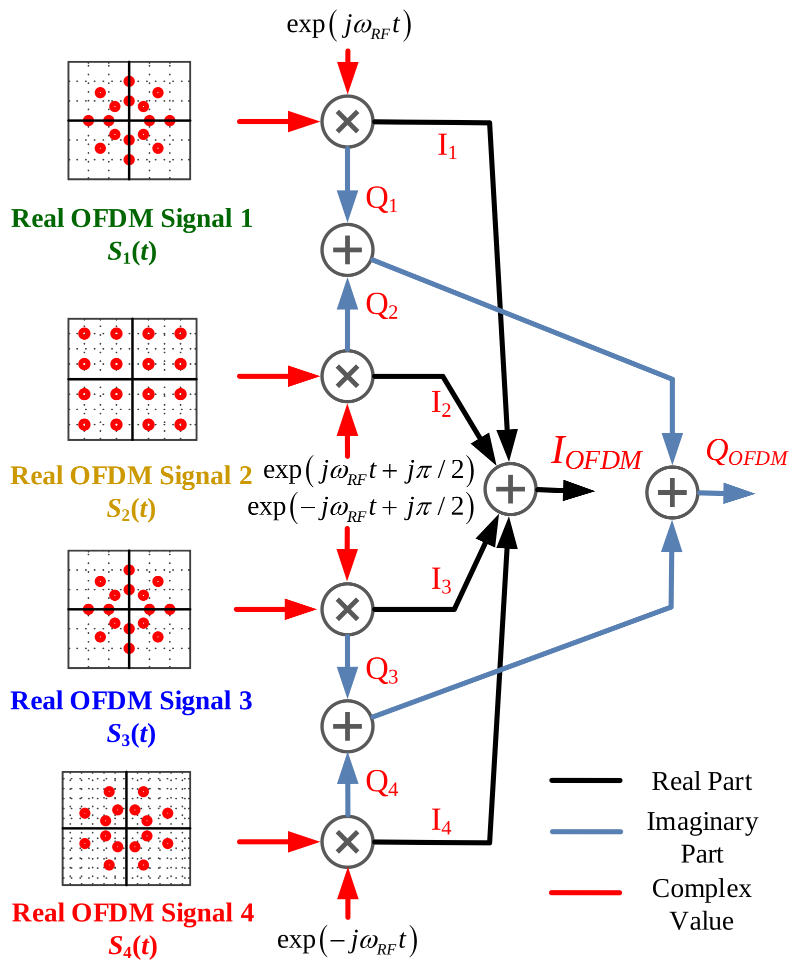

Fig. 6.2. Principle of the dual independent sideband generation with four real OFDM signals.

Secondly, the four baseband OFDM signals, $S_1(t)$, $S_2(t)$, $S_3(t)$ and $S_4(t)$, modulate the RF carriers in the form of complex sinusoidal. $S_1(t)$ is carried by the positive frequency carrier in the form of $\exp(j\omega_{RF}t)$, $S_2(t)$ is carried by the carrier with the same frequency having a $\pi/2$ initial phase, which is expressed as $\exp(j\omega_{RF}t+\pi/2)$. Apparently, the RF carriers of the two signals are orthogonal. While for $S_3(t)$ and $S_4(t)$, the two baseband signals are up converted to the same intermediate frequency at the negative side. The two carriers for $S_3(t)$ and $S_4(t)$ can be expressed as

$\exp\left(-j\omega_{RF}t\right)$ and $\exp\left(-j\omega_{RF}t+\pi/2\right)$. Again, they are also orthogonal. Note that in the proposed scheme, the frequencies of the four carries can be equal or not equal. Then, the real parts and imaginary parts of the four complex microwave OFDM signals are added together. Fig. 6.3 shows the spectrum of the complex signal after the four complex microwave OFDM signals are combined. As can be seen, the upper sideband contains OFDM signal 1 and OFDM signal 2 and the lower sideband contains OFDM signal 3 and OFDM signal 4. Fig. 6.4 shows the insertion of a pilot tone with an angular frequency of $2\omega_{RF}$, which is combined with the real parts of the complex microwave OFDM signals and used to separate the four OFDM signals at the receiver side. Fig. 6.5 shows the spectrum of the OFDM signals with the added pilot tone. Since the pilot tone is a real signal, the spectrum of the pilot tone is Hamilton symmetric. Finally, the real part and imaginary part of the combined complex signal, shown in Fig. 6.5, are applied to the DP-MZM via the two electrodes. To generate an OISB signal, the bias points of the three MZMs inside the DP-MZM are biased as follows: the main MZM is biased at the quadrature point, sub-MZM2 is biased at the null point, and sub-MZM1 is low biased. Mathematically, the optical field at the output of the DP-MZM is given by

$$\begin{aligned}
E_s(t) &= \frac{\sqrt{2P_sL_s}}{2}\begin{bmatrix}\cos\left(\pi I\left(t\right)/2V_{\pi RF}+\alpha\right)e^{j\left(\omega_c t+\varphi_c(t)\right)}\\ +\sin\left(\pi Q\left(t\right)/2V_{\pi RF}\right)e^{j\left(\omega_c t+\varphi_c(t)+\varphi_{DC}\right)}\end{bmatrix}\\
&\approx \frac{\sqrt{2P_sL_s}}{2}\begin{Bmatrix}\begin{bmatrix}\cos\left(\alpha\right)\\ -\pi\sin\left(\alpha\right)I\left(t\right)/2V_{\pi RF}\end{bmatrix}e^{j\left(\omega_c t+\varphi_c(t)\right)}\\ +\pi Q\left(t\right)/2V_{\pi RF}\cdot e^{j\left(\omega_c t+\varphi_c(t)+\varphi_{DC}\right)}\end{Bmatrix}
\end{aligned} \tag{6-1}$$

where P_s is the optical power at the input of the DP-MZM, ω_c is the angular frequency of the light wave, $\varphi_c\left(t\right)$ is the phase term of the transmitter laser source, $V_{\pi DC}$ is the half-wave voltage of the DP-MZM at DC, φ_{DC} is the phase difference between the two arms of the main MZM, L_s is the link loss between the coherent receiver and the transmitter, $I(t)$ is the real part of the complex signal, and $Q(t)$ is the imaginary part of the complex signal. The phase difference, $\alpha = \pi V_{bias} / 2V_{\pi DC}$, between the two arms of sub-MZM1 is controlled by a DC bias, V_{bias}. Both $I(t)$ and $Q(t)$ are small signals and can be expressed as

$$I(t) = S_1(t)\cdot\cos(\omega_{RF}t) - S_2(t)\cdot\sin(\omega_{RF}t) + S_3(t)\cdot\sin(\omega_{RF}t) + S_4(t)\cdot\cos(\omega_{RF}t) + A\cos(2\omega_{RF}t) \tag{6-2}$$

$$Q(t) = l\begin{bmatrix} S_1(t)\cdot\sin(\omega_{RF}t) + S_2(t)\cdot\cos(\omega_{RF}t) \\ +S_3(t)\cdot\cos(\omega_{RF}t) - S_4(t)\cdot\sin(\omega_{RF}t) \end{bmatrix} \tag{6-3}$$

where $S_1(t)$, $S_2(t)$, $S_3(t)$ and $S_4(t)$ are the four baseband real OFDM signals, ω_{RF} is the center frequency of the four microwave OFDM signals, A is the amplitude of the electrical pilot tone, and l is an attenuation factor. To generate an OISB signal, the optical power for the two optical sidebands at the output of sub-MZM1 ($\left[\pi\sin(\alpha)I(t)/2V_{\pi RF}\right]\exp\left[j\left(\omega_c t + \varphi_c(t)\right)\right]$) and sub-MZM2 ($\left[\pi Q(t)/2V_{\pi RF}\right]\exp\left[j\left(\omega_c t + \varphi_c(t) + \varphi_{DC}\right)\right]$) should be equal, thus l should be equal to $\sin(\alpha)$, which is done in the system by decreasing the electrical power of $Q(t)$. Since the main MZM is biased at the quadrature point, φ_{DC} can be equal to either $\pi/2$ or $-\pi/2$.

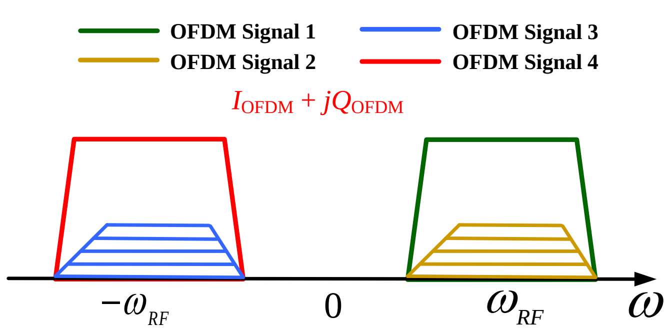

Fig. 6.3. The spectrum of the two independent sideband signals with four real OFDM signals.

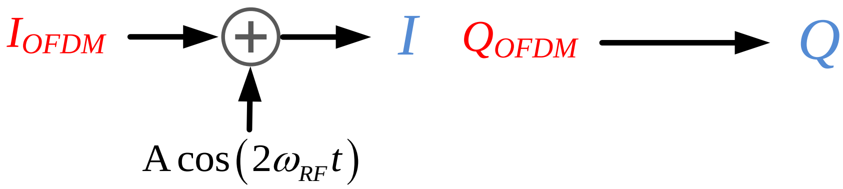

Fig. 6.4. The schematic diagram to show the pilot-tone insertion.

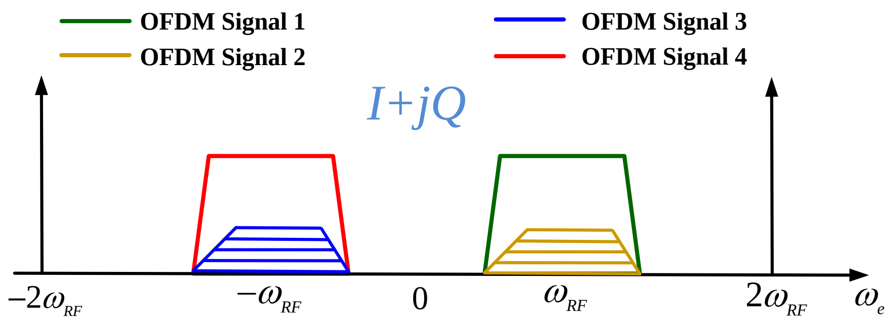

Fig. 6.5. The spectrum of the two independent sideband signals with the pilot tone.

Fig. 6.6 shows the optical spectrum of the OISB signal at the output of the DP-MZM when φ_{DC} is equal to $-\pi/2$. It can be seen that the signals shown in Fig. 6.5 are frequency up converted to ω_c. In addition, optical orthogonal modulation is realized. Each sideband contains two OFDM signals whose optical subcarriers are orthogonal. Fig. 6.7 shows the optical spectrum of the OISB signal at the output of the DP-MZM when φ_{DC} is equal to $\pi/2$. The only difference between the signals shown in Fig. 6.6 and Fig. 6.7 is that the positions of the signals at the lower and the upper sidebands are swapped. In addition, to separate the four microwave OFDM signals at the receiver side, the optical carrier is partially suppressed to make it have a power identical to that of either of the two pilot tones. In the following analysis, we assume that φ_{DC} is equal to $\pi/2$.

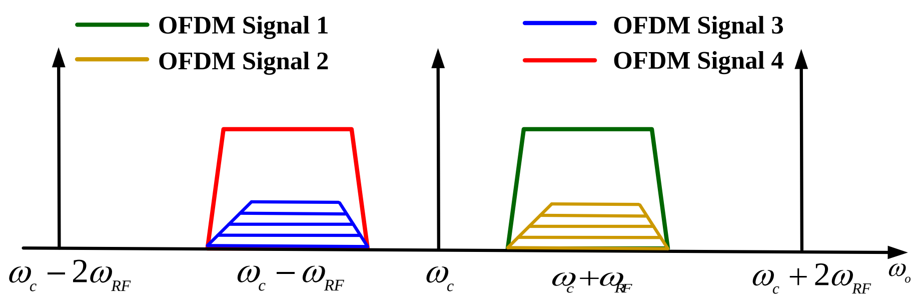

Fig. 6.6. The optical spectrum at the output of the DP-MZM for $\varphi_{DC} = -\pi/2$.

After transmission over an SMF, the optical signal is coherently detected by a coherent receiver while a free-running LO laser source is used as an LO source. The optical field of the light wave from the LO laser source is given by

$$E_{LO}(t) = \sqrt{2P_{LO}} e^{j(\omega_{LO}t + \varphi_{LO}(t))} \tag{6-4}$$

where P_{LO} is the optical power, $\varphi_{LO}(t)$ is the phase term, and ω_{LO} is the angular frequency.

The optical signal from the transmitter and the light wave from the LO laser source are co-polarized and are applied to a 90° optical hybrid. At the four outputs of the 90° optical hybrid, we have four optical signals with the electrical fields given by

$$E_1 = \sqrt{L}(E_s + E_{LO}) \tag{6-5}$$

$$E_2 = \sqrt{L}(E_s - E_{LO}) \tag{6-6}$$

$$E_3 = \sqrt{L}(E_s + E_{LO}e^{j\pi/2}) \tag{6-7}$$

$$E_4 = \sqrt{L}(E_s - E_{LO}e^{j\pi/2}) \tag{6-8}$$

where L is the insertion loss caused by the 90° optical hybrid.

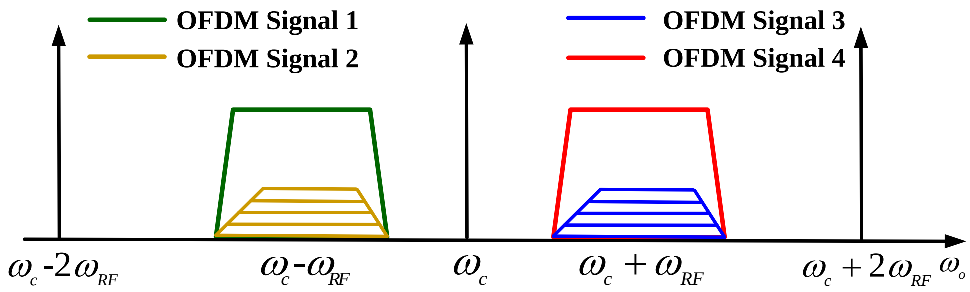

Fig. 6.7. The optical spectrum at the output of the DP-MZM for $\varphi_{DC}=\pi/2$.

By applying E_1 and E_2, and E_3 and E_4 to two balanced photodetectors, we have two output photocurrents given by

$$I_{PD1}=2RL\sqrt{P_sP_{LO}L_s}\left(I_{EC1}+I_{PR1}+I_{PL1}+S_{lower1}+S_{upper1}\right) \tag{6-9}$$

with

$$I_{EC1}=\cos\left(\alpha\right)\cos\left[\left(\Delta\omega\right)t+\varphi(t)\right]$$

$$I_{PR1}=-0.5AB\cos\left[\left(\Delta\omega\right)t+\varphi(t)+2\omega_{RF}t\right]$$

$$I_{PL1}=-0.5AB\cos\left[\left(\Delta\omega\right)t+\varphi(t)-2\omega_{RF}t\right]$$

$$\begin{aligned}S_{lower1}=&-BS_1\left(t\right)\cos\left[\left(\Delta\omega\right)t+\varphi(t)-\omega_{RF}t\right]\\&-BS_2\left(t\right)\cdot\sin\left[\left(\Delta\omega\right)t+\varphi(t)-\omega_{RF}t\right]\end{aligned}$$

$$\begin{aligned}S_{upper1}=&-BS_3\left(t\right)\sin\left[\left(\Delta\omega\right)t+\varphi(t)+\omega_{RF}t\right]\\&-BS_4\left(t\right)\cos\left[\left(\Delta\omega\right)t+\varphi(t)+\omega_{RF}t\right]\end{aligned}$$

$$B=\pi l/2V_{\pi RF}=\pi\sin\left(\alpha\right)/2V_{\pi RF}$$

and

$$I_{PD2}=2RL\sqrt{P_sP_{LO}L_s}\left(I_{EC2}+I_{PR2}+I_{PL2}+S_{lower2}+S_{upper2}\right) \tag{6-10}$$

with

$$I_{EC2}=\cos\left(\alpha\right)\sin\left[\left(\Delta\omega\right)t+\varphi(t)\right]$$

$$I_{PR2} = -0.5AB\sin\left[\left(\Delta\omega\right)t + \varphi(t) + 2\omega_{RF}t\right]$$

$$I_{PL2} = -0.5AB\sin\left[\left(\Delta\omega\right)t + \varphi(t) - 2\omega_{RF}t\right]$$

$$\begin{aligned} S_{lower2} = &-BS_1\left(t\right)\sin\left[\left(\Delta\omega\right)t + \varphi(t) - \omega_{RF}t\right] \\ &+BS_2\left(t\right)\cos\left[\left(\Delta\omega\right)t + \varphi(t) - \omega_{RF}t\right] \end{aligned}$$

$$\begin{aligned} S_{upper2} = &BS_3\left(t\right)\cos\left[\left(\Delta\omega\right)t + \varphi(t) + \omega_{RF}t\right] \\ &-BS_4\left(t\right)\sin\left[\left(\Delta\omega\right)t + \varphi(t) + \omega_{RF}t\right] \end{aligned}$$

$$B = \pi l / 2V_{\pi RF} = \pi\sin\left(\alpha\right) / 2V_{\pi RF}$$

where $\Delta\omega = \omega_c - \omega_{LO}$ is the frequency difference between the transmitter and the LO laser sources, $\varphi(t)$ is the phase noise introduced by the transmitter laser source and the LO laser source, $\varphi(t) = \varphi_c(t) - \varphi_{LO}(t)$, R is the responsivity of the PD. As can be seen, the photocurrents I_{PD1} contains one electrical carrier (I_{EC1}), one left pilot tone (I_{PL1}), one right pilot tone (I_{PR1}) and four microwave OFDM signals. Apparently, the lower sideband (S_{lower1}) contains two OFDM signals which are orthogonal. The same for the two signals in the upper sideband (S_{upper1}). For I_{PD2} , it also contains one electrical carrier (I_{EC2}), one left pilot tone (I_{PL2}), one right pilot tone (I_{PR2}) , the lower sideband (S_{lower2}) including $S_1(t)$ and $S_2(t)$ and the upper sideband (S_{upper2}) which contains S_3(t) and S_4(t).

Then, the two photocurrents (I_{PD1} and I_{PD2}) are sent to the DSP unit where the four microwave OFDM signals are separated and the phase noise from the transmitter and the LO laser sources and unstable frequency difference between the transmitter and the LO laser sources are cancelled. Fig. 6.8 to Fig. 6.11 show the DSP flow charts. Firstly, the electrical carrier (I_{EC1}), the left pilot tone (I_{PL1}), the right pilot tone (I_{PR1}), the lower sideband (S_{lower1}) and the upper sideband (S_{upper1}) are separated via electrical filters. Through signal processing, we can easily separate the four microwave signals and cancel the phase noise and unstable frequency difference. The detailed signal processing can be expressed by the following expressions.

$$S_1(t)\cos(\omega_{RF}t) \propto F[S_{lower1} \cdot I_{EC1} + S_{lower1} \cdot I_{PL1}]$$
$$= -\frac{1}{2}B\left[\cos(\alpha) - \frac{1}{2}AB\right]S_1(t)\cos(\omega_{RF}t) \qquad (6\text{-}11)$$
$$-\frac{1}{2}B\left[\cos(\alpha) + \frac{1}{2}AB\right]S_2(t)\sin(\omega_{RF}t)$$

$$S_2(t)\cos(\omega_{RF}t) \propto F[S_{lower1} \cdot I_{EC2} + S_{lower1} \cdot I_{PL2}]$$
$$= -\frac{1}{2}B\left(\cos\alpha - \frac{1}{2}AB\right)S_2(t)\cos(\omega_{RF}t) \qquad (6\text{-}12)$$
$$-\frac{1}{2}B\left(\cos\alpha + \frac{1}{2}AB\right)S_1(t)\sin(\omega_{RF}t)$$

$$S_3(t)\cos(\omega_{RF}t) \propto F[S_{upper1} \cdot I_{EC2} + S_{upper1} \cdot I_{PR2}]$$
$$= -\frac{1}{2}B\left[\cos\alpha - \frac{1}{2}AB\right]S_3(t)\cos(\omega_{RF}t) \qquad (6\text{-}13)$$
$$-\frac{1}{2}B\left[-\cos\alpha - \frac{1}{2}AB\right]S_4(t)\sin(\omega_{RF}t)$$

$$S_4(t)\cos(\omega_{RF}t) \propto F[S_{upper1} \cdot I_{EC1} + S_{upper1} \cdot I_{PR1}]$$
$$= -\frac{1}{2}B\left[\cos\alpha - \frac{1}{2}AB\right]S_4(t)\cos(\omega_{RF}t) \qquad (6\text{-}14)$$
$$-\frac{1}{2}B\left[-\cos\alpha - \frac{1}{2}AB\right]S_3(t)\sin(\omega_{RF}t)$$

where $F[\cdot]$ represents the function of a band-pass filter which is used to select the microwave OFDM signal. As can be seen in (6-11) - (6-14), to separate the four microwave OFDM signals, $\cos(\alpha)$ should be equal to $-0.5BA$. Thus, the power for the electrical carrier and either of the pilot tones are controlled equal. Note that the upper sideband, lower sideband, the carriers and the pilot tones have the same phase noise and unstable frequency difference introduced from the transmitter and the LO laser sources, through microwave mixing between a sideband and one of the pilot tones or carriers, the phase noise and the unstable frequency difference can be cancelled.

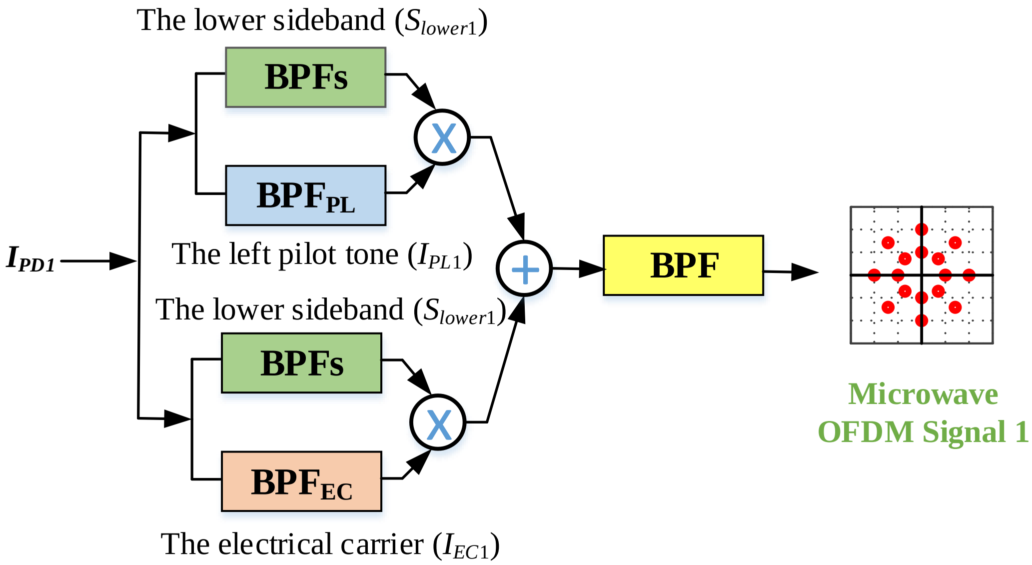

Fig. 6.8. DSP for recovering microwave OFDM signal 1 and cancelling the phase noise and the unstable frequency difference.

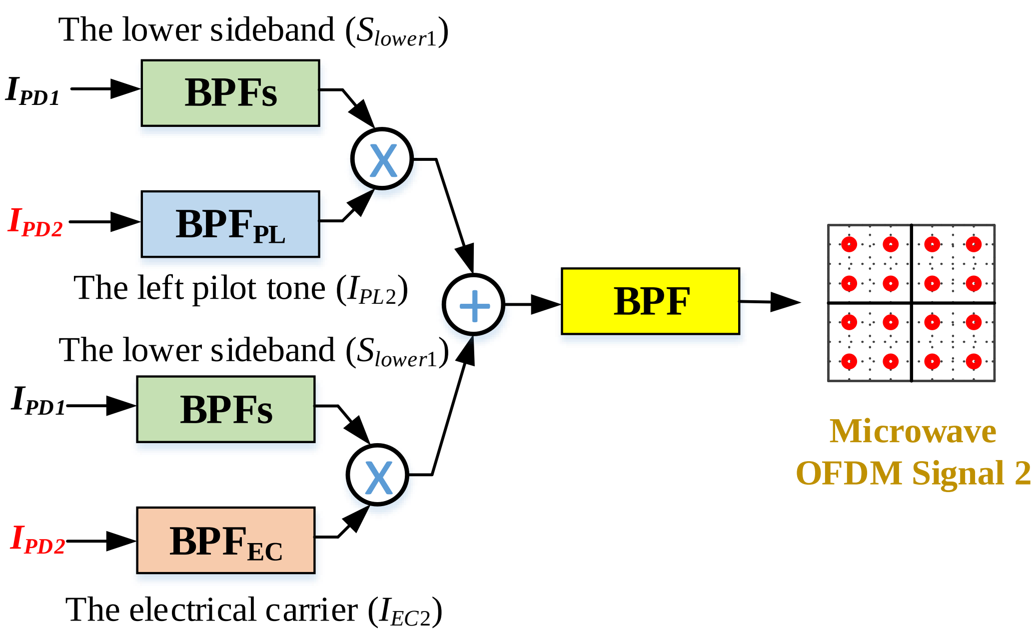

Fig. 6.9. DSP for recovering microwave OFDM signal 2 and cancelling the phase noise and the unstable frequency difference.

As can be seen from (6-11) - (6-14), the four microwave OFDM signals are free from the phase noise and the unstable frequency difference.

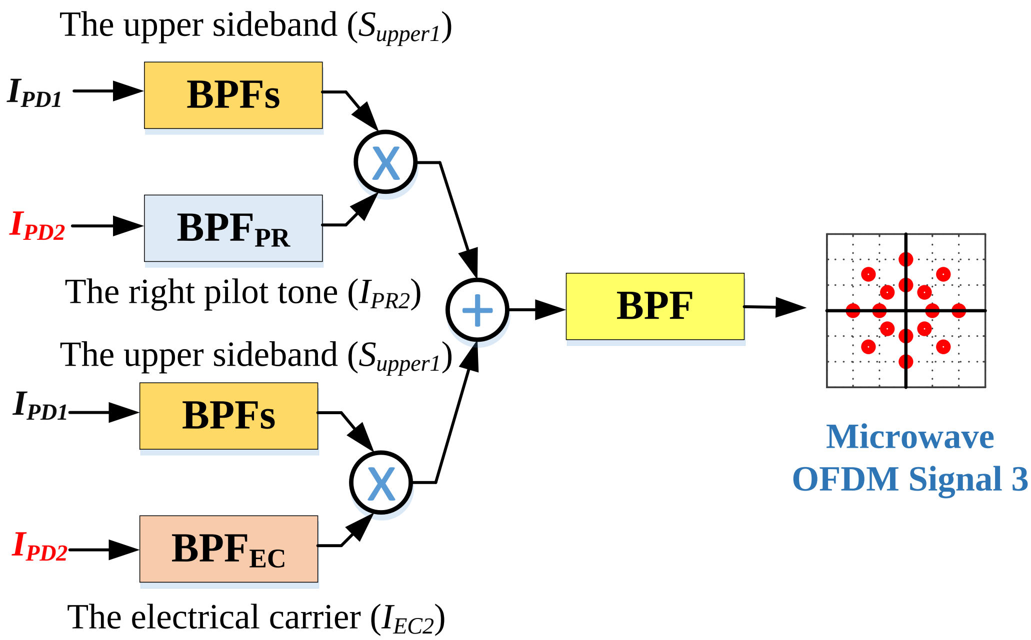

Fig. 6.10. DSP for recovering microwave OFDM signal 3 and cancelling the phase noise and the unstable frequency difference.

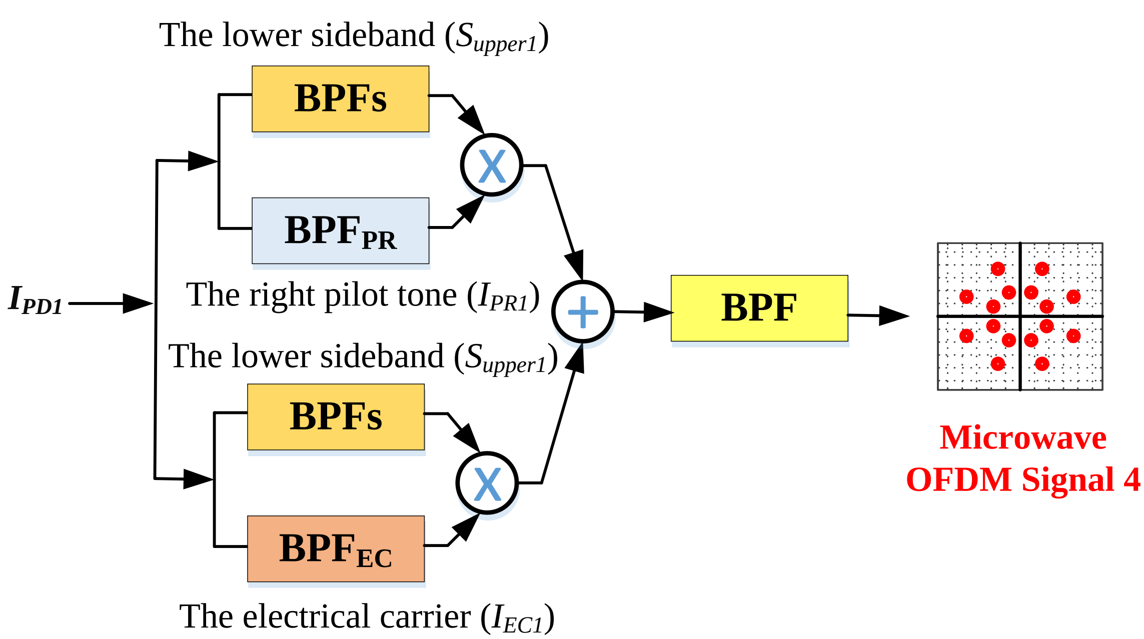

Fig. 6.11. DSP for recovering microwave OFDM signal 4 and cancelling the phase noise and the unstable frequency difference.

6.1.2. Experiment

To verify that the proposed coherent RoF link can transmit, detect and separate the four microwave OFDM signals, an experiment is performed based on the setup shown in Fig. 6.1. A picture of the experimental setup is shown in Fig. 6.12. A linearly-polarized CW light at 1550.435 nm from a tunable laser source (TLS, Agilent N7714A) with a linewidth of 100 KHz and an optical power of 16 dBm is sent to the DP-MZM (JDSU) via a polarization controller (PC1). The two signals, $I(t)$ and $Q(t)$, applied to the DP-MZM are generated by an arbitrary waveform generator (AWG, Keysight M8915A), with a program composed according to the flow chat shown in Fig. 6.2 and loaded to the AWG, to generate the two signals. Both $I(t)$ and $Q(t)$ contains four different microwave OFDM signals with an identical center frequency at 2.91 GHz. The modulation format for three of the four OFDM signals (OFDM Signal 1, OFDM Signal 3 and OFDM Signal 4) is star 16-QAM. The data rate is 1 Gbps each. The other OFDM signal (OFDM Signal 2) is rectangular 16-QAM with a data rate of 1.5 Gbps. In the signal $I(t)$, the frequency of the electrical pilot tone is 5.82 GHz and the amplitude is 0.3548 V. As indicated, since $\cos(\alpha)$ should be equal to -0.5*AB*, thus α should be equal to -1.527. Sub-MZM1 is low biased to introduce a phase shift of -1.527 and sub-MZM2 is biased at the null point, while the main MZM is biased at the quadrature point ($\varphi_{DC} = \pi / 2$). The DP-MZM has a bandwidth of 10 GHz and a half-wave voltage of around 6.33 V. Then, the generated OISB signal (the lower sideband carries OFDM Signal 1 and OFDM Signal 2, while the upper sideband carries OFDM Signal 3 and OFDM Signal 4) with two optical pilot tones and an optical carrier are sent to the coherent receiver over a 10-km SMF. At the receiver, coherent detection (Discovery Semiconductors DP-QPSK 40/100 Gbps Coherent Receiver Lab Buddy) with a free running LO laser source (TLS, Yokogawa AQ2201) operating at 1550.485 nm is performed to detect the optical signal.

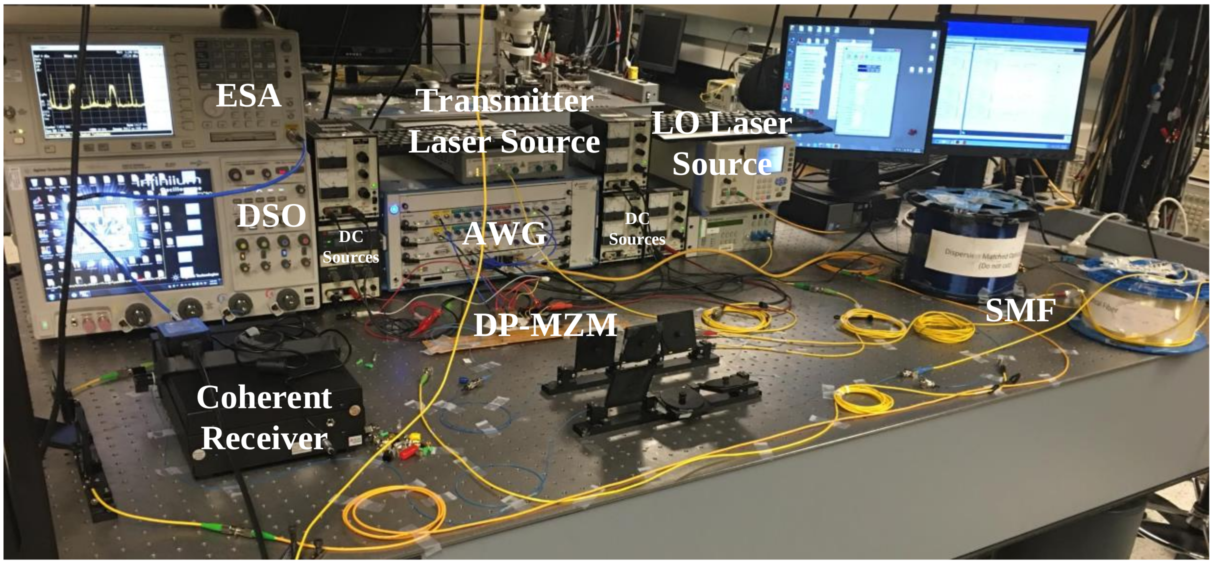

Fig. 6.12. Photograph showing the experimental setup of the proposed coherent microwave photonic link with optical independent sideband and optical orthogonal modulation. AWG: arbitrary-wave generator, DC Sources: direct current sources, DP-MZM: dual-parallel Mach-Zehnder modulator, DSO: digital storage oscilloscope, ESA: electrical spectrum analyzer, LO laser source: local oscillator laser source, SMF: single-mode fiber.

The LO laser source has a linewidth of 1 MHz and an optical power of 9 dBm. Through tuning PC_2 and PC_3, the light wave from the LO laser source is co-polarized with the received optical signal. Note that in a practical system, PC_2 can be replaced by a dynamic polarization controller, to accommodate the random polarization state of the input optical signal [100, 101]. At the output of the coherent receiver, two photocurrents are generated, which are sampled by a Digital Storage Oscilloscope (Agilent DSO-X 93204A) with a sampling rate of 80 GSa/s. Then, the signal is processed offline in a computer.

We would like to point out that according to the analysis ((6-11)-(6-14)), the signal processing functions can be realized using pure analog signal processing where analog circuits to functions as splitters, band-pass filters and mixers, thus, a high speed analog-to-digital converter (ADC) is not needed. In addition, since no ELOs are needed at the receiver the system complexity and cost would be significantly reduced. Fig. 6.13 shows the spectrum of the photocurrent of I_{PD1}. As indicated in Fig. 6.6 or Fig. 6.7, the lower sideband contains one 1 Gbps microwave OFDM signal and one 1.5 Gbps microwave OFDM signal (Signal 1 and Signal 2), and the upper sideband contains two 1 Gbps microwave OFDM signals (Signal 3 and Signal 4).

To verify the performance of the coherent RoF link, the EVMs and estimated BERs of the four microwave OFDM signals as a function of received optical power are measured for back-to-back and with 10-km fiber transmission. Fig. 6.14 shows the EVMs at different received optical power levels for the four OFDM signals and Fig. 6.15 show the BERs at different received optical power levels for the four OFDM signals. As can be seen, after 10-km transmission, even the received optical power is only -20.3 dBm, the raw BERs for the microwave OFDM signals are still less than 3×10^{-3}, which would enable error-free transmission, if FEC can be employed. The power penalty caused by the fiber transmission is less than 1 dB, which is small and can be ignored. The corresponding constellations of the signals are shown in Fig. 6.16.

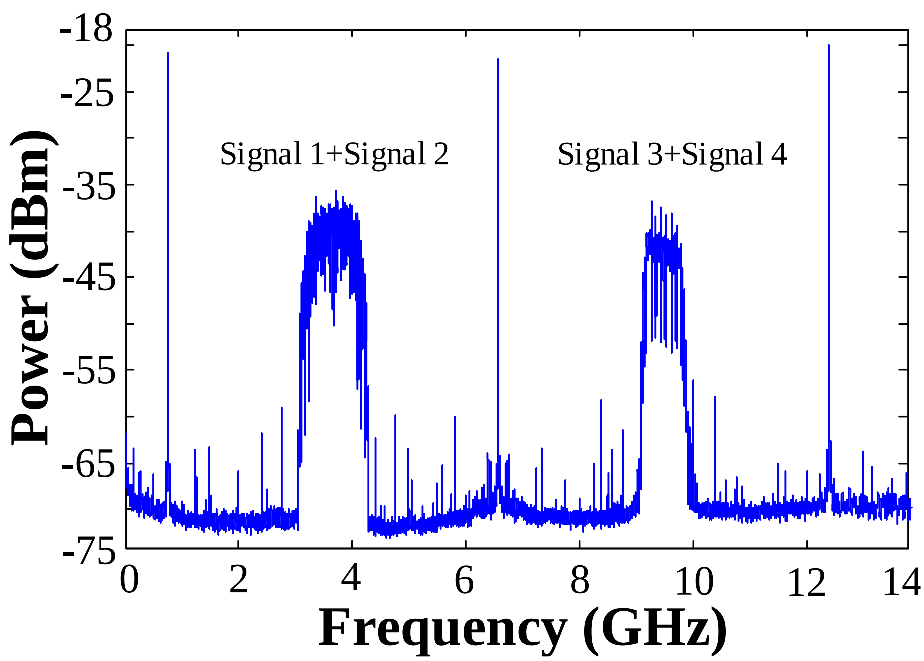

Fig. 6.13. Spectrum of the signal at the output of the coherent receiver (I_{PD1}).

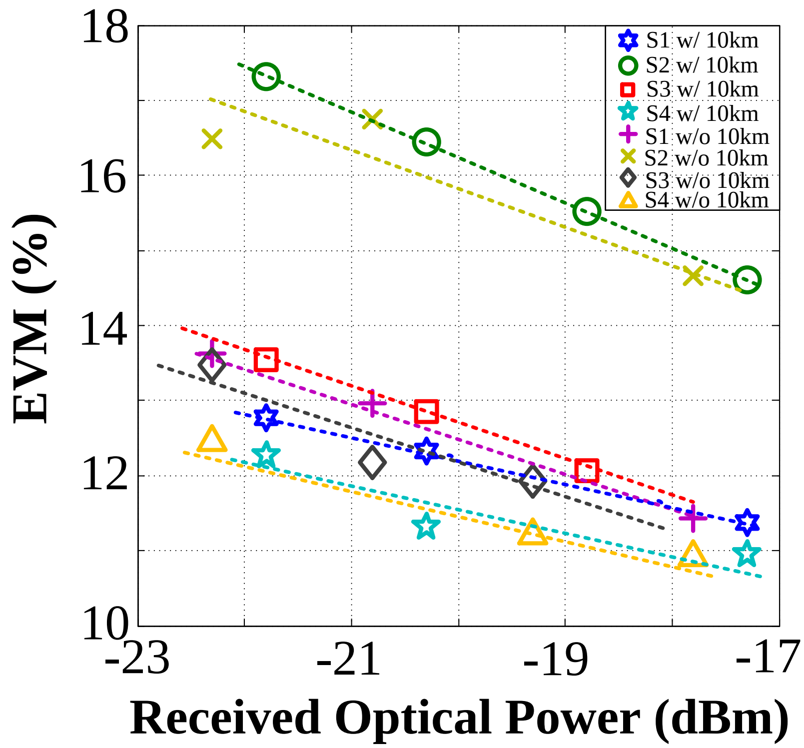

Fig. 6.14. EVMs at different received optical power levels for the four OFDM signals, S1: Signal 1, S2: Signal 2, S3: Signal 3, S4: Signal 4.

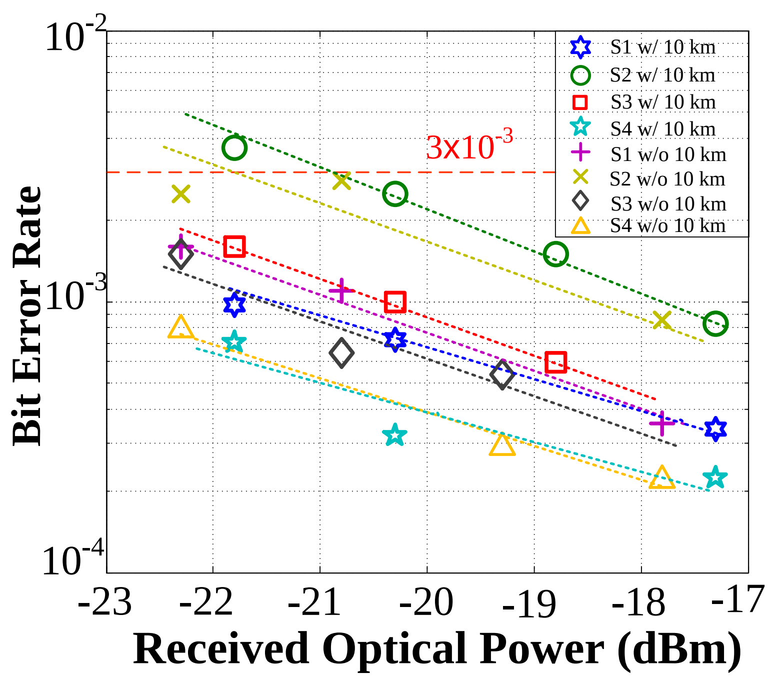

Fig. 6.15. BERs at different received optical power levels for the four OFDM signals, S1: Signal 1, S2: Signal 2, S3: Signal 3, S4: Signal 4.

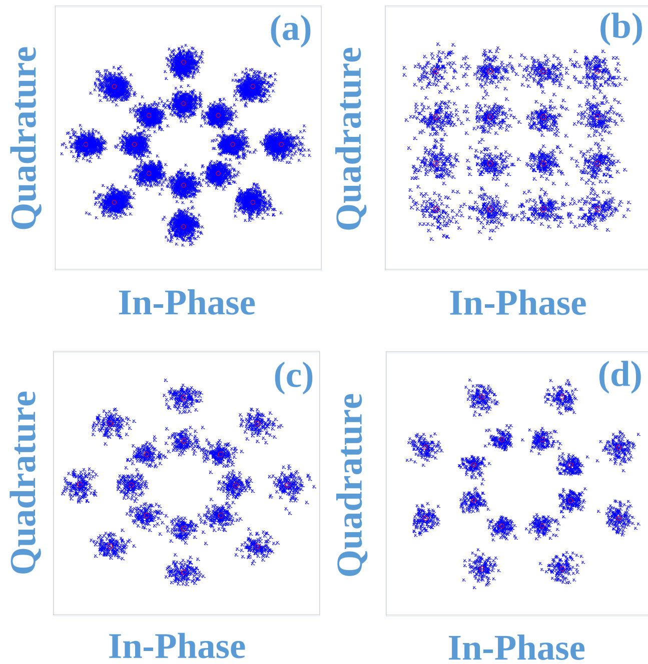

Fig. 6.16. The measured constellations for the recovered microwave OFDM signals (fiber length: 10 km, the received optical power: -20.3 dBm). (a) Signal 1, (b) Signal 2, (c) Signal 3, and (d) Signal 4.

As can be seen the constellations are clear after 10-km transmission, which confirms that the four microwave OFDM signals are well separated and the phase noise and the unstable frequency difference are effectively cancelled. In addition, it can be seen that the power penalty caused by the 10-km SMF transmission is very small, about 1 dB, and can be ignored.

6.2. A data rate quadrupled coherent microwave photonic link

In chapter 6.1, for the proposed 4 × 4 MIMO coherent RoF link, to separate the multiple signals, two pilot tones at different frequencies have to be transmitted to the receiver which would decrease the energy efficiency. In addition, the center frequency of the transmitted wireless signals is not transparent to the RoF link due to the need of two bandpass filters to eliminate the two pilot tones. For future optical-wireless systems, the center frequency and the data rate should be transparent to the optical link. Also, such an RoF link is only suitable for downlink transmission, since digital signal processing (DSP) is needed in a RRH, making the RRH complicated and costly.

In this section, a novel RoF link based on coherent detection and DSP with quadrupled data rate improved by employing both intensity and phase modulation and polarization multiplexing to transmit four microwave signals over a single optical carrier is proposed. Since no pilot tones are used, the center frequencies of the wireless signals and their data rates are transparent to the RoF link, and polarization multiplexing is employed, to double the spectral efficiency.

At the transmitter, a light wave from a laser source is divided into two channels, and the light wave in each channel is phase modulated by a microwave signal and then intensity modulated by a second microwave signal. The two modulated optical signals from the two channels are polarization multiplexed at a polarization beam combiner (PBC) and transmitted over a single-mode fiber (SMF). At the receiver, coherent detection with a free-running local oscillator (LO) laser source is used to detect the two orthogonally polarized optical signals. After DSP, the four microwave vector signals are separated and the phase noise and the unstable frequency difference are cancelled. The proposed scheme is validated by an experiment. The transmission of four 2.5-Gbps 16 quadrature amplitude modulation (16-QAM) microwave signals with an identical center frequency of 2.5 GHz over 10-km SMF with a total data rate of 10 Gbps is achieved. The error vector magnitudes (EVMs) are measured to be 9.5%. If forward error correction (FEC) is employed, error-free transmission can be achieved. Since four wireless signals are simultaneously transmitted, the RoF link is suitable for the implementation of 4×4 MIMO. In the experiment, limited by the number of channels of an arbitrary waveform generator (AWG) to generate the wireless signals, two orthogonal frequency division multiplexing (OFDM) signals are generated and transmitted, a 2 × 2 MIMO RoF link is experimentally demonstrated. The total data rate is 0.9 Gbps. The EVMs for the two received wireless signals at the wireless terminal are measured to be 8.6%.

6.2.1. Principle

Fig. 6.17 shows the schematic diagram of the proposed DSP-assisted coherent RoF link. At the transmitter, a light wave from a continuous-wave (CW) laser source is split into two channels (Ch-1 and Ch-2) by a 3-dB optical coupler (OC), with each of the light wave being firstly phase modulated by a 16-QAM microwave signal, and then intensity modulated by a second 16-QAM microwave signal. The modulated optical signals from the two channels are polarization multiplexed at a polarization beam splitter (PBS1), and transmitted to the receiver over a SMF. Since the four microwave signals have an identical center frequency, frequency-division multiplexing (FDM) in the microwave domain can be employed to incorporate more microwave channels to further increase the data rate of the RoF link. At the receiver, a coherent receiver with a free-running LO is used to coherently detect the two orthogonally polarized optical signals. The two orthogonally polarized optical signals are sent to a second PBS (PBS2), to separate the orthogonally polarized optical signals into two channels (Ch-X and Ch-Y), with Ch-X corresponding to CH-1 and Ch-Y corresponding to CH-2. Then, the two signals from the Ch-X and Ch-Y channels and an LO signal from a LO laser source are sent to two optical hybrids and detected by four balanced photodetectors (balanced PDs). At the output of the coherent receiver, four electrical signals, I_{PD1} and I_{PD2} from Ch-X and I_{PD3} and I_{PD4} from Ch-Y, are obtained, which are sent to a DSP unit, where the four 16-QAM microwave signals are separated and recovered, and the phase noise introduced from the transmitter laser source and the LO laser source and the unstable frequency difference between the transmitter laser source and the LO laser source are cancelled.

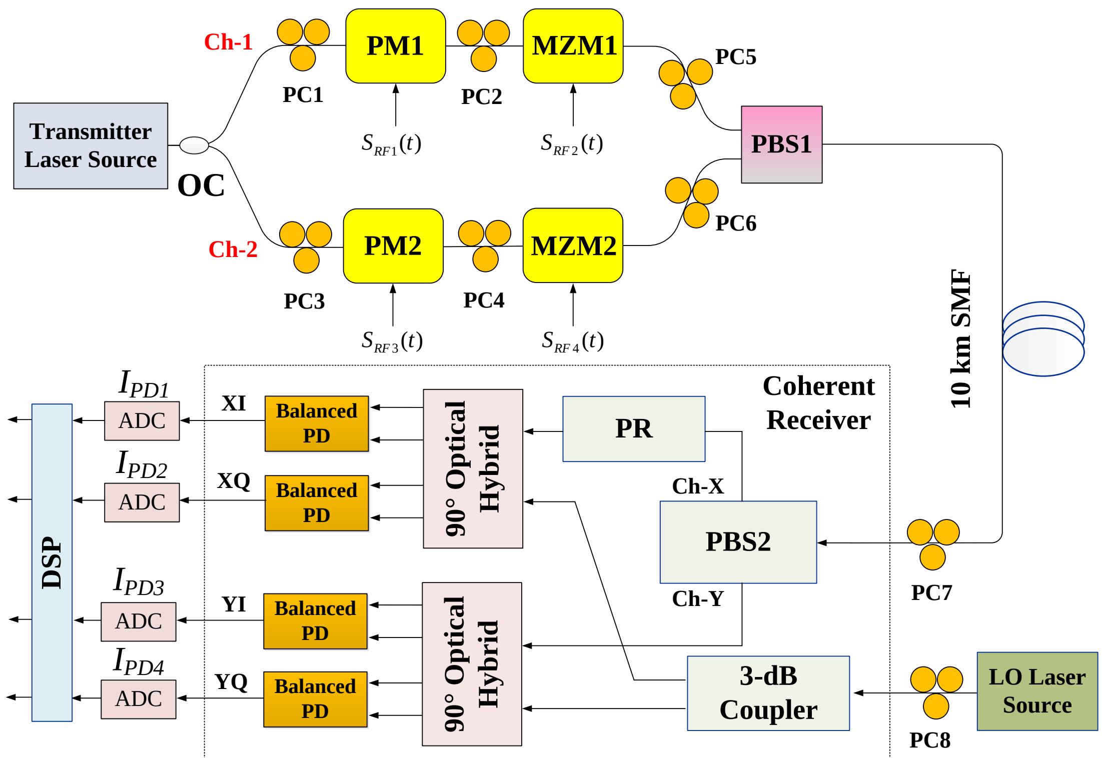

Fig. 6.17. Schematic of the proposed RoF link. ADC: analog-to-digital converter, PC: polarization controller, PD: photodetector, MZM: Mach-Zehnder modulator, DSP: digital signal processing, PBS: polarization beam splitter, PR: polarization rotator, PM: phase modulator.

At the transmitter, a phase modulators (PMs) and a Mach-Zehnder modulators (MZM) in each of the two channels are used for phase and intensity modulation. The MZMs are both biased at the quadrature point. Mathematically, the optical fields of the two orthogonally polarized optical signals at the output of PBS1 can be expressed as

$$E_1(t) = \sqrt{P_s L_1} \cos\left(\frac{\pi S_{RF2}(t)}{2V_{\pi IM1}} + \frac{\pi}{4}\right) e^{j\left[\omega_c t + \varphi_{c1}(t) + \frac{\pi S_{RF1}(t)}{V_{\pi PM1}}\right]} \tag{6-15}$$

$$E_2(t) = \sqrt{P_s L_2} \cos\left(\frac{\pi S_{RF4}(t)}{2V_{\pi IM2}} + \frac{\pi}{4}\right) e^{j\left[\omega_c t + \varphi_{c2}(t) + \frac{\pi S_{RF3}(t)}{V_{\pi PM2}}\right]} \tag{6-16}$$

where P_s is the optical power of the light wave at the output of the transmitter laser source, ω_c is the angular frequency of the light wave, $S_{RF1}(t)$ and $S_{RF3}(t)$ are the two 16-QAM microwave signals applied to the two phase modulators (PM1 and PM2), $S_{RF2}(t)$ and $S_{RF4}(t)$ are the two 16-QAM microwave signals applied to the two MZMs (MZM1 and MZM2), $\varphi_{c1}(t)$ and $\varphi_{c2}(t)$ are the phase terms of the light waves from the transmitter laser source for Ch-1 and Ch-2, $V_{\pi IM1}$ and $V_{\pi IM2}$ are the half-wave voltages of MZM1 and MZM2, $V_{\pi PM1}$ and $V_{\pi PM2}$ are the half-wave voltages of PM1 and PM2, and L_1 and L_2 are the link losses between the OC and PBS1 for Ch-1 and Ch-2, respectively.

Then, the optical signal at the output of PBS1 is transmitted over a SMF and detected by a coherent receiver. To perform coherent detection, a LO laser source is needed. In the proposed RoF link, a free-running laser source is used. The optical field at the output of the LO laser source is given by

$$E_{LO}(t) = \sqrt{2P_{LO}}e^{j(\omega_{LO}t+\varphi_{LO}(t))} \tag{6-17}$$

where P_{LO} is the optical power, ω_{LO} is the angular frequency, and $\varphi_{LO}(t)$ is the phase term. The two orthogonally polarized optical signals are demultiplexed by PBS2 into Ch-X and Ch-Y. After coherent detection, four electrical signals at the outputs of the coherent receiver are obtained, which are given by

$$I_{PD1}(t) = A(t)\cos\left(\Delta\omega t + \varphi_1(t) - \varphi_x + \pi S_{RF1}(t)/V_{\pi PM1}\right) \tag{6-18}$$

$$I_{PD2}(t) = A(t)\sin\left(\Delta\omega t + \varphi_1(t) - \varphi_x + \pi S_{RF1}(t)/V_{\pi PM1}\right) \tag{6-19}$$

$$I_{PD3}(t) = B(t)\cos\left(\Delta\omega t + \varphi_2(t) - \varphi_y + \pi S_{RF3}(t)/V_{\pi PM2}\right) \tag{6-20}$$

$$I_{PD4}(t) = B(t)\sin\left(\Delta\omega t + \varphi_2(t) - \varphi_y + \pi S_{RF3}(t)/V_{\pi PM2}\right) \tag{6-21}$$

with

$$\Delta\omega = \omega_c - \omega_{LO}, \varphi_1(t) = \varphi_{c1}(t) - \varphi_{LO}(t), \varphi_2(t) = \varphi_{c2}(t) - \varphi_{LO}(t)$$

$$\mathrm{A}(t) = 2RL_h\sqrt{P_s P_{LO} L_f L_1}\cos\left(\pi S_{RF2}(t)/2V_{\pi IM1} + \pi/4\right)$$

$$B(t) = 2RL_h\sqrt{P_s P_{LO} L_f L_2}\cos\left(\pi S_{RF4}(t)/2V_{\pi IM2} + \pi/4\right)$$

where $\Delta\omega$ is the frequency difference between the transmitter laser source and the LO laser source, R is the responsivity of the PD, L_f is the link loss caused by the SMF, $\varphi_1(t)$,and $\varphi_2(t)$ are the phase noise terms introduced by the transmitter laser source and the LO laser source, and φ_x and φ_y are the phase terms arising from the polarization mismatch between the received optical signals and the light wave from the LO laser source. To recover $S_{RF2}(t)$ while cancelling the phase noise and the unstable frequency difference, we sum the square of the two currents (I_{PD1} and I_{PD2}) using DSP [99],

$$\begin{aligned} I_1(t) &= I_{PD1}^2(t) + I_{PD2}^2(t) \\ &\approx 2R^2 L_h^2 L_f P_s P_{LO} L_1\left[1 - \pi S_{RF2}(t)/V_{\pi IM1}\right] \end{aligned} \tag{6-22}$$

Also, by summing the squared of the other two signals (I_{PD3} and I_{PD4}), $S_{RF4}(t)$, as shown in Fig. 6.17, can be recovered. As can be seen the two recovered signals are both free from the phase noise and the unstable frequency difference.

To recover $S_{RF1}(t)$, zero padding is applied to $S_{RF1}(t)$ at the transmitter. At the coherent receiver, the detected zero padding signal, $I'_{PD1}(t)$ and $I'_{PD2}(t)$ can be rewritten as

$$I'_{PD1}(t) = A(t)\cos\left(\Delta\omega t + \varphi'_1(t) - \varphi_x\right) \tag{6-23}$$

$$I'_{PD2}(t) = A(t)\sin\left(\Delta\omega t + \varphi'_1(t) - \varphi_x\right) \tag{6-24}$$

where $\varphi'_1(t)$ is the phase noise in the detected signal when the phase-modulated signal is zero padded.

Through DSP, we obtain,

$$\begin{aligned} I_2(t) &= \text{atan}\left[\left(I_{PD2} \times I'_{PD1} - I_{PD1} \times I'_{PD2}\right) / \left(I_{PD1} \times I'_{PD1} + I_{PD2} \times I'_{PD2}\right)\right] \\ &= \text{atan}\left\{\tan\left[\pi S_{RF1-16QAM}(t) / V_{\pi PM1} + \varphi(t)\right]\right\} \end{aligned} \tag{6-25}$$

with

$$\varphi(t) = \varphi_1(t) - \varphi'_1(t)$$

Apparently, if the spectrum of the noise $\varphi(t)$ does not overlap with that of the transmitted $S_{RF1}(t)$, $S_{RF1}(t)$ can be selected by a bandpass filter which is free from the phase noise and unstable frequency difference. Also, $S_{RF3}(t)$ can be recovered by the same method. Note, due to instability of the frequency difference ($\Delta\omega$ in (6-23) and (6-24) may not be equal to $\Delta\omega$ in (6-18)-(6-21)), the frequency difference may not be cancelled completely through (6-25). Then, a residual frequency difference will be preserved. If we consider the residual frequency difference is much smaller than the symbol rate of $S_{RF1}(t)$, (6-25) can be rewritten as

$$I'_2(t) = \text{atan}\left\{\tan\left[\pi S_{RF1}(t) / V_{\pi PM1} + \varphi(t) + \sum_{i=1}^{\infty} \omega_i t\right]\right\} \tag{6-26}$$

where $\sum_{i=1}^{\infty} \omega_i$ is the residual frequency difference. Apparently $\sum_{i=1}^{\infty} \omega_i t$ will accumulate over time and phase jumps will occur. To eliminate the phase jumps, phase unwrapping should be employed [106].

6.2.2. Experiment

An experiment is performed based on the setup shown in Fig. 6.17. A picture of the experimental setup is shown in Fig. 6.18.

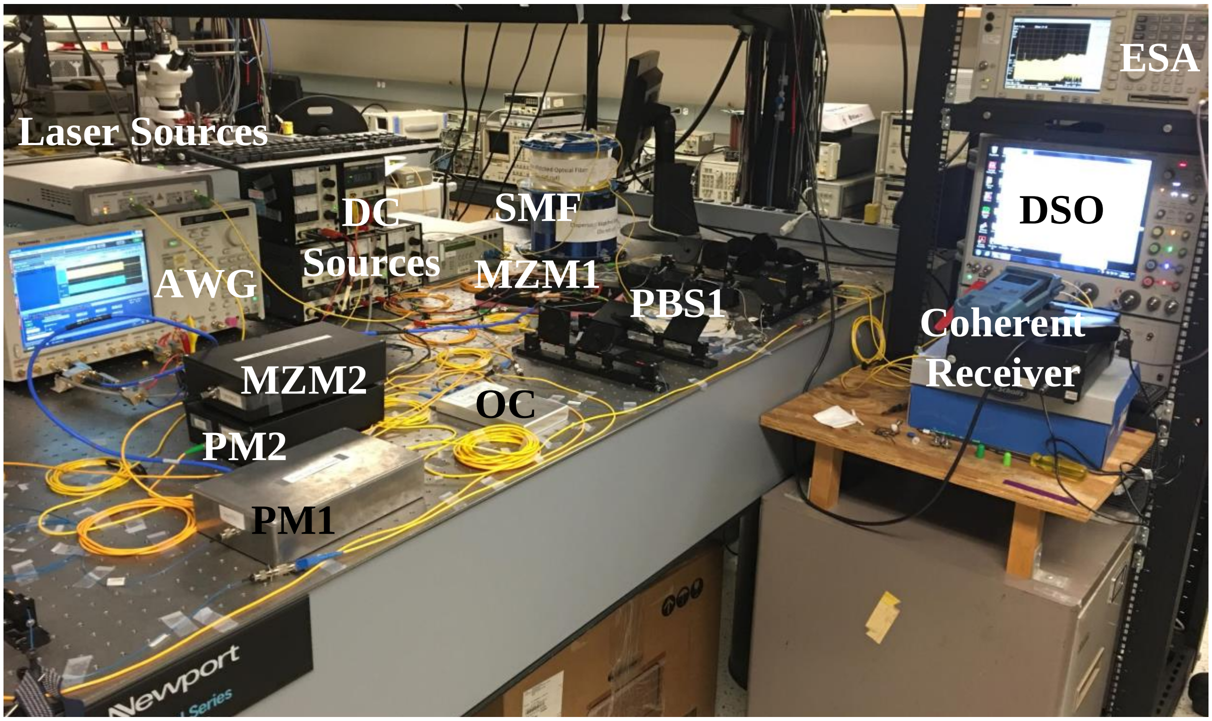

Fig. 6.18. Photograph showing the experimental setup of the proposed data rate quadrupled coherent microwave photonic link with optical independent sideband and optical orthogonal modulation. AWG: arbitrary-wave generator, DC Sources: direct current sources, DSO: digital storage oscilloscope, ESA: electrical spectrum analyzer, MZM: Mach-Zehnder modulator, PBS: polarization beam splitter, PM: phase modulator, SMF: single-mode fiber.

At the transmitter, an optical wave at 1550.0 nm from a tunable laser source (TLS, Agilent N7714A) with a power of 14 dBm and a linewidth of 100 KHz is divided into two channels (Ch-1 and Ch-2) by a 3-dB OC, with the optical wave in each channel being first phase modulated by a microwave 16-QAM signal and then intensity modulated by a second 16-QAM signal. The intensity modulator is a chirp-free single-electrode MZM which is biased at the quadrature point. The four microwave 16-QAM signals are generated by an arbitrary waveform generator (Tektronix AWG7102). Then, the two optical signals from the two channels are polarization multiplexed at PBS1 and sent to the receiver over a 10-km SMF. At the receiver, optical coherent detection is performed using a Discovery Semiconductors DP-QPSK 40/100 Gbps Coherent Receiver, with a free running LO laser source (Agilent N7714A) as a LO laser source to detect the two orthogonally polarized optical signals. The optical power and the wavelength of the light wave from the LO laser source are 9.5 dBm and 1550.051 nm. Through tuning PC7, the two polarization multiplexed light waves can be demultiplexed into two channels (Ch-X and Ch-Y) by PBS2. Note that PC7 can be replaced by a dynamic polarization controller [100, 101] in a practical system to avoid manual tuning. In the coherent receiver, Ch-X is used to detect the optical signal from Ch-1, and Ch-Y is used to detect the signal from Ch-2. A Digital Storage Oscilloscope (Keysight DSO-Z 504A) with a sampling rate of 80 GSa/s is employed to perform the analog-to-digital conversion. The four sampled signals are processed offline in a computer. As mentioned in chapter 6.2.1, to recover $S_{RF1}(t)$ and $S_{RF3}(t)$, zero padding is needed for the two transmitted signals. In the experiment, the length ratio between the zero padding portion and the signal portion is 1:3. In a practical system, the ratio can be as small as 1:20. The center frequencies of the four 16-QAM microwave signals are 2.5 GHz, and the symbol rate is 625 MSymbol/s, with the total data rate is 10 Gbps. Since the four microwave signals have an identical center frequency, FDM in the microwave domain can be employed to incorporate more microwave channels to further increase the data rate of the RoF link. Fig. 6.19 shows the spectrum of the signal (I_{PD1}) which contains $S_{RF1}(t)$ and $S_{RF2}(t)$ at the output of the coherent receiver. The received optical power for each channel is -10 dBm. As can be seen, the spectra of the two microwave signals are completely overlapped and are up converted to 3.875 GHz and 8.875 GHz because of the wavelength difference between the transmitter laser source and LO laser source.

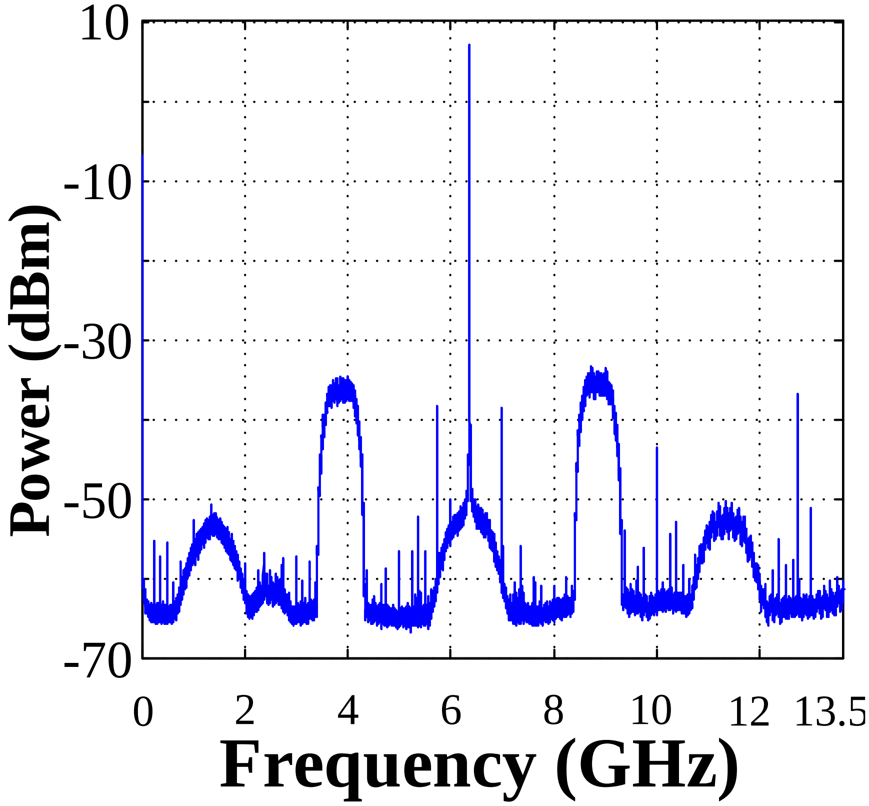

Fig. 6.19. Spectrum of the signal at the output of the coherent receiver (I_{PD1}).

Since the two laser sources are not phase locked, the frequency difference is not stable. The two 16-QAM microwave signals are separated by DSP. In addition, the phase noise and the unstable frequency difference are also eliminated by DSP.

Fig. 6.20 shows the bit error rates (BERs) of the recovered microwave signals versus the received optical power. As can be seen, when the optical received optical power is -18 dBm, the BERs are still less than 10^{-3}. If state-of-art FEC is employed, error-free transmission can be achieved. The constellations for the four recovered 16-QAM microwave signals when the received optical power for each channel is -18 dBm are also shown in Fig. 6.20. They are very clear which proves the effectiveness of the proposed technique to cancel the unstable frequency difference and phase noise introduced from the two laser sources.

When the received optical power for each channel is -10 dBm, the measured error vector magnitudes (EVMs) are around 9.5% and the corresponding signal-to-noise ratios (SNRs) are estimated to be 20 dB. For a vector signal with an SNR of 20 dB, error-free detection with 64-QAM vector signal can be achieved by using Soft-Decision FEC (overhead 15%). Thus, the sub-band spectrum efficiency of the proposed scheme can reach 20.62 bit/s/Hz.

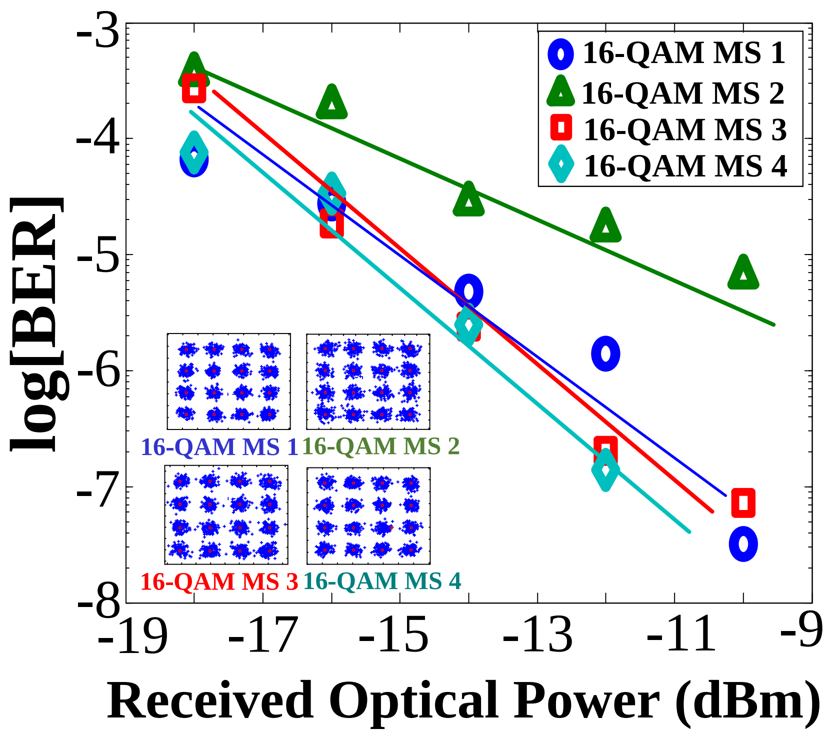

Fig. 6.20. BERs at different received optical power levels of each channel for the four 16-QAM microwave signals transmitted over a 10-km SMF.

Since four microwave signals are transmitted over a single fiber link over a single optical carrier, the proposed RoF link is suitable for the implementation of 4×4 MIMO. In our experimental demonstration, since the AWG can only generate two different microwave signals at the same time, the performance of the proposed RoF link with 2×2 MIMO is evaluated. In the experiment, two MIMO-OFDM microwave signals are generated by the AWG and are applied to PM2 and MZM2. The center frequency of the two MIMO-OFDM signals is 2.5 GH and the total data rate is 0.9 Gbps. Each of the two OFDM signals contains 64 subcarriers of which 44 subcarriers are used to carry data. The modulation format for each subcarrier is QPSK. The two MIMO-OFDM signals are received and recovered after offline DSP. In the demonstration, the AWG is also used to perform digital-to-analog conversion (DAC) to generate the two recovered MIMO-OFDM microwave signals after DSP, which are amplified by two electrical amplifiers and sent to two antennas. Each of the electrical amplifiers and the antennas has a gain of 10 dB and 16 dBi, respectively. After 1 meter wireless transmission, the two MIMO-OFDM microwave signals are received by another two antennas, and the received signals are sampled and processed offline in a computer.

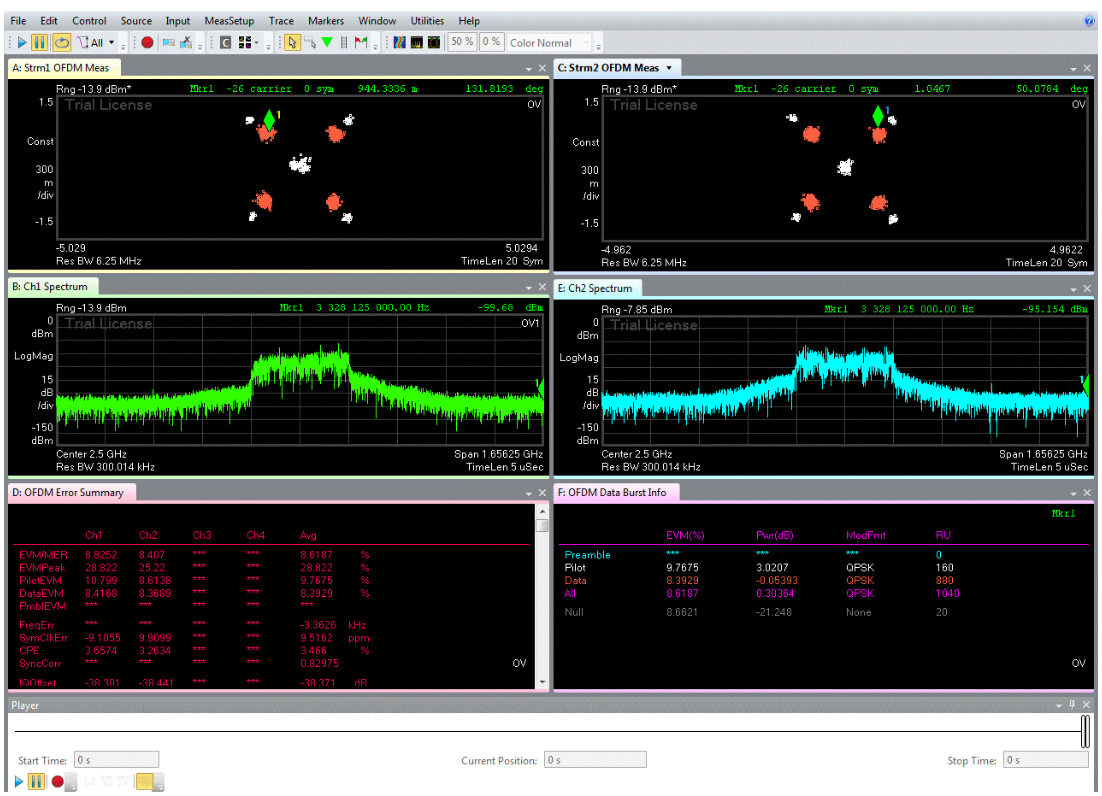

Fig. 6.21. EVMs and constellations for two received OFDM signals at the wireless terminal.

The measured EVMs for the two OFDM signals are 8.8% and 8.4%. Fig. 6.21 shows the constellations for the two received OFDM signals.

6.3. Conclusions

Firstly, a 4 × 4 coherent RoF link based on OISB modulation and optical orthogonal modulation was proposed and experimentally demonstrated. The proposed scheme was able to support the transmission of four microwave OFDM signals with an identical center frequency without using electrical FDM and optical wavelength-division multiplexing (WDM). If polarization multiplexing is employed, the data transmission capacity would be doubled, that is, eight microwave signals can be transmitted which would enable 8 × 8 MIMO. In the proposed scheme, no ELOs were needed for frequency conversion at the receiver which simplifies significantly the system. In addition, since the OISB modulation and optical orthogonal modulation were employed, the spectral efficiency was improved. The proposed approach was experimentally evaluated. Three 1 Gbps OFDM signals and one 1.5 Gbps OFDM signal at an identical microwave carrier frequency of 2.91 GHz were transmitted over a 10-km SMF. The estimated BERs showed that error-free transmission was ensured even for a low received optical power of -20.3 dBm and the power penalty caused by the10-km fiber was small and could be ignored.

Secondly, a data rate quadrupled RoF link based on coherent detection and DSP was proposed and experimentally demonstrated. Four microwave signals were carried by a single optical carrier based on both phase modulation and intensity modulation, and polarization multiplexing. The four microwave signals were coherently detected at a coherent receiver and recovered by DSP. The phase noise and the unstable frequency difference introduced from the transmitter laser source and LO laser source were cancelled also by DSP. An experiment was performed. Error-free transmission of four 2.5-Gbps16-QAM microwave signals with an identical center frequency of 2.5 GHz over a 10-km SMF with a total data rate of 10 Gbps was achieved if FEC was employed. The measured SNRs for the four recovered signals were 20 dB. Thus, the sub-band spectral efficiency of the proposed RoF link was calculated to be

20.62 bit/s/Hz. In addition, the proposed RoF link could be used to implement 4 × 4 MIMO. In the experiment, limited by the number of channels of the AWG to generate multiple microwave signals, two OFDM signals were generated and transmitted, and a 2×2 MIMO RoF link was demonstrated. The measured EVMs of the MIMO-OFDM signals at the wireless terminal were 8.6%.

CHAPTER 7 SUMMARY AND FUTURE RESEARCH

7.1. Summary

The work of the thesis was focused on the investigation of phase noise and unstable frequency difference cancellation for the RoF link based on coherent detection, high spectral efficiency coherent RoF links, wavelength reuse in a coherent radio over WDM-PONs and coherent RoF links with MIMO.

The IM/DD RoF link was widely studied and applied in different areas, since it was easy to implement and low cost. But the IM/DD RoF link could only detect the intensity information of the optical carrier, thus the spectral efficiency was very low. However, the RoF link with coherent detection could detect both the amplitude and phase information of the optical carrier. In addition, compared with the conventional IM/DD RoF link, the RoF link with coherent detection could provide a higher receiver sensitivity. But the coherent detection was sensitive to the phase noise, so we proposed a technique to cancel the phase noise and unstable frequency difference introduced from the transmitter laser source and LO laser source. Compared with other phase noise cancellation techniques, the proposed scheme was easy to implement and low cost. To further increase the spectral efficiency of the RoF link, a coherent RoF link supporting both amplitude and phase modulation with phase noise cancellation was proposed. A novel DSP algorithm was proposed to separate the information on the amplitude and phase of the optical carrier while cancelling the phase noise and the unstable frequency difference.

To increase the capacity of the full duplex RoF, WDM-PON techniques could be applied. Since the access network environment was very cost-sensitive, colorless ONUs were essential. Thus, we proposed two different approaches to realize radio over colorless WDM-PONs with polarization multiplexing and coherent detection incorporating phase noise cancellation. Compared with conventional RSOA based or FP-LD based wavelength reuse techniques, in principle these two schemes did not have any limitation for the ER of the downstream signal. In addition, there was no requirement of the power or wavelength for the downstream signal to realize wavelength reuse.

To further increase the capacity of the RoF link, UDWDM-PON techniques had to be used. However, ODSB+C modulation was not suitable for the UDWDM-PON system due to the low spectral efficiency. Thus, a coherent RoF link based on OSSB modulation with low-cost free-running laser sources for UDWDM-PONs was proposed. The proposed scheme could utilize the spectrum of each channel efficiently in UDWDM-PON system. In the experiment, the channel spacing could be as narrow as 3 GHz and the data rate for each channel could reach 2.5 Gbps.

To realize seamless integration of RoF links and 4 × 4 MIMO, two coherent RoF links to transmit four wireless signals with an identical microwave center frequency without using FDM over a single optical wavelength were proposed. For the first scheme, to enable 4 × 4 MIMO, each of the two optical sidebands carried two independent microwave OFDM signals. By using optical coherent detection, the four microwave OFDM signals were separated. To further increase the spectral efficiency and make the RoF link be transparent to the center frequencies of transmitted wireless signals, a 20.62 bit/s/Hz coherent RoF by employing both intensity and phase modulation and polarization multiplexing to transmit four microwave signals over a single optical carrier was proposed.

7.2. Future research

In the research work, to realize a colorless ONU in a UDWDM-PON, an expensive tunable laser source has to be used. We will find a cost-effective solution to realize coherent radio over colorless UDWDM-PONs in the future work.

In addition, WDM-PON technology is unable to dynamically allocate a bandwidth with sub-λ granularity for multiple services, which would significantly reduce the flexibility. However, in an OFDMA-PON, the optical OFDM subcarriers can be assigned to different services in different time slots, which enables dynamic bandwidth allocation. The seamless integration of coherent RoF and OFDMA-PON will be next research focus.

Finally, to further increase the capacity of the coherent RoF link, optical spatial division multiplexing (SDM) based on few-mode fiber (FMF) for RoF links will be investigated. Each mode of the fiber in principle can be used to independently transmit a data signal as a channel. However, during the propagation, different transmission channels may have spatial overlap, thus the signals would couple randomly among the modes. To unravel the mixing and improve the link performance, optical MIMO techniques will be studied.

REFERENCES

[1] C. Lam, Passive Optical Networks Principles and Practice, Burlington, MA, USA: Academic Press, 2007, pp. 1-143.

[2] Cisco visual networking index: global mobile data traffic forecast update, 2015-2020.

[3] IEEE 802.11 Working Group, http://ieee802.org/11/.

[4] X. Liu, H. Zeng, N. Chand, and F. Effenberger, “Efficient mobile fronthaul via DSP-based channel aggregation,” J. Lightw. Techol., vol. 34, no.6, pp. 1556-1564, Mar. 15, 2016.

[5] A. Pizzinat, P. Chanclou, F. Saliou, and T. Diallo, “Things you should know about fronthaul,” J. Lightw. Techol., vol. 33, no.5, pp. 1077-1083, Mar. 2015.

[6] A. J. Seeds, “Microwave photonics,” IEEE Trans. Microw. Theory Tech., vol. 50, no. 3, pp. 877-887, Mar. 2002.

[7] J. P. Yao “Microwave photonics,” J. Lightw. Technol., vol. 27, no. 3, pp. 314-335, Feb. 2009.

[8] J. Capmany and D. Novak, “Microwave photonics combines two worlds,” Nature Photon., vol. 1, no. 6, pp. 319–330, Jun. 2007.

[9] X. Chen and J. P. Yao, “A high spectral efficiency coherent microwave photonic link employing both amplitude and phase modulation with digital phase noise cancellation,” J. Lightw. Technol., vol. 33, no. 14, pp. 3091-3097, Jul. 15, 2015.

[10] S. Camatel, V. Ferrero, R. Gaudino, and P. Poggiolini, “Optical phase-locked loop for coherent detection optical receiver,” Electron. Lett., vol. 40, no. 6, pp. 384-385, Mar. 2004.

[11] M. Hyodo, S. Saito and Y. Kasai, “Optical phase-locked loop with fibre lasers for low phase noise millimeter-wave signal generation,” Electron. Lett., vol. 45, no. 17, pp. 878-880, Aug. 2009.

[12] T. Kuri and K. Kitayama, “Optical heterodyne detection technique for densely multiplexed millimeter-wave-band radio-on-fiber systems,” J. Lightw. Techol., vol. 21, no.12, pp. 3167-3179, Dec. 2003.

[13] T. Kuri and K. Kitayama, “Laser phase noise free optical hetero-dyne detection technique for 60-GHz-band radio-on-fiber systems,” Int. Topical Meeting Microwave Photonics (MWP2000) Tech. Dig., vol. WE1.5, Oxford, UK, Sept. 2000, pp. 141-144.

[14] D. K. Jung, S. K. Shin, C. -H. Lee, and Y. C. Chung, “Wavelength-division-multiplexed passive optical network based on spectrum-slicing techniques,” IEEE Photon. Technol. Lett., vol. 10, no. 9, pp. 1334-1336, Sep. 1998.

[15] B. Zhang, C. Lin, L. Huo, Z. Wang, and C. -K. Chan, “A simple high speed WDM PON utilizing a centralized supercontinuum broadband light source for colorless ONUs,” Optical Fiber Communication Conf., Anaheim, CA, Mar. 5-10, 2006, paper OTuC6.

[16] D. J. Shin, Y.C. Keh, J.W. Kwon, E.H. Lee, J.K. Lee, M.K. Park, J. W. Park, Y. K. Oh, S. W. Kim, I. K. Yun, H.C. Shin, D. Heo, J. S. Lee, H. S. Shin, H.S. Kim, S. B. Park, D. K. Jung, S. Hwang, Y. J. Oh, D. H. Jang, and C. S. Shim, “Low-cost WDM-PON with color-less bidirectional transceivers,” J. Lightw. Technol., vol. 24, no. 1, pp. 158–165, Jan. 2006.

[17] H. D. Kim, S. G. Kang, and C. H. Lee, “A low-cost WDM source with an ASE injected Fabry–Perot semiconductor lasers,” IEEE Photon. Technol. Lett., vol.12, no. 8, pp. 1067–1069, Aug. 2000.

[18] S. B. Park, D. K. Jung, D. J. Shin, H. S. Shin, I.K. Yun, J.S. Lee, Y.K. Oh, and Y.J. Oh, "Demonstration of WDM-PON with 50 GHz channel spacing employing spectrum-sliced reflective semi-conductor optical amplifiers," Electron. Lett., vol. 42, no. 20, pp. 1172–1173, Sep. 2006.

[19] S. Hann, T.-Y. Kim, and C.-S. Park, "Direct-modulated upstream signal transmission using a self-injection locked F-P LD for WDM-PON," in Proc. ECOC, Glasgow, Scotland, Sep. 25-29, 2005, Paper We3.3.3.

[20] E. Wong, K. L. Lee, and T. Anderson, "Low-Cost WDM passive optical network with directly-modulated self-seeding reflective SOA," Electron. Lett., vol. 42, no. 5, pp. 299–300, Mar. 2006.

[21] E. Wong, K. L. Lee, and T. Anderson, "Directly modulated self-seeding reflective semiconductor optical amplifiers as colorless transmitters in wavelength division multiplexed passive optical networks," J. Lightw. Technol., vol. 25, no. 1, pp. 67–74, Jan. 2007.

[22] W. Cui, T. Shao, and J. P. Yao, "Wavelength reuse in a UWB Over WDM-PON based on injection locking of a Fabry-Pérot laser diode and polarization multiplexing," J. Lightw. Technol., vol. 32, no. 2, pp. 220-227, Jan. 2014.

[23] F. Xiong, W.-D. Zhong, and H. Kim, "A broadcast-capable WDM-PON based on polarization-sensitive weak-resonant-cavity Fabry–Pérot laser diodes," J. Lightw. Technol., vol. 30, no. 3, pp. 355–361, Feb. 2012.

[24] H. Takesue and T. Sugie, "Wavelength channel data rewrite using saturated SOA modulator for WDM networks with centralized light sources," J. Lightw. Technol., vol. 21, no. 11, pp. 2546–2556, Nov. 2003.

[25] A. T. Nguyen, K. Lefebvre, and L. A. Rusch, “Multi-service OFDM uplink transmission in full-duplex FTTx Systems using RSOA-based WDM-PON architecture,” Optical Fiber Communication Conf., San Fran-cisco, CA, USA, 2014, paper Tu2C.1.

[26] K. Lefebvre, A. T. Nguyen, and L. A. Rusch, “Enabling in-band bidirectional OFDM-uplink and OOK-downlink transmission in long-reach RSOA-based WDM-PON systems,” J. Lightw. Technol., vol. 32, no. 20, pp. 3854–3860, Oct. 15, 2014.

[27] P.-T. Shih, C.-T. Lin, W.-J. Jiang, Y.-H. Chen, J. Chen, and S. Chi, “Full duplex 60-GHz RoF link employing tandem single sideband modulation scheme and high spectral efficiency modulation for-mat,” Opt. Express, vol. 17, no. 22, pp. 19501–19508, Oct. 2009.

[28] L. Chen, Y. Shao, X. Lei, H. Wen, and S. Wen, “A novel radio-over-fiber system with wavelength reuse for upstream data connection,” IEEE Photon. Technol. Lett., vol. 19, no. 6, pp. 387–389, Mar. 15 2007.

[29] Z. Wu, M. Xu, J. Zheng, C.-T. Tsai, Y.-C. Chi, G.-R. Lin, and G.-K. Chang, “Efficient centralized light sources for RoF-WDM-PON based on weak-resonant-cavity Fabry-Pérot laser diode,” Optical Fiber Communication Conf., Los Angeles, CA, Mar. 22-26, 2015, paper W1F.4.

[30] J. Yu, Z. Jia, T. Wang, and G.-K. Chang, “A novel radio-over-fiber configuration using optical phase modulator to generate an optical mm-wave and centralized lightwave for uplink connection,” IEEE Photon. Technol. Lett., vol. 19, no. 3, pp. 140–142, Feb. 2007.

[31] X. Yu, T.-B. Gibbon, and I.-T. Monroy, “Bidirectional radio-over-fiber system with phase-modulation downlink and RF oscillator-free uplink using a reflective SOA,” IEEE Photon. Techol. Lett., vol. 20, no. 24, pp. 2180–2182, Dec. 2008.

[32] T. Shao and J. P. Yao, “Wavelength reuse in a bidirectional UWB over fiber system,” Opt. Express, vol. 21, no. 10, pp. 11921-11927, Apr. 2013.

[33] J. Zheng, H. Wang, L. Wang, N. Zhu, J. Liu, and S. Wang, “Implementation of wavelength reusing upstream service based on distributed intensity conversion in ultrawideband-over-fiber system,” Opt. Lett., vol. 38, no. 7, pp. 1167–1169, Apr. 2013.

[34] B. Wu, M. Zhu, J. Zhang, J. Wang, M. Xu, F. Yan, S. Jian, and G. -K. Chang, “Multi-service RoF links with colorless upstream transmission based on orthogonal phase-correlated modulation,” Opt. Express, vol. 23, no. 14, pp. 18323–18329, Jul. 2015.

[35] R. Waterhouse and D. Novak, “Realizing 5G: microwave photonics for 5G mobile wireless systems,” IEEE Microwav. Mag., vol. 16, no. 8, pp. 84-92, Sept. 2015.

[36] W. J. Jiang, C. T. Lin, P. T. Shih, J. Chen, P. C. Peng, and S. Chi, “A Full duplex radio-over-fiber link with Multi-level OFDM signal via a single-electrode MZM and wavelength reuse with a RSOA,” Opt. Express, vol. 18, no. 3, pp. 2170-2718, Feb. 2010.

[37] W. J. Jiang, C. T. Lin, A. Ng’oma, P. T. Shih, J. Chen, M. Sauer, F. Annunziata, and S. Chi, “Simple 14 Gbps Short-Range Radio-over-Fiber System Employing a Single-Electrode MZM for 60 GHz Wireless Applications,” J. Lightw. Technol., vol. 28, no. 16, pp. 2238-2246, Aug. 2010.

[38] C. T. Lin, J. Chen, P. T. Shih, W. J. Jiang, and S. Chi, “ Ultra-high Data-rate 60 GHz Radio-over-Fiber Systems Employing Optical Frequency Multiplication and OFDM Formats,” J. Lightw. Technol., vol. 28, no. 16, pp. 2296-2306, Aug. 15, 2010.

[39] W. J. Jiang, C. T. Lin, P. T. Shih, L. Y. Wang-He, J. Chen, and S. Chi, "Simultaneous Generation and Transmission of 60-GHz Wireless and Baseband Wireline Signals With Uplink Transmission Using an RSOA," IEEE Photon. Techol. Lett., vol. 22, no. 15, pp. 1099-1101, Aug. 2010.

[40] P. T. Shih, C. T. Lin, W. J. Jiang, H. S. Huang, J. Chen, A. Ng'oma, M. Sauer, and S. Chi, "Transmission of 20-Gb/s OFDM signals occupying 7-GHz license-free band at 60 GHz using a RoF system employing frequency sextupling optical up-conversion," Opt. Express, vol. 18, no. 12, pp. 12748-12755, Jun. 2010.

[41] W. J. Jiang, C. T. Lin, C. H. Ho, C. C. Wei, P. T. Shih, J. Chen, and S. Chi, "Photonic Vector Signal Generation Employing an Novel Optical Direct-Detection I/Q Up-Conversion," Opt. Lett., vol.35, no. 23, pp. 4069-4071, Dec. 2010.

[42] C. T. Lin, P. T. Shih, J. Chen, W. Q. Xue, P. C. Peng, and S. Chi, "Optical Millimeter-Wave Signal Generation Using Frequency Quadrupling Technique and No Optical Filtering," IEEE Photon. Techol. Lett., vol. 20, no. 12, pp. 1027-1029, Jun. 2008.

[43] C. T. Lin, Y. M. Lin, J. Chen, S. P. Dai, P. T. Shih, P. C. Peng, and S. Chi, "Optical direct-detection OFDM signal generation for radio-over-fiber link using frequency doubling scheme with carrier suppression," Opt. Express, vol. 16, no. 9, pp. 6056-6063, Apr. 2008.

[44] C. T. Lin, W. J. Jiang, J. Chen, P. T. Shih, P. C. Peng, E. Z. Wong, and S. Chi, "Novel optical vector signal generation with carrier suppression and frequency multiplication based on a single-electrode Mach-Zehnder modulator," IEEE Photon. Techol. Lett., vol. 20, no. 24, pp. 2060-2062, Dec. 2008.

[45] C. T. Lin, P. T. Shih, J. Chen, W. J. Jiang, S. P. Dai, P. C. Peng, Y. L. Ho, and S. Chi, "Optical millimeter-wave up-conversion employing frequency quadrupling without optical filtering," IEEE Trans. Microw. Theory Tech., vol. 57, no. 8, pp. 2084-2092, Aug. 2009.

[46] C. T. Lin, P. T. Shih, W. J. Jiang, E. Z. Wong, J. Chen, and S. Chi, "Photonic vector signal generation at microwave/millimeter-wave band employing optical frequency quadrupling scheme," Opt. Lett., vol.34, no. 14, pp. 2171-2173, Jul. 2009.

[47] P. T. Shih, J. Chen, C. T. Lin, W. J. Jiang, H. S. Huang, P. C. Peng, and S. Chi, "Optical millimeter-wave signal generation via Frequency 12-tupling," J. Lightw. Technol., vol. 28, no. 1, pp. 71-78, Jan. 2010.

[48] A. Kanno, K. Inagaki, I. Morohashi, T. Sakamoto, T. Kuri, I. Hosako, T. Kawanishi, Y. Yoshida, and K. Kitayama, "40 Gb/s W-band (75-110 GHz) 16-QAM radio-over-fiber signal generation and its wireless transmission," Opt. Express, vol. 19, no. 26, pp. B56-B63, Dec. 2011.

[49] T. Kuri, H. Toda, J. J. Vegas Olmos, and K. Kiatayama, "Reconfigurable dense wavelength division multiplexing millimeter-wave-band radio-over-fiber access system technologies," J. Lightwave Technol., vol. 28, no. 16, pp. 2247-2257, Aug. 15, 2010.

[50] J. J. Vegas Olmos, T. Kuri, T. Sono, K. Tamura, H. Toda, and K. Kitayama, "Reconfigurable 2.5-Gb/s baseband and 60-GHz (155-Mb/s) millimeter-waveband radio-over-fiber (Interleaving) access network," J. Lightwave Technol., vol. 26, no. 15, pp. 2506-2512, Aug. 2008.

[51] J. J. Vegas Olmos, T.Kuri, and K.Kitayama, “Half-duplex 12-channel dense WDM 2.6-GHz-band radio-over-fiber system employing a 1.5 GHz bandwidth reflective semiconductor optical amplifier,” J. Opt. Netw. vol. 7, no. 12, pp. 989-994, Dec. 2008.

[52] X. Li, J. Yu, and G. -K. Chang, “Frequency-quadrupling vector mm-wave signal generation by only one single-drive MZM,” IEEE Photon. Techol. Lett., vol. 28, no. 12, pp. 1302-1305, Dec. 2016.

[53] X. Li, Y. Xu, J. Xiao, and J. Yu, “W-Band millimeter-wave vector signal generation based on precoding-assisted random photonic frequency tripling scheme enabled by phase modulator,” IEEE Photon. J., vol. 8, no. 2, pp. 1-10, Apr. 2016.

[54] Y.-T. Hsueh, Z. Jia, H.-C. Chien, A. Chowdhury, J. Yu, and G.-K. Chang, “Multiband 60-GHz wireless over fiber access system with high dispersion tolerance using frequency tripling technique,” J. Lightwave Technol., vol. 29, no. 8, pp. 1105-1111, Feb. 2011.

[55] J. Liu, H.-C. Chien, S.-H. Fan, B. Chen, J. Yu, S. He, and G.-K. Chang, “Efficient Optical Millimeter-Wave Generation Using a Frequency-Tripling Fabry–Pérot Laser With Sideband Injection and Synchronization,” IEEE Photon. Techol. Lett., vol. 23, no. 18, pp. 1325-1327, Sep. 15, 2011.

[56] M. Pasandi, M. Ebrahim, M. M. Sisto, S. Doucet, Y. Kim, L. A. Rusch, and S. LaRochelle, “Low-Distortion Optical Null-Steering Beamformer for Radio-Over-Fiber OFDM Systems,” J. Lightw. Technol., vol.27, no.22, pp. 5173-5182, Nov. 2009.

[57] D. Wake, A. Nkansah, and N. J. Gomes, “Radio over fiber link design for next generation wireless systems,” J. Lightw. Technol., vol. 28, no. 16, pp. 2456-2464, Aug.15, 2010.

[58] Nathan J. Gomes, M. Morant, A. Alphones, B. Cabon, J. E. Mitchell, C. Lethien, M. Csörnyei, A. Stöhr, and S. Iezekiel, "Radio-over-fiber transport for the support of wireless broadband services.," J. Opt. Netw. vol. 8, no. 2, pp. 156-178, Feb. 2009.

[59] C. Cox, *Analog optical links*: Theory and Practice, Cambridge University Press, 2004.

[60] B. Hraimel and X. Zhang, "Low-cost broadband predistortion-linearized single-drive x-cut Mach-Zehnder modulator for radio-over-fiber system," IEEE Photon. Technol. Lett., vol. 24, no. 18, pp. 1571-1573, Sep. 2012.

[61] M. Huang, J. Fu, and S. Pan, "Linearized analog photonic links based on a dual-parallel polarization modulator," Opt. Lett., vol. 37, no. 11, pp. 1823-1825, Jun. 2012.

[62] Y. Cui, Y. Dai, F. Yin, J. Dai, K. Xu, J. Li, and J. Lin, "Intermodulation distortion suppression for intensity-modulated analog fiber-optic link incorporating optical carrier band processing," Opt. Express, vol. 21, no. 20, pp. 23433-23440, Oct. 2013.

[63] W. Li and J. P. Yao, "Spurious-free dynamic range improvement of a microwave photonic link based on bi-directional use of a polarization modulator in a Sagnac loop," Opt. Express, vol. 21, no. 13, pp. 15692-15697, Jul. 2013.

[64] W. Li and J. P. Yao, "Microwave and terahertz generation based photonically assisted microwave frequency twelvetupling with large tenability," IEEE Photon. J., vol. 2, no. 6, pp. 954-959, Dec. 2010.

[65] A. Agarwal, T. Banwell, P. Toliver, and T. K. Woodward, "Pre-distortion compensation of nonlinearities in channelized RF photonic links using a dual-port optical modulator," IEEE Photon. Technol. Lett., vol. 23, no. 1, pp. 24-26, Jan. 2011.

[66] K. Kitayama, A. Maruta, and Y. Yoshida, "Digital coherent technology for optical fiber and radio-over-fiber transmission systems," J. Lightwave Technol., vol. 32, no. 20, pp. 3411-3420, Oct. 15, 2014.

[67] X. Li and J. Yu, "Generation and heterodyne detection of > 100-Gb/s Q-band PDM-64QAM mm-Wave signal," IEEE Photon. Techol. Lett., vol. 29, no. 1, pp. 27-30, Jan. 2017.

[68] X. Li, Y. Xu, and J. Yu, "Over 100-Gb/s V-band single-carrier PDM-64QAM fiber-wireless-integration system," IEEE Photon. J., vol. 8, no. 5, pp. 1-7, Oct. 2016.

[69] X. Li, J. Yu, J. Zhang, F. Li, Y. Xu, Z. Zhang, and J. Xiao, "Fiber-wireless-fiber link for 100-Gb/s PDM-QPSK signal transmission at W-band," IEEE Photon. Techol. Lett., vol. 26, no. 18, pp. 1825-1828, Sep. 15, 2014.

[70] D. Zibar, R. Sambaraju, A. Caballero, J. Herrera, U. Westergren, A. Walber, J. B. Jensen, J. Marti, and I. T. Monroy, "High-capacity wireless signal generation and demodulation in 75- to 110-GHz band employing all-optical OFDM," IEEE Photon. Techol. Lett., vol. 23, no. 12, pp. 810-812, Jun. 15, 2011.

[71] A. Stöhr, B. Shih, S. T. Abraha, A. G. Steffan, and A. Ng' oma, "High spectral-efficient 512-QAM-OFDM 60 GHz CRoF system using a coherent photonic mixer (CPX) and an RF envelope detector," Optical Fiber Communication Conf., Anaheim, CA, USA, 2016, Paper Tu3B.4.

[72] A. Caballero, D. Zibar, and I. T. Monroy, "Digital cohrerent detection of multi-gigabit 40 GHz carrier frequency radio-over-fibre signals using photonic downconversion," Electron. Lett., vol. 46, no. 1, pp. 58-59, Jan. 2010.

[73] D. Zibar, R. Sambaraju, R. Alemany, A. Caballero, J. Herrera, and I. T. Monroy, "Radio-frequency transparent demodulation for broadband hybrid wireless-optical links," IEEE Photon. Technol. Lett., vol. 22, no. 11, pp. 784-786, Jun. 2010.

[74] R. Sambaraju, D. Zibar, A. Caballero, I. T. Monroy, R. Alemany, and J. Herrera, "100-GHz wireless-over-fibre links with up to 16 Gb/s QPSK modulation using optical heterodyne generation and digital coherent detection," IEEE Photon. Technol. Lett., vol. 22, no. 22, pp. 1650-1652, Nov. 2010.

[75] N. G. Gonzalez, A. Caballero, R. Borkowski, V. Arlunno, T. T. Pham, R. Rodes, X. Zhang, M. B. Othman, K. Prince, X. Yu, J. B. Jensen, D. Zibar, and I. T. Monroy, "Reconfigurable digital coherent receiver for metro-access networks supporting mixed modulation formats and bit-rates," Optical Fiber Communication Conf., Los Angeles, CA, Mar. 6-10, 2011, paper OMW7.

[76] A. Caballero, S. Wong, D. Zibar, L. Kazovsky, and I. T. Monroy, "Distributed MIMO antenna architecture for wireless-over-fiber backhaul with multicarrier optical phase modulation," Optical Fiber Communication Conf., Los Angeles, CA, Mar. 6-10, 2011, paper OWT8.

[77] A. Caballero. N. G. Gonzalez, F. Amaya, D. Zibar, and I. T. Monroy, "Long reach and enhanced power budget DWDM radio-over-fibre link supported by Raman amplification and coherent detection," European Conference on Optical Communication., Vienna, Austria, Sept. 20-24, 2009, paper P6.09.

[78] A. Caballero, D. Zibar, and I. T. Monroy, “Performance evaluation of digital coherent receivers for phase modulated radio-over-fiber links,” J. Lightw. Technol., vol. 29, no. 21, pp. 3282-3292, Nov. 2011.

[79] A. Caballero, D. Zibar, R. Sambaraju, J. Marit, and I. T. Monroy, “High capacity 60 GHz and 75-110 GHz band links employing all-optical OFDM generation and digital coherent detection,” J. Lightw. Technol., vol. 30, no. 1, pp. 147-155, Jan. 2012.

[80] A. Caballero. D. Zibar, R. Sambaraju, N. G. Gonzalez, and I. T. Monroy, “Engineering rules for optical generation and detection of high speed wireless millimeter-wave band signals,” European Conference on Optical Communication., Geneva, Switzerland, Sept. 18-22, 2011, paper We. 10. P1. 115.

[81] M. Nakazawa, K. Kikuchi, and T. Miyazaki, *High Spectral Density Optical Communication Technologies*. New York: Springer-Verlag, 2010, pp. 11-50.

[82] S. Norimatsu, K. Iwashita, and K. Sato, “PSK optical homodyne detection using external cavity laser diodes in costas loop,” IEEE Photon. Techol. Lett., vol. 2, no. 5, pp. 374-376, May 1990.

[83] J. Zhang and A. Ansari, “Design of WDM PON with tunable lasers: the upstream scenario,” J. Lightw. Technol., vol. 28, no. 2, pp. 228–236, Jan. 2010.

[84] T. Pfeiffer, “Next generation mobile fronthaul and midhaul architectures,” J. Opt. Netw. vol. 7, no. 11, pp. B38-B44, Nov. 2015.

[85] L. Cheng, X. Liu, N. Chand, F. Effenberger, and G.-K. Chang, “Experimental demonstration of sub-Nyquist sampling for bandwidth- and hardware-efficient mobile fronthaul

supporting 128×128 MIMO with 100-MHz OFDM signals," Optical Fiber Communication Conf., Anaheim, CA, USA, 2016, paper W3C.3.

[86] F. Lu, Y. -C. Chi, M. Xu, L. Cheng, J. Wang, C. -T. Tsai, G.-R. Lin, and G.-K. Chang, "Cost-effective bi-directional mobile fronthaul employing WRC-FPLD for beyond LTE-advanced services," Optical Fiber Communication Conf., Anaheim, CA, USA, 2016, paper TU2B.5.

[87] M. Xu, J. Zhang, F. Lu, J. Wang, L. Cheng, H. J. Cho, M. I. Khalil, D. Guidotti, and G.-K. Chang, "FBMC in Next-Generation Mobile Fronthaul Networks with Centralized Pre-Equalization," IEEE Photon. Technol. Lett., vol. 27, no. 4, Jun. 2016.

[88] J. Wang, C. Liu, J. Zhang, M. Zhu, M. Xu, F. Lu, L. Cheng, and G.-K. Chang, "Nonlinear inter-band subcarrier intermodulation for multi-RAT OFDM wireless services in 5G heterogeneous mobile fronthaul networks," J. Lightw. Technol., vol. 34, no. 17, pp. 4089-4103, Jun. 2016.

[89] J. -Y. Sung, C. -W. Chow, C. -H. Yeh, and G. -K. Chang, "Two-level modulation scheme to reduce latency for optical mobile fronthaul networks," Opt. Express, vol. 24, no. 22, pp. 25767-25773, 2016.

[90] M. Zhu, F. Li, F. Lu, J. Yu, C. Su, G. Gu, and G. -K. Chang, "Wavelength resource sharing in bidirectional optical mobile fronthaul," J. Lightw. Technol., vol. 33, no. 55, pp. 3182-3188, Apr. 2015.

[91] CPRI specification V6.1, "Common public radio interface (CPRI): Interface specification," Jul. 2014.

[92] X. Liu, F. Effenberger, N. Chand, L. Zhou, and H. Lin, “Demonstration of bandwidth-efficient mobile fronthaul enabling seamless aggregation of 36 E-UTRA-like wireless signals in a single 1.1-GHz wavelength channel,” Optical Fiber Communication Conf., Los Angeles, CA, USA, 2015, Paper M2J.2.

[93] X. Liu, F. Effenberger, N. Chand, L. Zhou, and H. Lin, “Efficient mobile fronthaul transmission of multiple LTE-A signals with 36.86-Gb/s CPRI-equivalent data rate using a directly-modulated laser and fiber dispersion mitigation,” the Asia Communications Photonics Conf., Shanghai, China, 2014, Paper AF4B.5.

[94] X. Liu, H. Zeng, N. Chand, and F. Effenberger, “Bandwidth-efficient mobile fronthaul transmission for future 5G wireless networks,” the Asia Communications Photonics Conf., Hong Kong, China, 2015, Paper ASu3E.4.

[95] X. Liu, H. Zeng, N. Chand, and F. Effenberger, “Experimental demonstration of high-throughput low-latency mobile fronthaul supporting 48 20-MHz LTE signals with 59-Gb/s CPRI-equivalent rate and 2-μs processing latency,” 2015 European Conference on Optical Communication, Valencia, Spain, 2015, pp. 1-3.

[96] X. Liu, H. Zeng, N. Chand, L. Zhou, and F. Effenberger, “CPRI-compatible efficient mobile fronthaul transmission via equalized TDMA achieving 256 Gb/s CRPI-equivalent data rate in a single 10-GHz-bandwidth IM-DD channel,” Optical Fiber Communication Conf., Anaheim, CA, USA, 2016, Paper W1H.3.

[97] R. B. Taylor and S. R. Forrest, “Optically coherent direct modulated FM analog link with phase noise canceling circuit,” J. Lightwave Technol., vol. 17, no. 4, pp. 556-563, Apr. 1999.

[98] W. Kwong, P. Prucnal, and M. Teich, "Coherent subcarrier fiber-optic communication systems with phase-noise cancellation," IEEE Trans. Commun., vol. 42, no. 6, pp. 2208-2212, Jun. 1994.

[99] X. Chen, T. Shao, and J. P. Yao, "Digital phase noise cancellation for a coherent-detection microwave photonic link," IEEE Photon. Technol. Lett., vol. 26, no. 8, pp. 805-808, Apr. 2014.

[100] X. S. Yao, L. -S. Yan, B. Zhang, A. E. Willner, and J. Jiang, "All-optic scheme for automatic polarization division demultiplexing," Opt. Express, vol. 15, no. 12, pp. 7407-7414, Jun. 2007.

[101] Datasheet for Mini dynamic polarization controller – PolaRITE™ III (General Photonics), http://www.generalphotonics.com/wp-content/uploads/2015/04/MPC-3-4X.pdf.

[102] D. H. Wolaver, "Measure error rates quickly and accurately," Electron. Des., vol. 43, no. 11, pp. 89-98, May. 1995.

[103] R. Schmogrow et al., "Error vector magnitude as a performance measure for advanced modulation formats," IEEE Photon. Technol. Lett., vol. 24, no. 1, pp. 61-63, Jan. 2012.

[104] G. P. Agrawal, Fiber-Optic Communication Systems, 3rd ed. Hoboken, NJ: Wiley, 2002, pp. 478-479.

[105] Y. Chen, T. Shao, A. Wen, and J. P. Yao, "Microwave vector signals transmission over an optical fiber based on IQ modulation and coherent detection, " Opt. Lett., vol. 39, no. 6, pp. 1509-1512, Mar. 2014.

[106] Y. Pei, J. P. Yao, K. Xu, J. Li, Y. Dai, and J. Lin, "Advanced DSP technique for dynamic range improvement of a phase-modulation and coherent-detection microwave photonic link ," in Proc. IEEE Int. Topical Meeting Microw. Photon. Conf., Oct. 2013, pp. 72-75.

[107] T. R. Clark and M. L. Dennis, "Coherent optical phase-modulation link," IEEE Photon. Technol. Lett., vol. 19, no. 16, pp. 1206-1208, Aug. 2007.

[108] T. R. Clark, S. R. O'Connor, and M. L. Dennis, "A phase-modulation I/Q-demodulation microwave-to-digital photonic link," IEEE Trans. Microw. Theory Tech., vol. 58, no. 11, pp. 3069-3058, Nov. 2010.

[109] A. Caballero, D. Zibar, and I. Tafur Monroy, "Performance evaluation of digital coherent receivers for phase-modulated radio-over-fiber links," J. Lightw. Technol., vol. 29, no. 21, pp. 3282-3292, Nov. 2011.

[110] A. Caballero, D. Zibar, and I. Tafur Monroy, "Digital coherent detection of multi-gigabit 40 GHz carrier frequency radio-over-fibre signals using photonic downconversion," Electron. Lett., vol. 46, no. 1, pp. 57–58, Jan. 2010.

[111] X. Chen and J. P. Yao "A coherent microwave photonic link with digital phase noise cancellation," in Proc. IEEE Int. Topical Meeting Microw. Photon. Conf., Oct. 2014, pp. 438-441.

[112] A. Brillant, Digital and Analog Fiber Optic Communication for CATV and FTTx Applications, Bellingham, Washington: SPIE, 2008, pp. 653-660.

[113] V. J. Urick, J. X. Qiu, and F. Bucholtz, “Wide-band QAM-over-fiber using phase modulation and interferometric demodulation,” IEEE Photon. Technol. Lett., vol. 16, no. 10, pp. 2374-2376, Oct. 2004.

[114] G. P. Agrawal, Fiber-Optic Communication Systems, 4th ed. Hoboken, NJ: Wiley, 2010, pp. 151-157.

[115] G. Hill, *The Cable and Telecommunications Professionals' Reference: Transport Networks. Vol. 3. Burlington*, MA: Focal Press, 2008, pp. 203-206.

[116] R. Schmogrow, D. Hillerkuss, S. Wolf, B. Bäuerle, M. Winter, P. Kleinow, B. Nebendahl, T. Dippon, P. C. Schindler, C. Koos, W. Freude, and J. Leuthold, “512QAM Nyquist sinc-pulse transmission at 54 Gbit/s in an optical bandwidth of 3 GHz,” Opt. Express, vol. 20, no.6, pp. 6439-6447, Mar. 2012.

[117] X. Chen and J. P. Yao, “Radio over colorless WDM-PON with wavelength reuse based on polarization multiplexing and coherent detection incorporating digital phase noise cancellation,” Optical Fiber Communication Conf., Los Angeles Convention Center, Los Angeles, California, USA, Mar. 22-26, 2015, paper W1F.2.

[118] X. Chen and J. P. Yao, “Wavelength reuse in a symmetrical radio over WDM-PON based on polarization multiplexing and coherent detection,” J. Lightw. Technol., vol. 34, no. 4, pp. 1150-1157, Feb. 15, 2016.

[119] C. H. Cox III, E. I. Ackerman, G. Betts, and J. Prince, “Limits on the performance of RF-over-fiber links and their impact on device design,” IEEE Trans. Microw. Theory Techn., vol. 54, no. 2, pp. 906-920, Feb. 2006.

[120] G. H. Smith, D. Novak, and Z. Ahmed, “Technique for optical SSB generation to overcome dispersion penalties in fibre-radio systems,” Electron. Lett., vol. 33, no. 1, pp. 74-75, Jan. 1997.

[121] S. Shimotsu, S. Oikawa, T. Saitou, N. Mitsugi, K. Kubodera, T. Kawanishi, and M. Izutsu, “Single side-band modulation performance of a LiNbO3 integrated modulator consisting of four-phase modulator waveguides ,” IEEE Photon. Technol. Lett., vol. 13, no. 4, pp.364-366, Apr. 2001.

[122] G. H. Smith, D. Novak, and Z. Ahmed, “Overcoming chromatic-dispersion effects in fiber-wireless systems incorporating external modulators,” IEEE Trans. Microw. Theory Techn., vol. 45, no. 8, pp. 1410–1415, Aug. 1997.

[123] M. Xue, S. Pan, and Y. Zhao, “Optical single-sideband modulation based on a dual-drive MZM and a 120° hybrid coupler,” J. Lightw. Technol., vol. 32, no. 19, pp. 3317–3323, Oct. 2014.

[124] B. Hraimel, X. Zhang, Y. Pei, T. Liu, T, Xu, and Q. Nie, “Optical single-sideband modulation with tunable optical carrier to sideband ratio in radio over fiber,” J. Lightw. Technol., vol. 29, no. 5, pp. 775–781, Mar. 2011.

[125] Y. Zhang, F. Zhang, and S. Pan, “Optical single sideband modulation with tunable optical carrier-to-sideband ratio,” IEEE Photon. Technol. Lett., vol. 26, no. 7, pp. 653-655, Apr. 2014.

[126] J. L. Wei, X. Q. Jin, and J. M. Tang, “The influence of directly modulated DFB lasers on the transmission performance of carrier-suppressed single-sideband optical OFDM signals over IMDD SMF systems,” J. Lightw. Technol., vol. 27, no. 13, pp. 2412–2419, Jul. 2009.

[127] C. Lim, M. Attygalle, A. Nirmalathas, D. Novak, and R. Waterhouse, “Analysis of optical carrier-to-sideband ratio for improving transmission performance in fiber-radio links,” IEEE Trans. Microw. Theory Techn., vol. 54, no. 5, pp. 2181-2186, May 2006.

[128] X. Chen and J. P. Yao, “High Spectral Efficiency Coherent RoF System Based On OSSB Modulation With Low-Cost Free-Running Laser Sources For UDWDM-PONs,” IEEE/OSA J. Lightw. Technol., vol. 34, no. 11, pp. 2789-2795, Jun. 2016.

[129] J. G. Proakis and M. Salehi, Digital Communications, 5th ed, New York, NY: McGraw-Hill, 2008, pp. 97-104.

[130] A. D. Poularikas, The Handbook of Formulas and Tables for Signal Processing, Boca Raton, FL: CRC, 1999.

[131] L. W. Couch, Digital and Analog Communication System, 8th ed, Upper Saddle River, NJ: Pearson, 2013, pp. 324-325.

[132] J. Lu, K. B. Letaief, J. C. -I. Chuang, and M. L. Liou, “M-PSK and M-QAM BER computation using signal-space concepts,” IEEE Trans. Commu., vol. 47, no. 2, pp.181-184, Feb. 1999.

[133] L. Hanzo, M. Münster, B. J. Choi, and T. Keller, OFDM and MC-CDMA for Broadband Multi-User Communications, WLANs and Broadcasting, Hoboken, NJ: Wiley, 2003, pp. 419-429.

[134] China Mobile Research Institute, “C-RAN: The road towards green RAN,” Whitepaper v. 2.6, Sep. 2013.

[135] Z. Shen, A. Papasakellariou, J. Montojo, D. Gerstenberger, and F. Xu, “Overview of 3GPP LTE- advanced carrier aggregation for 4G wireless communications,” IEEE Commun. Mag., vol. 50, no. 2, pp. 122-130, Feb. 2012.

[136] K. Werner, H. Asplund, B. Halvarsson, N. Jalden, and D. Figueiredo, “LTE-A field measurements : 8 × 8 MIMO and carrier aggregation,” IEEE Vehicular Technology Conf., Dresden, Germany, 2013.

[137] Y. Okumura and J. Terada, “Optical network technologies and architectures for backhaul/fronthaul of future radio access supporting big mobile data,” Optical Fiber Communication Conf., San Francisco, CA, USA, 2014, Paper Tu3F.1.

[138] N. Cvijetic, A. Tanaka, K. Kanonakis, and T. Wang, “SDN-controlled topology-reconfigurable optical mobile fronthaul architecture for bidirectional CoMP and low latency inter-cell D2D in the 5G mobile era,” Opt. Exp., vol. 22, no. 17, pp. 20809-20815, 2014.

[139] J. Wang, Z. Yu, K. Ying, J. Zhang, F. Lu, M. Xu, and G.-K. Chang, “Delta-Sigma modulation for digital mobile fronthaul enabling carrier aggregation of 32 4G-LTE / 30 5G-FBMC signlas in a single-λ 10-Gb/s IM-DD Channel,” Optical Fiber Communication Conf., Anaheim, CA, USA, 2016, Paper W1H.2.

[140] M. Zhu, X. Liu, N. Chand, F. Effenberger, and G.-K. Chang, “High capacity mobile fronthaul supporting LTE-advanced carrier aggregation and 8 × 8 MIMO,” Optical Fiber Communication Conf., Los Angeles, CA, USA, 2015, Paper M2J.3.

[141] H. -T Huang, C.-T Lin, Y.-T Chiang, C-C Wei, and C.-H Ho, “Simple 2 × 2 MIMO 60-GHz optical/wireless system with extending fiber transmission distance,” J. Lightw. Technol., vol. 32, no. 20, pp. 3660-3667, Oct. 2014.

[142] C. -T Lin, C.-H Ho, H.-T Huang, and Y.-H Cheng, "Ultrahigh capacity 2 × 2 MIMO RoF system at 60 GHz employing single-sideband single-carrier modulation," Opt. Lett., vol. 39, no. 6, pp. 1358-1361, Mar. 2014.

[143] J. Zhang, J. Yu, N. Chi, Z. Dong, X. Li, and G. -K. Chang, "Multichannel 120-Gb/s data transmission over 2 × 2 MIMO fiber-wireless link at W-band," IEEE Photon. Technol. Lett., vol. 25, no. 8, pp. 780-783, Apr. 15, 2013.

[144] F. Li, Z. Cao, X. Li, Z. Dong, and L. Chen, "Fiber-wireless transmission system of PDM-MIMO-OFDM at 100 GHz frequency," J. Lightw. Technol., vol. 31, no. 14, pp. 2394-2399, Jul. 15, 2013.

[145] L. Tao, Z. Dong, J. Yu, N. Chi, J. Zhang, X. Li, Y. Shao, and G.-K. Chang, "Experimental demonstration of 48-Gb/s PDM-QPSK radio-over-fiber system over 40-GHz mm-wave MIMO wireless transmission," IEEE Photon. Technol. Lett., vol. 24, no. 24, pp. 2276-2279, Dec. 15, 2013.

[146] X. Li, Z. Dong, J. Yu, N. Chi, Y. Shao, and G.-K. Chang, "Demonstration of ultra-high bit rate fiber wireless transmission system of 108-Gb/s data over 80-km fiber and 2 x 2 MIMO wireless links at 100 GHz W-band frequency," Optical Fiber Communication Conf., 2013, Paper JW2A.75.

[147] X. Li, J. Yu, Z. Zhang, and Y. Xu, "Field trial of 80-Gb/s PDM-QPSK signal delivery over 300-m wireless distance with MIMO and antenna polarization multiplexing at W-band," Optical Fiber Communication Conf., Los Angeles, CA, USA, 2015, Paper Th5A.5.

[148] X. Li, J. Yu, J. Xiao, F. Li, Y. Xu, N. Chi, and G. -K. Chang, "Mm-wave vector signal generation and transport for W-band MIMO system with intensity modulation and direct detection," Optical Fiber Communication Conf., Anaheim, CA, USA, 2016, Paper M3B. 2.

[149] X. Li, Y. Xu, J. Xiao, and J. Yu "A 2 × 2 MIMO optical wireless system at D-band," Optical Fiber Communication Conf., Anaheim, CA, USA, 2016, Paper Th4A.7.

[150] Y. Xu, J. Yu, X. Li, J. Xiao, and Z. Zhang "Experimental investigation on fiber-wireless MIMO system with different LO at W band," IEEE Photon. J., vol. 7, no. 2, pp. 1-7, Apr. 2015.

[151] X. Li and J. Yu, "Over 100 Gb/s ultra-broadband MIMO wireless signal delivery system at the D-band," IEEE Photon. J., vol. 8, no. 5, pp. 1-10, Oct. 2016.

[152] J. Yu, X. Li, and N. Chi, "Faster than fiber: over 100-Gb/s signal delivery in fiber wireless integration system," Opt. Express, vol. 21, no. 19, pp. 22885-22904, Sep. 2013.

[153] J. Xiao, J. Yu, X. Li, Y. Xu, Z. Zhang, and L. Chen, "40-Gb/s PDM-QPSK signal transmission over 160-m wireless distance at W-band," Opt. Lett., vol. 40, no. 6, pp. 998-1001, Mar. 15, 2015.

[154] N. P. Diamantopoulos, S. Inudo, Y. Yoshida, A. Maruta, A. Kanno, P. T. Dat, T. Kawanishi, R. Maruyama, N. Kuwaki, S. Matsuo, and K. Kitayama, "Mode-division multiplexed W-band RoF transmission for higher-order spatial multiplexing," Optical Fiber Communication Conf., Los Angeles, CA, USA, 2015, paper W4G.2.

[155] A. Kanno, T. Kuri, I. Hosako, T. Kawanishi, Y. Yasumura, Y. Yoshida, Y. Yasumura, and K. Kitayama, "Optical and millimeter-wave radio seamless MIMO transmission based on a radio over fiber technology," Opt. Express, vol. 20, no. 28, pp. 29395-29403, Dec. 2012.